IOCCG Protocol Series

Ocean Optics & Biogeochemistry Protocols for Satellite Ocean Colour Sensor Validation

Volume 3: Protocols for Satellite Ocean Colour Data Validation: In Situ Optical Radiometry (v3.0)

Authors
Giuseppe Zibordi, Kenneth J. Voss, B. Carol Johnson and James L. Mueller

International Ocean Colour Coordinating Group (IOCCG) in collaboration with National Aeronautics and Space Administration (NASA)

IOCCG, Dartmouth, Canada

December 2019

IOCCG Ocean Optics and Biogeochemistry Protocols for Satellite Ocean Colour Sensor Validation

IOCCG Protocol Series Volume 3.0, 2019

Protocols for Satellite Ocean Colour Data Validation: *In Situ* Optical Radiometry (v3.0)

Authors:

Giuseppe Zibordi	European Commission, Joint Research Centre, Ispra, Italy
Kenneth J. Voss	University of Miami, Coral Gables, Florida, USA
B. Carol Johnson	National Institute of Standards and Technology, Gaithersburg, Maryland, USA
James L. Mueller	Salinas, California, USA

Correct citation for this volume:

IOCCG Protocol Series (2019). Protocols for Satellite Ocean Colour Data Validation: In Situ Optical Radiometry. Zibordi, G., Voss, K. J., Johnson, B. C. and Mueller, J. L. IOCCG Ocean Optics and Biogeochemistry Protocols for Satellite Ocean Colour Sensor Validation, Volume 3.0, IOCCG, Dartmouth, NS, Canada.
http://dx.doi.org/10.25607/OBP-691

Acknowledgements:

The authors gratefully acknowledge the assistance of the following colleagues who provided valuable comments and suggestions improving the quality of the protocols (in alphabetical order): Emmanuel Boss, Susanne Craig, Robert Foster, Philipp Grotsch, Antonio Mannino, and Dariusz Stramski. The authors also thank the Associate Editorial Peer-Reviewers for their constructive comments on this document:

Susanne Craig	NASA Goddard Space Flight Center, Greenbelt, MD, USA
Robert Foster	U.S. Naval Research Laboratory, Washington, D.C., USA
Dariusz Stramski	Scripps Institution of Oceanography, CA, USA

http://www.ioccg.org

Published by the International Ocean Colour Coordinating Group (IOCCG), Dartmouth, NS, Canada, in conjunction with the National Aeronautics and Space Administration (NASA).

Doi: http://dx.doi.org/10.25607/OBP-691

Contents

Preface

This document aims to support the ocean color community with protocols for the collection, quality check, and processing of *in situ* measurements of radiometric quantities and the subsequent determination of apparent optical properties of natural water for the validation of satellite radiometric products. In addition to a general introduction on *Elements of Marine Optical Radiometry Data and Analysis* (Chapter 1), the document addresses *Radiometer Specifications* (Chapter 2), *Calibration and Characterization of Optical Radiometers* (Chapter 3), *In-water Radiometry Measurements and Data Analysi*s (Chapter 4), and *Above-water Radiometry Measurements and Data Analysis* (Chapter 5).

The overall structure and content of the various chapters are based on, and benefit from, the Ocean Optics Protocols promoted and published by the National Aeronautics and Space Administration within the framework of the Sea-Viewing Wide Field-of-View Sensor (SeaWiFS) and Sensor Intercomparison for Marine Biological and Interdisciplinary Ocean Studies (SIMBIOS) programs (Mueller and Austin 1995, Mueller *et al.* 2003a, Mueller *et al.* 2003b).

Optical radiometry is heavily affected by the presence of clouds, which challenges both *in situ* measurements and satellite observations. It is emphasized, therefore, that the protocols detailed herein focus on radiometric measurements performed during clear sky conditions necessary for rigorous validation of satellite ocean color data products. It is acknowledged that the collection of radiometric data during suboptimal conditions (*e.g.*, non-favorable illumination) is still highly recommended to support different applications (*e.g.*, bio-optical modeling). However, a strict ranking of measurements based on application needs must be enforced to correctly identify data for the various uses and specifically those meeting validation requirements.

Finally, it is anticipated that the chapters on in-water and above-water radiometry provide comprehensive details on those measurement methods sharing large consensus inside the community and whose application is strongly encouraged. Conversely, only brief summaries are provided for those methods already well represented by the previous ones, still requiring consolidation, or that may be difficult to implement in the field.

References

Mueller J.L., and Austin R.W,. 1995: Ocean Optics Protocols for SeaWiFS Validation, Revision 1. *NASA Tech. Memo. 104566, Vol. 25*, Hooker S.B., Firestone E.R. and Acker J.G., Eds., NASA Goddard Space Flight Center, Greenbelt, Maryland, 67 pp.

Mueller J.L., Pietras C., Hooker S.B., Austin R.W., Miller M., Knobelspiesse K.D., Frouin R., Holben B.N. and Voss K.J., 2003a. Ocean Optics Protocols for Satellite Ocean Color Sensor Validation, Revision 4, Volume II: Instrument Specifications, Characterization and Calibration. *NASA/TM-2003-21621/Rev-Vol II*. Mueller J.L., Fargion G.S. and McClain C.R., Eds., NASA Goddard Space Flight Center, Greenbelt, Maryland, 63 pp.

Mueller J.L., Morel A, Frouin R., Davis C., Arnone R., Carder K., Lee Z.P, Steward R.G., Hooker S.B., Mobley C.D., McLean S., Holben B.N., Miller M., Pietras C, Knobelspiesse K.D., Fargion G.S., Porter J. and Voss K.J., 2003b: Ocean Optics Protocols for Satellite Ocean Color Sensor Validation, Revision 4, Volume III: Radiometric Measurements and Data Analysis Protocols. *NASA/TM-2003-21621/Rev-Vol III*. Mueller J.L., Fargion G.S. and McClain C.R., Eds., NASA Goddard Space Flight Center, Greenbelt, Maryland, 84 pp.

Chapter 1: Elements of Marine Optical Radiometry Data and Analysis

Giuseppe Zibordi[1] and Kenneth J. Voss[2]

[1] *European Commission, Joint Research Centre, Ispra, Italy*
[2] *University of Miami, Coral Gables, Florida, USA*

1. INTRODUCTION

This chapter introduces a few complementary elements relevant to both in-water and above-water radiometry. It specifically embraces the spectral classification of radiometers and a general description of irradiance and radiance sensors. Further, it addresses the need to account for a number of corrections generally resulting from characterizations of radiometer's performance. Additionally, by focusing on the basic radiometric quantity, *i.e.*, the water leaving radiance $L_w(\lambda)$, methods are introduced for its normalization to remove the dependence on illumination conditions. Finally, the uncertainty budget for the normalized water-leaving radiance $L_{WN}(\lambda)$ determined from a multispectral in-water radiometer system is provided as an elementary example for radiometric data products.

2. RADIOMETERS

Spectral classification

Radiance and irradiance sensors are commonly classified according to their capability of spectrally resolving light (Zibordi and Voss 2014). Specifically, optical radiometers relevant for the validation of satellite ocean color products can be classified as either hyperspectral or multispectral in order of decreasing spectral resolution.

A large number (generally tens to hundreds) of narrow spectral bands, typically less than 10 nm wide, distributed continuously across the spectrum identify hyperspectral radiometers. These sensors, exhibiting a spectral resolution greater than the sampling interval at which the spectrum is measured, use a dispersive optical element (*i.e.*, diffraction grating or prism) with one- or two-dimensional detector arrays to sample the light spectrum.

As opposed to hyperspectral radiometers, multispectral sensors measure the light field at a few discrete spectral bands typically 10 nm wide ideally equivalent to those of satellite sensors. The individual spectral bands of these radiometers are commonly realized by coupling photodetectors and spectral band-pass filters.

The response of optical radiometers exhibits dependence on a number of factors (see Chapter 3 on *Calibration and Characterization of Optical Radiometers*), including non-linearity, temperature dependence, polarization sensitivity, out-of-band response, and stray light perturbations. Among these, stray light and sensitivity to polarization can be a major source of uncertainty for hyperspectral sensors. Specifically, stray light resulting from scattering or reflections in the optical system causes light from one region of the spectrum to interfere with light from another region. Sensitivity to polarization, which may vary as a function of wavelength, may spectrally affect measurements of polarized natural light fields.

Similar to the stray light problems in hyperspectral systems, the spectral responsivity of multispectral sensors may exhibit responsivity outside the central band (out-of-band response), introducing errors in radiometric measurements dependent on the spectral shape of the incoming light. Sensitivity to the polarization of multispectral radiometers is generally less pronounced than that of hyperspectral systems. Still, it may vary with the optical design and components.

Irradiance sensors

Plane irradiance measured with a cosine collector (hereafter simply called *irradiance*) is a measure of the light flux per unit surface area. Typical quantities measured in the field are the downward or upward

irradiance, which is the light energy per unit time going through a flat horizontal surface with a given area either in the downward or upward directions.

For any cosine collector, the spectral angular response must be measured to determine the error in the cosine response (Mekaoui and Zibordi 2013). The effects of this error in irradiance measurements depend both on the spectral angular response of the collector and the radiance distribution of the light field being measured.

One important characteristic is the immersion factor that quantifies the change in responsivity of a sensor as a function of the refractive index of the external medium (Mueller and Austin 1995). Since radiometers have their absolute calibration performed in air, the immersion factor must be determined to account for the difference in their responsivity while in water.

Radiance sensors

Radiance is the flux per unit solid angle and per unit projected area. It is generally measured by limiting the field-of-view of the radiometer and assuming radiance is spatially invariant, or at the least slightly changing, over the projected solid angle. The simplest radiance sensor, commonly referred to as a Gershun tube radiometer (Gershun 1939), is formed by combining an irradiance collector and a tube restricting its full-angle field-of-view (FOV). Its nominal FOV is defined by $\theta_{FOV} = 2 \tan^{-1}[D/(2h)]$ where D is the front aperture of the optics and h the distance between aperture and detector. The related solid angle field-of-view in sr for a conical full-angle FOV is given by $\Omega = 2\pi (1 - \cos(\theta_{FOV} / 2))$.

In general, an optical window is placed in front of the Gershun tube. Similar to the case of irradiance sensors, this affects the measured radiance when the radiometer is operated in water. This implies the need to determine the immersion factor for in-water radiance sensors (Mueller and Austin 1995).

3. CHARACTERIZATION AND ABSOLUTE CALIBRATION

This section addresses the basic need to ensure proper application of absolute calibration coefficients and correction factors resulting from instrument characterizations for field measurements. While absolute calibration coefficients are produced through laboratory activities necessarily performed on each sensor, the characterizations may result from both laboratory analysis specific for the sensor or, alternately, from investigations performed for a class of radiometers. Both correction factors from characterizations and absolute calibration coefficients contribute to the determination of the actual responsivity of each sensor, which relates the sensor output to the input radiometric quantity. Thus, calibration accounts for: absolute in-air responsivity to the radiometric source (either radiance or irradiance); in-water responsivity changes due to differences between the refractive index of air and that of water; and, additionally, factors correcting for the non-ideal performance of the radiometer such as stray light, polarization sensitivity, non-linearity, temperature dependence, sensitivity decay with time, and deviation from the ideal angular response.

The calibration concept is implemented through the application of the measurement equation yielding the radiometer output for a given source configuration (Zibordi and Voss 2014). Specifically, the conversion from relative to physical units of the radiometric quantity $\Im(\lambda)$ (either $E(\lambda)$ or $L(\lambda)$) at wavelength λ is performed through

$$\Im(\lambda) = F_{\Im}(\lambda)\, F_{i,\Im}(\lambda)\, \aleph(\lambda)\, \mathrm{DN}(\Im(\lambda)) \tag{1.1}$$

where $\mathrm{DN}(\Im(\lambda))$ indicates the digital output corrected for the dark-signal, $F_{\Im}(\lambda)$ the in-air absolute calibration coefficient (*i.e.,* the absolute responsivity), $F_{i,\Im}(\lambda)$ the immersion factor accounting for the change in responsivity of the sensor when immersed in water with respect to air, and $\aleph(\lambda)$ (for simplicity only expressed as a function of λ) corrections for any deviation from the ideal performance of the radiometer. In the case of an ideal sensor $\aleph(\lambda)=1$, but in general $\aleph(\lambda)\neq 1$ with

$$\aleph(\lambda) = \aleph_i(\mathrm{i}(\lambda))\, \aleph_j(\mathrm{j}(\lambda)) \ldots \aleph_k(\mathrm{k}(\lambda)) \tag{1.2}$$

where $\aleph_i(\mathrm{i}(\lambda))$, $\aleph_j(\mathrm{j}(\lambda))$, …, and $\aleph_k(\mathrm{k}(\lambda))$ are correction terms for different factors indexed by i, j, …, k affecting the non-ideal performance of the instrument, such as temperature, non-linearity, stray light, polarization, etc., all assumed independent.

The independence of terms $\aleph_i(i(\lambda))$, $\aleph_j(j(\lambda))$, …, and $\aleph_k(k(\lambda))$ is a clear idealization of Eq. 1.2 that may exhibit operational limits. For instance, stray light can exhibit dependence with temperature not captured by independent temperature and stray light characterizations. Still, it is expected that in the case of corrections restricted to a few percent of the input signal, the contributions due to the non-independence of corrections are of a second order and thus have a negligible impact on the overall uncertainty of corrections.

4. BASIC RADIOMETRIC QUANTITIES

The basic data product from *in-situ* radiometry is $L_w(\lambda)$, generally in units of $\mu W\ cm^{-2}\ nm^{-1}\ sr^{-1}$, whose amplitude varies with the illumination conditions. In view of removing such a dependence, Gordon and Clark (1981) introduced the concept of normalized water-leaving radiance, $L_{wn}(\lambda)$, to express the water-leaving radiance that would occur with no atmosphere, the sun at the zenith and at the mean sun-earth distance

$$L_{wn}(\lambda) = \frac{L_w(\lambda)}{E_s(\lambda)} E_0(\lambda) \tag{1.3}$$

where $E_0(\lambda)$ is the mean extra-atmospheric solar irradiance in units of $\mu W\ cm^{-2}\ nm^{-1}$ (Thuillier *et al.* 2003) and the ratio $L_w(\lambda)/E_s(\lambda)$ is commonly referred to as the remote sensing reflectance $R_{rs}(\lambda)$ in units of sr^{-1}.

In the case the above-water downward irradiance $E_s(\lambda)$ (also indicated as $E_d(0^+,\lambda)$) is not directly measured or alternatively determined from sub-surface values of the in-water downward irradiance $E_d(0^-,\lambda)$ (see Chapter 4 on *In-Water Radiometry Measurements and Analysis*), the ratio $E_0(\lambda)/E_s(\lambda)$ can be replaced by $[D^2\, t_d(\lambda)\, \cos\theta_0]^{-1}$ (Tanré *et al.* 1979), where θ_o is the solar zenith angle, $D = 1 + 0.0167 \cos [2\pi\ (d_y - 3)/365]$ accounts for the variation in the sun-earth distance as a function of the day of the year d_y (Gordon *et al.* 1983) and $t_d(\lambda)$ is the atmospheric diffuse transmittance. The latter is computed from measured or estimated values of the aerosol optical depth $\tau_a(\lambda)$ and calculated values of the Rayleigh optical depth $\tau_R(\lambda)$.

As previously indicated, both $L_{wn}(\lambda)$ and $R_{rs}(\lambda)$ are quantities which take into account illumination effects stemming from atmospheric transmittance, sun-earth distance, and to some extent the sun zenith angle. However, this initial correction does not account for the bidirectional effects implicit in anisotropic radiance distributions. Corrections for bidirectional effects were introduced by Morel and Gentili (1991) through the concept of *exact normalized water-leaving radiance*, $L_{WN}(\lambda)$. By applying their correction scheme to nadir-view $L_{wn}(\lambda)$, $L_{WN}(\lambda)$ is given by

$$L_{WN}(\lambda) = L_{wn}(\lambda) \frac{f(0,\lambda,\tau_a,IOP)}{Q_n(0,\lambda,\tau_a,IOP)} \left[\frac{f(\theta_0,\lambda,\tau_a,IOP)}{Q_n(\theta_0,\lambda,\tau_a,IOP)} \right]^{-1} \tag{1.4}$$

where the ratios $f(0,\lambda,\tau_a,IOP)/Q_n(0,\lambda,\tau_a,IOP)$ and $Q_n(\theta_0,\lambda,\tau_a,IOP)/f(\theta_0,\lambda,\tau_a,IOP)$ account for the effects of the anisotropic radiance distribution and $\theta_0 \neq 0$.

It is recalled that the above scheme and the $f(0,\lambda,\tau_a,IOP)/Q_n(0,\lambda,\tau_a,IOP)$ and $Q_n(\theta_0,\lambda,\tau_a,IOP)/f(\theta_0,\lambda,\tau_a,IOP)$ ratios from tabulated values (see Morel *et al.* 2002), were proposed for Case-1 waters where the values of the inherent optical properties (IOPs) are expressed as a sole function of the chlorophyll-*a* concentration (*Chla*). Because of the intrinsic limits of the previous *Chla*-based scheme to address corrections for bidirectional effects in optically complex waters, a number of alternative approaches have been investigated. However, they often require input parameters not accessible unless radiometric measurements are supported by a comprehensive characterization of the water IOPs and the determination of the concentration of the optically significant constituents. Among those approaches, that proposed by Lee *et al.* (2011) for both Case-1 and optically complex waters, solely requires the input radiometric quantity for which corrections need to be devised (*i.e.*, $L_{wn}(\lambda)$). This approach, which separates contributions due to geometry from those depending on IOPs, can also be broadly applied to the basic quantity obtained from above-water radiometry, $L_w(\theta,\phi,\lambda)$, where θ and ϕ are the viewing nadir and

azimuth angles, respectively (see Chapter 5 on *Above-water Radiometry Measurements and Data Analysis*).

In this IOP-based correction method, the following equation is used to determine essential inherent optical properties characterizing the measured $L_{wn}(\lambda)$

$$L_{wn}(\lambda) = E_0(\lambda)\left\{\left[G_0^w(0,0,\theta_0) + G_1^w(0,0,\theta_0)\cdot\frac{b_{bw}(\lambda)}{\kappa(\lambda)}\right]\cdot\frac{b_{bw}(\lambda)}{\kappa(\lambda)} + \left[G_0^p(0,0,\theta_0) + G_1^P(0,0,\theta_0)\cdot\frac{b_{bp}(\lambda)}{\kappa(\lambda)}\right]\cdot\frac{b_{bp}(\lambda)}{\kappa(\lambda)}\right\} \quad (1.5)$$

where the coefficients G_0^w, G_1^w, G_0^p, G_1^p are model parameters determined for nadir view and sun zenith angle θ_0 from simulations applying a phase function representing scattering of an assemblage of particles. Symbols $b_{bw}(\lambda)$ and $b_{bp}(\lambda)$ indicate the pure sea water and particle backscattering coefficients, respectively, while $\kappa(\lambda) = a(\lambda)+b_b(\lambda)$ with $b_b(\lambda) = b_{bw}(\lambda)+b_{bp}(\lambda)$ and $a(\lambda)$ is the total seawater absorption coefficient.

The correction process proceeds by estimating the values of $a(\lambda)$ and $b_b(\lambda)$ from Eq. 1.5. Then the derived IOPs are used to calculate $L_{WN}(\lambda)$ by applying the parameters G_0^w, G_1^w, G_0^p, G_1^p determined for $\theta_0 = 0$ from

$$L_{WN}(\lambda) = E_0(\lambda)\left\{\left[G_0^w(0,0,0) + G_1^w(0,0,0)\cdot\frac{b_{bw}(\lambda)}{\kappa(\lambda)}\right]\cdot\frac{b_{bw}(\lambda)}{\kappa(\lambda)} + \left[G_0^p(0,0,0) + G_1^P(0,0,0)\cdot\frac{b_{bp}(\lambda)}{\kappa(\lambda)}\right]\cdot\frac{b_{bp}(\lambda)}{\kappa(\lambda)}\right\}. \quad (1.6)$$

This correction approach was investigated in recent studies (Gleason *et al.* 2012, Talone *et al.* 2018) and, as expected showed a better performance in optically complex waters compared with Morel *et al.* (2002), which was proposed for Case-1 waters.

Figure 1.1 illustrates the *Chla*- and IOP-based approaches for the correction of bidirectional effects in $L_{wn}(\lambda)$.

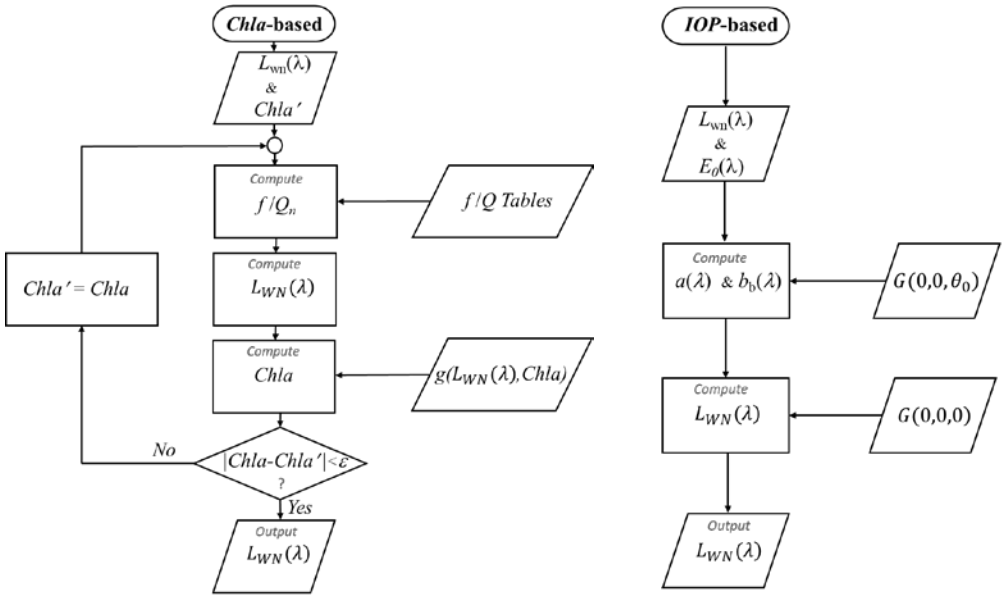

Figure 1.1. A schematic of the Chla- and IOP-based correction approaches. Rectangles designate processes, and parallelograms specify input/outputs. Chla′ indicates an initial value for Chla iteratively updated, and f/Q_n any of the $f(0,\lambda,\tau_a,IOP)/Q_n(0,\lambda,\tau_a,IOP)$ and $Q_n(\theta_0,\lambda,\tau_a,IOP)/f(\theta_0,\lambda,\tau_a,IOP)$ ratios determined from tabulated values (i.e., f/Q tables). $g(L_{WN}(\lambda), Chla)$ designates a bio-optical algorithm for the computation of Chla. The value ε specifies a Chla threshold (e.g., 0.05 mg m^{-3}) triggering the completion of the iterative Chla-

based correction. Finally, G(0,0,θ_0) and G(0,0,0) specify parameters G_0^w, G_1^w, G_0^p, G_1^p for the geometric configurations (0,0,θ_0) and (0,0,0), respectively.

5. UNCERTAINTIES

Errors and uncertainties are distinct quantities. Differences between values of measured quantities and the true values of measurands are indicated as errors. These may comprise i) systematic components indicating biases due to lack of accuracy, and ii) random components indicating dispersion due to lack of precision. Bias components are generally minimized through corrections.

Uncertainties quantify the incomplete knowledge of the measurand through the available information (see JCGM 2008). These are generally classified into type A when determined through statistical methods and type B when determined by means other than statistical (*e.g.*, models, published data, calibration certificates, or even experience). Type A and type B uncertainties can additionally be separated into additive (*i.e.*, independent of the measured value such as the dark-signal) or multiplicative (*i.e.*, dependent on the measured value such as those related to the responsivity of the radiometer). All uncertainties contribute to the overall measurement uncertainty through their combined values. When the various uncertainties are independent, multiplicative, and normally distributed, the combined uncertainty can be determined as the quadrature sum (*i.e.*, the root square sum) of the various contributions. The level of confidence of each uncertainty is defined by the coverage factor k (Johnson *et al.* 2014). Standard uncertainties refer to a confidence level of 68% determined by $k = 1$, while expanded uncertainties defined by $k > 1$ refer to confidence levels of approximately 95% ($k \approx 2$) or 99% ($k \approx 3$). Unless otherwise specified, $k = 1$ is used in this document.

Uncertainties, when possible, should be provided in both relative (*i.e.*, %) and physical units. The range of values for which the uncertainties are proposed should also be reported together with details on measurement conditions. In fact, uncertainties determined for a specific range of values may not necessarily be the same for other ranges or different measurement conditions.

The quantification of uncertainties of *in situ* measurements should comprehensively address contributions from the calibration source and its transfer, the performance of the radiometer and any model applied for data reduction, effects of environmental variability, and field perturbations by the instrument housing and deployment platform.

An uncertainty threshold of 5% was defined originally for satellite-derived $L_{WN}(\lambda)$ in the blue spectral region to restrict to within 35% the uncertainties in chlorophyll-*a* concentrations determined in oligotrophic waters with existing bio-optical algorithms (Gordon and Clark 1981). This 5% uncertainty threshold was then set as the target for $L_{WN}(\lambda)$ for most of the ocean color missions, regardless of the wavelength. The maximum uncertainty values given for $L_{WN}(\lambda)$ unavoidably prompted the need for uncertainties better than 5% for *in situ* optical radiometry data. This implied the need to constrain individual sources of uncertainty of *in situ* radiometry data to within the ideal threshold of 1%, which is commonly referred to as *1% radiometry* (McClain *et al.* 2004).

Table 1.1, which is populated using accessible information from various literature sources, provides a basic example of uncertainty budget produced for $L_{WN}(\lambda)$ data determined from a specific multispectral free-fall profiler. Neglecting uncertainty contributions due to instrumental performance such as temperature dependence, non-linearity, stray light, polarization sensitivity, all assumed marginal for the considered multispectral radiometer system, and also ignoring avoidable contributions to instrument deployment such as tilt assuming these are minimized by an aggressive filtering of data, the table summarizes spectral contributions at the 443, 555, and 665 nm center-wavelengths as resulting from:

1. Uncertainty of the absolute calibration of the L_u sensor accounting for specific contributions from an FEL lamp irradiance standard, reflectance plaque, and mechanical positioning of the various components (Hooker *et al.* 2002)
2. Uncertainty due to the experimental determination of the immersion factor of radiance sensors (Zibordi 2006)

3. Uncertainty of the correction factors applied for removing self-shading perturbations computed as 25% of the corrections applied to a specific commercial radiometer with 5 cm diameter and 1 cm aperture (the 25% value is heuristically selected to amply account for differences between computations and actual measurement errors (see Zibordi and Ferrari 1995))
4. Uncertainty of the absolute calibration of the E_s sensor accounting for contributions from an FEL lamp irradiance standard, and positioning of the various optics and mechanics components (Hooker *et al.* 2002)
5. Uncertainty of the corrections applied for the non-cosine response of the E_s collectors as resulting from maximum difference with respect to theoretical correction values performed with highly accurate radiative transfer simulations (Zibordi and Bulgarelli 2007)
6. Uncertainty in the application of bidirectional corrections computed as 25% of the applied corrections (in this case the 25% value is arbitrarily selected to tentatively account for errors affecting corrections (Talone *et al.* 2018))
7. Uncertainty in the determination of the value of E_0 as resulting from an uncertainty of ±1 nm in the center wavelength of a rectangular 10 nm spectral response function (this contribution could be accurately determined using the actual spectral bands of the radiometer)
8. Uncertainty in the extrapolation of sub-surface values due to wave perturbations and uncertainties due to changes in illumination and seawater optical properties during profiling (excluding contributions due to inelastic scattering addressed in Chapter 4 on *In-water Radiometry Measurements and Data Analysis*), cumulatively quantified as the average of the variation coefficients of $L_{WN}(\lambda)$ from a number of replicate measurements (Zibordi *et al.* 2004).

The estimated values provided in Table 1.1, quantified through the quadrature sum of all individual contributions assuming that each one is independent of the others, are in the range from 4 to 5% in the selected spectral bands. For this specific example, it is emphasized that the uncertainty values provided for absolute calibration are likely overestimated. Additionally, the proposed uncertainty analysis assumes fully independent calibrations of E_d and L_u sensors (*i.e.*, as obtained with different lamps and laboratory set-ups). The use of the same calibration lamp and set-up would lead to a reduction of approximately 1% of the quadrature sum of spectral uncertainties for $L_{WN}(\lambda)$, explained by correlations between absolute calibration uncertainties of $E_d(\lambda)$ and $L_u(\lambda)$ (Zibordi and Voss 2014, Johnson *et al.* 2014).

Table 1.1: Uncertainty budget (in percent) for $L_{wn}(\lambda)$ determined from in-water profile data

Uncertainty Source	**443 nm**	**555 nm**	**665 nm**
Absolute calibration of L_u	2.7	2.7	2.7
Immersion factor	0.2	0.2	0.2
Self-shading correction	0.5	0.3	1.3
Absolute calibration of E_s	2.3	2.3	2.3
Cosine response correction	0.5	0.5	0.5
Anisotropy correction	0.4	0.9	0.5
E_0 determination	1.9	0.8	0.2
Environmental effects	2.1	2.2	3.2
Quadrature sum	**4.6**	**4.4**	**5.0**

6. FUTURE DIRECTIONS

Future research and development activities should specifically address corrections for bidirectional effects and their uncertainties, both theoretically and experimentally. In this respect, uncertainties are a key element that should be further studied to produce a number of comprehensive examples covering the main measurement protocols and instruments.

REFERENCES

Gershun A., 1939: The light field. *Studies in Applied Mathematics*, 18(1-4), 51-151.

Gleason A.C., Voss K.J., Gordon H.R., Twardowski M., Sullivan J., Trees C., Weidemann A., Berthon J.-F., Clark D.K. and Lee Z.P., 2012: Detailed validation of the bidirectional effect in various Case I and Case II waters. *Optics Express*, 20(7), 7630-7645.

Gordon H.R. and Clark D.K., 1981: Clear water radiances for atmospheric correction of coastal zone color scanner imagery. *Applied Optics*, 20 (24), 4175-4180.

Gordon H.R., Clark D.K., Brown J.W., Brown O.B., Evans R.H. and Broenkow W.W., 1983: Phytoplankton pigment concentrations in the Middle Atlantic Bight: comparison of ship determinations and CZCS estimates. *Applied Optics*, 22(1), 20-36.

Hooker S.B., McLean S., Sherman J., Small M., Lazin G., Zibordi G. and Brown J.W., 2002: The Seventh SeaWiFS Intercalibration Round-Robin Experiment (SIRREX-7), March 1999. *NASA Tech. Memo. 2002-206892, Vol. 17*. Hooker S.B. and Firestone E.R., Eds., NASA Goddard Space Flight Center, Greenbelt, Maryland, 69 pp.

Johnson B.C., Yoon H., Rice J.P. and Parr A.C., 2014: Principles of Optical Radiometry and Measurement Uncertainty. In *Experimental Methods in the Physical Sciences* (*Vol.* 47, pp. 13-67). Academic Press.

Joint Committee for Guides in Metrology (JCGM), *Evaluation of Measurement Data—Guide to the Expression of Uncertainty in Measurement (GUM),* JCGM 100:2008 (2008).

Lee Z.P., Du K., Voss K.J., Zibordi G., Lubac B., Arnone R. and Weidemann A., 2011: An inherent-optical-property-centered approach to correct the angular effects in water-leaving radiance. *Applied Optics*, 50(19), 3155-3167.

McClain C.R., Feldman G.C. and Hooker S.B., 2004: An overview of the SeaWiFS project and strategies for producing a climate research quality global ocean bio-optical time series. *Deep Sea Research Part II: Topical Studies in Oceanography*, 51(1-3), 5-42.

Morel A., Antoine D. and Gentili B., 2002: Bidirectional reflectance of oceanic waters: accounting for Raman emission and varying particle scattering phase function. *Applied Optics*, 41(30), 6289-6306.

Morel A. and Gentili B., 1991: Diffuse reflectance of oceanic waters: its dependence on sun angle as influenced by the molecular scattering contribution. *Applied Optics*, 30(30), 4427-4438.

Mekaoui S. and Zibordi G., 2013: Cosine error for a class of hyperspectral irradiance sensors. *Metrologia*, 50(3), 187-189.

Mueller J.L. and Austin R.W., 1995: Ocean Optics Protocols for SeaWiFS Validation, Revision 1. *NASA Tech. Memo. 104566, Vol. 25*, Hooker S.B., Firestone E.R. and Acker J.G., Eds., NASA Goddard Space Flight Center, Greenbelt, Maryland, 67 pp.

Talone M., Zibordi G. and Lee Z.P., 2018: Correction for the non-nadir viewing geometry of AERONET-OC above water radiometry data: an estimate of uncertainties. *Optics Express*, 26(10), A541-A561.

Tanré D., Herman M., Deschamps P.Y. and De Leffe A., 1979: Atmospheric modeling for space measurements of ground reflectances, including bidirectional properties. *Applied Optics*, 18(21), 3587-3594.

Thuillier G., Hersé M., Foujols T., Peetermans W., Gillotay D., Simon P.C. and Mandel H., 2003: The solar spectral irradiance from 200 to 2400 nm as measured by the SOLSPEC spectrometer from the ATLAS and EURECA missions. *Solar Physics*, 214(1), 1-22.

Zibordi G., 2006: Immersion factor of in-water radiance sensors: assessment for a class of radiometers. *Journal of Atmospheric and Oceanic Technology*, 23(2), 302-313.

Zibordi G. and Bulgarelli B., 2007: Effects of cosine error in irradiance measurements from field ocean color radiometers. *Applied Optics* 46(22), 5529-5538.

Zibordi G., D'Alimonte D. and Berthon J.-F., 2004: An evaluation of depth resolution requirements for optical profiling in coastal waters. *Journal of Atmospheric and Oceanic Technology*, 21(7), 1059-1073.

Zibordi G. and Ferrari G.M., 1995: Instrument self-shading in underwater optical measurements: experimental data. *Applied Optics*, 34(15), 2750-2754.

Zibordi G. and Voss K.J., 2014: In situ optical radiometry in the visible and near infrared. In *Experimental Methods in the Physical Sciences* (*Vol.* 47, pp. 247-304). Academic Press.

Chapter 2: Radiometer Specifications

Kenneth J. Voss[1], James L. Mueller[2] and Giuseppe Zibordi[3]

[1] *University of Miami, Coral Gables, Florida, USA*
[2] *Salinas, California, USA*
[3] *European Commission, Joint Research Centre, Ispra, Italy*

1. INTRODUCTION

This chapter introduces requirements for the radiometric quantities relevant to the validation of data from satellite ocean color sensors, but also relevant to different applications such as bio-optical modeling. The specifications relate to radiometers to be operated on a variety of autonomous or manually operated systems to acquire the *in situ* data needed. These specifications should apply to instruments that exist or that can be developed with current state-of-the-art technology with a view to ensuring the collection of radiometric data with uncertainties that comply with requirements for the assessment of satellite ocean color radiometry data.

The following sections will address specifications for both in-water and above-water instruments. However, the emphasis will be on in-water radiometry, complemented by details relevant to above-water radiometry. In particular, the emphasis is placed on the characteristics of instruments measuring in-water $E_d(z,\lambda)$, $E_u(z,\lambda)$, and $L_u(z,\lambda)$ (*i.e.,* the downward irradiance, the upward irradiance and the upwelling radiance at nadir view, respectively, all measured at depth z and center wavelength λ). Most of the specifications provided for $E_d(z,\lambda)$, nevertheless, also apply to above-water $E_S(\lambda)$ (*i.e.,* the downward irradiance measured above the sea-surface, *i.e.*, ideally at depth 0^+). Similarly, some of the specifications provided for $L_u(z,\lambda)$ apply to measurements of $L_T(\theta,\phi,\lambda)$ and $L_i(\theta',\phi,\lambda)$ from above-water radiometry (*i.e.*, the total radiance from the sea and the sky-radiance measured above-water with relative azimuth ϕ between the instrument and the sun, and viewing angles θ and θ', respectively). Ultimately, the requirements for an above-water ocean color radiometer should ensure that the water-leaving radiance $L_w(\lambda)$ from above-water radiometry exhibits uncertainties comparable to those characterizing in-water measurements of $L_u(z,\lambda)$.

The specifications, leading to requirements, are applicable to multispectral radiometers equipped with interference filters and to hyperspectral radiometers based on dispersive devices (*e.g.*, gratings) or monochromators. Minimum performance characteristics are provided for spectral resolution, radiometric responsivity and resolution, signal-to-noise ratio (SNR), radiometric saturation and minimum detectable values, angular response, linearity, and stability.

2. SPECTRAL AND RADIOMETRIC CHARACTERISTICS

Spectral characteristics

Ideally, field radiometers should provide validation data at the specific satellite bands in the visible spectral range. However, with a few exceptions (*e.g.*, in the case of above-water radiometry over extremely turbid waters), it is recognized that it is difficult to produce reliable *in situ* data beyond 700 nm with current technology and measurement methods.

Measurement of *in situ* radiometric quantities must be performed in spectral bands complying with the characteristics given in Table 2.1 for the nominal bands of current ocean color sensors. Either this presumes performing measurements with filter radiometers matching the spectral bands of the satellite sensors, or alternatively with hyperspectral radiometers having spectral resolution high enough to allow accurate reconstruction of the satellite signal through spectral convolution.

Filter radiometers should ideally have all the satellite spectral bands as defined by center wavelengths and full-width at half-maximum (FWHM) bandwidths. This implies the use of properly blocked interference filters ensuring the required spectral bandpass and out-of-band rejection (ideally 10^{-6} or better of the normalized peak transmittance). Measurement of the out-of-band rejection should be done with a

double monochromator and/or confirmed with cut-on and cut-off filters. Extra care must be taken to avoid possible out-of-band leakage due to fluorescence by the materials constituting the filter or any other optical component.

The center wavelength and bandwidth of filter radiometers should be determined on the assembled instrument. A desirable maximum ±2 nm uncertainty for the center wavelength of a 10 nm FWHM filter installed in an *in situ* radiometer in view of best mirroring the spectral bands of satellite sensors, can be satisfied with filters exhibiting ±1 nm center wavelength uncertainty and 8.5 ± 1 nm FWHM bandwidth. In fact, when filters are installed in a radiometer with a 20^o full-angle FOV, the spectral bandpass is broadened by a few nm (McCluney 2014), and the center wavelength is also shifted. Furthermore, as filters age in use, their transmission curve may undergo changes, including broadening the FWHM bandpass and shifting the peak. Thus, the tolerances indicated above include an allowance for some degradation. In a single instrument system comprising multiple filter radiometers (*e.g.*, measuring $E_s(\lambda)$, $E_d(z,\lambda)$, $E_u(z,\lambda)$, and/or $L_u(z,\lambda)$), it is desirable that all channels at a given nominal wavelength match within 1 nm. This would imply all filters at any nominal center wavelength are from a single manufacturing lot. If this is accomplished, all the radiometric quantities measured with such a system would have a greater likelihood of having matching spectral bands. In any event, the actual spectral response function of each radiometer band should be characterized with a wavelength uncertainty of 0.2 nm.

Table 2.1: Spectral bands of current satellite ocean color sensors (rows are aligned to enable the comparison of overlapping bands). Note that either the validation of radiometric data products or the indirect calibration (*i.e.*, System Vicarious Calibration (SVC)) of the satellite sensor for center wavelengths greater than 700 nm are not generally performed relying on *in situ* radiometry, but rather by satellite measurements over open ocean gyres where the water-leaving radiance can be assumed to be zero.

MODIS bands[1] [nm]	**VIIRS bands**[2] [nm]	**OLCI bands**[3] [nm]
		400 (15)
405–420	402–422	412 (10)
438–448	436–454	442 (10)
483–493	478–498	490 (10)
526–536		510 (10)
546–556	545–565	560 (10)
		620 (10)
662–672	662–682	665 (10)
		709 (10)
743–753	739–754	754 (7.5)
862–877	846–885	865 (20)
		940 (20)
		1020 (40)

1. Moderate Resolution Imaging Spectroradiometer (MODIS).
2. Visible Infrared Imaging Radiometer Suite (VIIRS) onboard the Suomi National-Polar Orbiting Partnership.
3. Ocean Land Colour Instrument (OLCI) specified as nominal center wavelengths and band width (as opposed to the actual values for each of the five cameras composing the satellite optical system).

Hyperspectral radiometers based on dispersive elements with a spectral resolution between 3 and 10 nm and spectral sampling in the range of 1 and 3 nm, are a valuable alternative to filter radiometers and provide high flexibility for a comprehensive validation of data from each visible band of the various satellite ocean color sensors. Hyperspectral radiometers with sub-nanometer spectral resolution are

required for System Vicarious Calibration (SVC) in view of supporting forthcoming satellite sensors exhibiting increased spectral resolution with respect to the current ones (Zibordi *et al.* 2017).

Stray light is a major issue affecting hyperspectral systems. Their characterization requires considerable effort to accurately determine the spectral stray light response distribution function across the spectrometer wavelength range. Stray light should be characterized and minimized with maximum residuals after correction for this effect, below 1% in each band across the full spectral range.

Table 2.2 summarizes recommended specifications for hyperspectral radiometers applicable for validation activities. Requirements for SVC are significantly higher.

Table 2.2: Recommended specifications for hyperspectral radiometers applied for validation activities.

Optical Sensors	
Spectral Range	380 to 900 nm (an extension in the ultraviolet is desirable)
Spectral Resolution	3-10 nm (FWHM)
Spectral Sampling	1-3 nm (or at least 2 times the spectral resolution)
Wavelength Accuracy	10% FWHM resolution
Wavelength Stability	5% FWHM of resolution
Signal-to-Noise Ratio	1000:1 (at minimum)
Stray Light Rejection	10^{-5} (of the maximum radiometric signal at each spectral band)
FOV Maximum (full-angle)	5°, 20° (for above-water and in-water, respectively)
Temperature Stability	Specified for the range from 0 °C to 45 °C
Linearity	Correctable to 0.1%

Responsivity, signal-to-noise ratio, and resolution

The expected operating limits for radiometric responsivities, signal-to-noise ratio (SNR), and digital resolution are specified in Table 2.3 as resulting from the following assumptions and requirements.

1. An $E_d(z,\lambda)$ and $E_s(\lambda)$ saturation value of 300 μW cm^{-2} nm^{-1} is tentatively required at all wavelengths, assuming a typical collector diameter of 25 mm or greater. For radiometers with fixed acquisition time on the order of milliseconds, this large saturation value is required to properly deal with in-water downward intense wave-focusing events (Zaneveld *et al.* 2001). These events are averaged out in the case of longer integration times. Smaller collectors would require a higher saturation value (Darecki *et al.* 2011).

2. The minimum required $E_s(\lambda)$ is 20 μW cm^{-2} nm^{-1}. It is considered not appropriate to perform validation measurements when illumination is less than this threshold.

3. The minimum $E_s(\lambda)$ implies a minimum detectable $E_d(z,\lambda)$ value of 1 μW cm^{-2} nm^{-1} at 3 optical depths (*i.e.*, at a depth determined by the ratio 3 over the diffuse attenuation coefficient $K_d(\lambda)$ from the $E_d(z,\lambda)$ values of the sub-surface layer (see Chapter 4 on *In-Water Radiometry Measurements and Data Analysis*)).

4. Digital resolution must be less than or equal to 0.5% of the reading to maintain a very minimum 100:1 SNR. To permit an ideal target of 1% uncertainty in absolute calibration with $k = 1$ (likely challenged by the uncertainty affecting 1000 W FEL irradiance standards below 400 nm), the instrument must digitally resolve 0.1% of the irradiance (radiance) produced by the laboratory standards used. The *Calibration Irradiance* and *Calibration Radiance*, and related *Digital Resolution (irradiance or radiance cal.)* provided in Table 2.3 are for typical irradiance and radiance values applied during calibrations performed with 1000 W FEL irradiance standard lamps traceable to National Measurement Institutes (NMIs). A SNR of 100:1 requires a resolution in $E_d(z,\lambda)$ at three optical depths to within 0.005 μW cm^{-2} nm^{-1} per count. At the surface, $E_d(0^-, \lambda)$ or $E_s(\lambda)$ should be resolved to within 0.05 μW cm^{-2} nm^{-1} per count.

Table 2.3: Required sensitivities for satellite validation as a function of the radiometric measured variable and sample wavelength (after Mueller *et al.* 2003).

Quantity	Variable	410 nm	488 nm	665 nm	Description
$E_d(z, \lambda)$	$E_d(0^-, \lambda)_{max}$	300	300	300	Saturation irradiance
	$E_d\left(\frac{3}{K_d}, \lambda\right)$	1	1	1	Minimum expected irradiance
	$\frac{\Delta E}{\Delta N}$	5×10^{-3}	5×10^{-3}	5×10^{-3}	Digital resolution (profiles)
	$\frac{\Delta E}{\Delta N}$	5×10^{-2}	5×10^{-2}	5×10^{-2}	Digital resolution (surface unit)
$E_u(z, \lambda)$	$E_u(0^-, \lambda)_{max}$	120	120	60	Saturation irradiance (Case-2 / coccoliths)
	$E_u(0^-, \lambda)_{max}$	37	22	1.5	Saturation irradiance (Case-1)
	$E_u\left(\frac{3}{K_d}, \lambda\right)$	1×10^{-2}	2×10^{-2}	1.5×10^{-3}	Minimum expected irradiance
	$\frac{\Delta E}{\Delta N}$	$5\ 10^{-5}$	$1\ 10^{-4}$	$7.5\ 10^{-6}$	Digital resolution (profiles)
	$\frac{\Delta E}{\Delta N}$	1×10^{-3}	2×10^{-3}	1.5×10^{-4}	Digital resolution (surface unit)
$L_u(z, \lambda)$	$L_u(0^-, \lambda)$	38	38	13	Saturation radiance (Case-2 / coccoliths)
	$L_u(0^-, \lambda)$	12.0	7.2	0.5	Saturation radiance (Case-1)
	$L_u\left(\frac{3}{K_d}, \lambda\right)$	2×10^{-3}	4×10^{-3}	2.25×10^{-4}	Minimum expected radiance
	$\frac{\Delta L}{\Delta N}$	$1\ 10^{-5}$	$2\ 10^{-5}$	$1\ 10^{-6}$	Digital resolution (profiles)
	$\frac{\Delta L}{\Delta N}$	2×10^{-4}	4×10^{-4}	2×10^{-5}	Digital resolution (surface unit)
$E_{cal}(\lambda)$	E_{cal}	2	5	15	Calibration irradiance
	$\frac{\Delta E}{\Delta N}$	2×10^{-3}	5×10^{-3}	1×10^{-2}	Digital resolution (E_d, E_s, E_u cal.)
$L_{cal}(\lambda)$	L_{cal}	0.6	1.5	4.5	Calibration radiance
	$\frac{\Delta L}{\Delta N}$	6×10^{-4}	1×10^{-3}	4×10^{-3}	Digital resolution (L_u cal.)

Notes: 1. E_u and E_d are in units of $\mu W\ cm^{-2}\ nm^{-1}$, while L_u is in units of $\mu W\ cm^{-2}\ nm^{-1}\ sr^{-1}$.

2. Responsivity resolution in radiometric units per digital count at the minimum required signal level.

3. ΔN indicates the change in digital counts corresponding to a change in radiance ΔL or irradiance ΔE.

4. Specified ranges should maintain a 100:1 SNR.

5. The saturation values of $E_u(0^-,\lambda)$ are estimated for the maximum reflectance expected in ordinary Case-1 waters: 12.5% at 410 nm, 7.5% at 488 nm, and 0.5% at 670 nm (Mueller and Austin 1992). These saturation values are too low for measurements in Case-2 waters, or coccolithophorid blooms. In these conditions, a maximum expected reflectance of 40% for $\lambda < 660$ nm and 20% for $\lambda \geq 660$ nm is assumed. This implies that the expected maximum irradiance in $E_u(0^-,\lambda)$ should be 120 $\mu W\ cm^{-2}\ nm^{-1}$ for $\lambda < 660$ nm and 60 $\mu W\ cm^{-2}\ nm^{-1}$ for $\lambda \geq 660$ nm.

6. The minimum required irradiance at three optical depths assumes a minimum reflectance of 1% at 410 nm, 2% at 488 nm, and 0.15% at 670 nm.

7. The saturation and minimum radiances, and the related radiance responsivity resolutions for $L_u(0^-,\lambda)$ and $L_u(3/K_d,\lambda)$ are calculated as $L_u = E_u \cdot Q^{-1}$ accounting for the corresponding specification for $E_u(0^-,\lambda)$ or $E_u(z,\lambda)$. Mueller and Austin (1995) assumed $Q = 5\ sr^{-1}$, constant at all wavelengths and depths. Morel and Gentili (1996) showed that Q actually varies between approximately 3.14 sr^{-1} and 5 sr^{-1} at 410 nm and 488 nm, and between approximately 3.14 sr^{-1} and 5.7 sr^{-1} at 670 nm in Case-1 waters. Saturation radiances, for the extreme minimum case of Q = 3.14 sr^{-1} (very clear waters with the sun nearly overhead), are increased by a factor of 1.6 at all three wavelengths relative to Mueller and Austin (1995). For the extreme maximum case of Q = 5.7 sr^{-1} (waters exhibiting high chlorophyll-*a* concentration and solar zenith angle $\theta_0 > 60^o$), minimum radiances at 670 nm are decreased by a factor of 0.75, which implies a corresponding change of the digital resolution at 670 nm. Minimum expected radiances and required digital resolution at 410 nm and 488 nm are unchanged with respect to Mueller and Austin (1995).

The specifications in Table 2.3 are intended as guidance for the implementation and handling of the following performance requirements:

i. The instrument must maintain at least a 100:1 SNR at every operating range encountered during field measurements.

ii. The data for measurements obtained in the field must be recorded with a digital resolution less than or equal to 0.5% of the reading.

iii. The dynamic range of the instrument must cover the signal levels encountered during laboratory calibrations, and the calibration signals must be recorded with a digital resolution of at least 0.1% of reading to permit to support the 1% ideal target uncertainty in calibration.

By recalling that the above requirements have been drawn for *in situ* sensors designed to operate in the visible spectral region beyond 400 nm, the performance specifications do not create engineering challenges, with the possible exception of the full dynamic range implied by Case-2 or coccolith saturation radiance at $L_u(z,665)$ to minimum expected value in oligotrophic waters. In any event, this requires specially designed radiometers (see also the section on *Red and near-infrared wavelengths*). In fact, every radiometer used for satellite ocean color sensor validation does not need to operate over the full dynamic ranges given in Table 2.3. A radiometer is only required to maintain the above performance specifications over the dynamic ranges of irradiance and radiance existing at locations and associated illumination conditions where it is operated.

Finally, it is recognized that future satellite radiometers such as the Plankton, Aerosol, Cloud, ocean Ecosystem (PACE) would have bands in the ultraviolet (UV) spectral region below 400 nm. The validation of data products from such a sensor would entail *in situ* radiometric measurements in the UV. This would require new efforts to overcome technological challenges associated with the low response of silicon detectors commonly applied for *in situ* ocean color measurements and also the low flux of FEL lamp irradiance standards limiting the calibration accuracy.

Red and near-infrared bands

The fact that red and near-infrared bands between approximately 700 nm and 900 nm have such short attenuation lengths in water requires that special attention be paid to measurements. In fact, instrument self-shading (Gordon and Ding 1992) and very large attenuation of $L_u(z,\lambda)$ make radiometers with large

diameter and large system packages, ill-suited for these measurements. Additionally, $L_w(\lambda)$ from above-water radiometry is primarily affected by uncertainties due to sky-glint correction. Thus, fiber optic probes carrying light back to a remote instrument (Yarbrough, *et al.* 2007), or very small single-wavelength discrete instruments, both combined with small floating platforms, are likely the sole alternative to allow extending radiometric measurements in the near-infrared. Still, care must be taken to avoid direct shading by the deployment platform, even though at these wavelengths the high attenuation coefficient of water makes any shadowing by objects more than a few meters away irrelevant.

Ideally, the minimum measurement scheme should include two discrete (*e.g.*, 10 nm FWHM) channels at 780 nm and 875 nm. Obviously, when in-water measurements are performed at these bands, the $E_s(\lambda)$ sensor should also include the same bands. Because of their importance in the atmospheric correction algorithms, these measurements should be performed in cases of extremely turbid waters or in coccolithophorid blooms. It is anticipated that in the majority of cases, and particularly in Case-1 waters, these measurements would show negligible upwelling light.

3. ADDITIONAL CHARACTERISTICS

Polarization sensitivity

Radiometers may exhibit sensitivity to polarization. In particular, polarization sensitivity is likely to affect any radiometer having mirrors, prisms, or gratings in its optical path. However, the problem is generally of relevance only for radiance measurements because diffusers, constituting the fore optics of irradiance sensors, act as depolarizers. For radiance measurements, the polarization sensitivity must be decreased to values of less than 1% in all bands by depolarizing the aperture radiance either through fiber optics or a *pseudo-depolarizer*. Obviously, an exception is provided by those radiometers designed to actually measure the polarization components of the radiance (*e.g.*, Fougnie *et al.* 1999).

Linearity and short-term stability

The combined uncertainties attributable to linearity and stability should be well below 0.5% of the instrumental readings over the dynamic ranges specified in Table 2.2, although the actual dynamic range required is significantly lower. This is a challenging goal, but one of those that must be met if the equally challenging goal of achieving the ideal target of 1% uncertainty in absolute radiometric calibration is to be meaningful.

Angular response

Irradiance: The response of a *cosine collector* to a collimated light source incident at an angle θ from the normal must be such that:

i. for $E_u(z,\lambda)$ measurements the integrated response to a radiance distribution of the form $L(\lambda,\theta) \propto 1+4\sin\theta$ (*i.e.,* an idealized radiance distribution for the in-water upward light field) should vary as $\cos\theta$, within 2%;
ii. for $E_d(z,\lambda)$ measurements, the response in-water to a collimated source should vary as $\cos\theta$ within 2% for angles $0 \le \theta \le 65°$ and 10% for angles $65° < \theta < 90°$; and
iii. for $E_s(\lambda)$ measurements the response in air to a collimated source should vary as $\cos\theta$ within 1% for $0 \le \theta \le 65°$, and within 5% for $65° < \theta < 90°$.

It is recalled that departures from $\cos\theta$ translate directly to approximately equal errors in $E_s(\lambda)$ or near-surface $E_d(z,\lambda)$ in the case of direct sunlight.

It is recognized that the above cosine response requirements are very demanding. Because of this, in the case of collectors exhibiting some deviation from the above thresholds, the application of correction schemes supported by radiative transfer simulations should be applied to satisfy uncertainty requirements (see Chapter 3 on *Calibration and Characterization of Optical Radiometers*).

Radiance: The in-water full-angle FOV for the upwelling radiance bands should be smaller than 20^o. The resulting solid angle FOV (approximately 0.1 sr) is large enough to provide reasonable levels of flux

using silicon detectors, yet small enough to be unaffected by the small angular variations characterizing the upwelling radiance at nadir. Smaller FOV sensors are appropriate, of course, if all of the other performance specifications are satisfied.

The full-angle FOV of above-water radiometers applied for $L_T(\theta,\phi,\lambda)$ and $L_i(\theta',\phi,\lambda)$ measurements should tentatively be lower than 5^o, and all bands must be co-registered to within a high portion of the FOV.

Operating depths and accuracy

Instruments used for profiling in clear to moderately turbid waters shall be capable of operating to several tens of meters depth. Instruments used for profiling in very turbid waters require a much lower maximum pressure rating.

The accuracy required for depth measurements can be determined by relating it to the uncertainty induced in propagating the measurement to the surface. With a desired target of 1%, the upper level of the required measurement accuracy is given by $\ln(1.01)/K_{\Im}(\lambda)$, where $K_{\Im}(\lambda)$ is the diffuse attenuation coefficient for the specific radiometric quantity $\Im(z,\lambda)$ (*e.g.*, $E_d(z,\lambda)$). For example, in clear water, in the blue bands where $K_{\Im}(\lambda)$ may reach values as low as 0.03 m^{-1}, this requirement is not stringent. In fact, it leads to an uncertainty on the order of 0.3 m. For more turbid waters, or in the red bands, were $K_{\Im}(\lambda)$ can be on the order of 0.5 m^{-1}, the required uncertainty is much more stringent and approaches 0.02 m. Thus, a target uncertainty of 0.01 m in depth values would tentatively satisfy extrapolation requirements across the whole visible spectrum for most water types.

Instrument attitude

The orientation of the instrument with respect to the vertical should be well within 5° and the attitude shall be measured with orthogonally oriented sensors from 0° to 30° with an uncertainty better than 0.5°. It is not intended that, in the case of in-water systems, this uncertainty is maintained while the instrument is subject to large accelerations induced by surface waves. In the case of above-water radiometers, $L_T(\theta,\phi,\lambda)$ and $L_i(\theta',\phi,\lambda)$ should be measured with tilts limits not exceeding 2° and 5°, respectively.

Due to the high accuracy requirements of derived radiometric data products, ideally, only $E_s(\lambda)$ measurements exhibiting tilt within 1° should be retained for successive processing. In fact, as a first approximation (*i.e.*, by neglecting the diffuse component of the total downward irradiance), a 1° tilt may lead up to 1% uncertainty in $E_s(\lambda)$ for a sun zenith angle $\theta_0 = 30°$ and up to 3% with $\theta_0 = 60°$.

Time response

The time response of the instrument to a full-scale step change (saturation to dark) in irradiance or radiance, should be less than one second to arrive at a value within 0.1%, or one digitizing step, whichever is greater, of steady-state. In addition, the electronic *e*-folding time constant of the instrument must be consistent with the rate at which the channels are sampled, *i.e.*, if data are to be acquired at 10 Hz, the *e*-folding time constant should be 0.2 s to avoid aliasing.

Temperature sensitivity

An important criteria in the instrument design should be to minimize any sensitivity to changes in ambient temperature. An in-water instrument can experience temperatures ranging from tentatively 0 °C to 35 °C, while an instrument operated in air may work over an expanded range of at least 0 °C to 45 °C. Sensors with temperature coefficients greater than 0.01% per °C should be characterized and a correction applied to the data to constrain residual temperature dependence below 0.01% per °C.

Dark-signal

At the low end of the responsivity range, sensor dark current and electronic offsets (contributing to the dark-signal) can become important. Thus, it is required that these be characterized to allow their removal from the measured signals. As these are often temperature dependent, one must use the appropriate

dark-signal value when doing this correction. The residual of this correction must allow the lower end of the responsivity to satisfy the required SNR.

4. FUTURE DIRECTIONS

Attention should be given to requirements and specifications for measurements in the ultraviolet bands incorporated in forthcoming ocean color missions. Additionally, requirements for polarized radiometers should be considered. Finally, because of the increasing use of hyperspectral systems for both above- and in-water measurements, more detailed specifications should be determined accounting for spectral response differences of silicon detector arrays across the visible spectral region in combination with the expected spectral shape of the radiance/irradiance to be measured.

REFERENCES

Darecki M., Stramski D. and Sokolski M., 2011: Measurements of high-frequency light fluctuations induced by sea surface waves with an Underwater Porcupine Radiometer System. *Journal of Geophysical Research* 116(C7), doi: 10.1029/2011JC007338.

Fougnie B., Frouin R., Lecomte P. and Deschamps P.Y., 1999: Reduction of skylight reflection effects in the above-water measurement of diffuse marine reflectance. *Applied Optics*, 38(18), 3844-3856.

Gordon H.R. and Ding K., 1992: Self shading of in-water optical instruments. *Limnology and Oceanography* 37, 491-500.

McCluney W.R., 2014: *Introduction to radiometry and photometry*. Artech House, London, 461 pp.

Morel A. and Gentili B., 1996: Diffuse reflectance of oceanic waters. III. Implication of bidirectionality for the remote-sensing problem. *Applied Optics*, 35(24), 4850-4862.

Mueller J.L. and Austin R.W., 1995: Ocean Optics Protocols for SeaWiFS Validation, Revision 1. *NASA Tech. Memo. 104566, Vol. 25,* Hooker S.B. and Firestone E.R., Eds., NASA Goddard Space Flight Center, Greenbelt, Maryland, 66 pp.

Mueller J.L., Pietras C., Hooker S.B., Austin R.W., Miller M., Knobelspiesse K.D., Frouin R., Holben B.N. and Voss K.J., 2003: Ocean Optics Protocols for Satellite Ocean Color Sensor Validation, Revision 4, Volume II: Instrument Specifications, Characterization and Calibration. *NASA/TM-2003-21621/Rev-Vol II*. Mueller J.L., Fargion G.S. and McClain C.R., Eds., NASA Goddard Space Flight Center, Greenbelt, Maryland, 63 pp.

Yarbrough M.A., Feinholz M.E., Flora S., Houlihan T., Johnson B.C., Kim Y.S., Murphy M.Y., Ondrusek M. and Clark D.K., 2007: Results in coastal waters with high resolution in-situ spectral radiometery: The Marine Optical System ROV. Proceedings Vol 6680, *Coastal Ocean Remote Sensing, SPIE, 668001*, doi: 10.117/12.735064.

Zaneveld J.R.V., Boss E. and Barnard A., 2001: Influence of surface waves on measured and modeled irradiance profiles. *Applied Optics* 40(9), 1442-1449.

Zibordi G., Talone M., Voss K.J. and Johnson B.C., 2017: Impact of spectral resolution of in situ ocean color radiometric data in satellite matchup analysis. *Optics Express*, 25(16) A798-A812.

Chapter 3: Calibration and Characterization of Optical Radiometers

Giuseppe Zibordi[1], Kenneth J. Voss[2], B. Carol Johnson[3] and James L. Mueller[4]

[1] *European Commission, Joint Research Centre, Ispra, Italy*
[2] *University of Miami, Coral Gables, Florida, USA*
[3] *National Institute of Standards and Technology, Gaithersburg, Maryland, USA*
[4] *Salinas, California, USA*

1. INTRODUCTION

Procedures for calibrating and characterizing optical radiometers, including the determination of characteristics peculiar to underwater sensors, are presented in this chapter. These calibrations and characterizations are essential to ensure compliance with specifications of those radiometers used to acquire field data for satellite ocean color validation. The calibrations and characterizations required are:

1. Spectral radiometric responsivity (*i.e.*, absolute response) traceable to National Measurement Institutes (NMI) standards
2. Spectral response functions (*i.e.*, bandpass) of the various radiometer bands
3. Out-of-band response and stray light perturbations
4. Responsivity change with the refractive index of the medium in which the radiometer operates
5. Angular response, in either air or water, depending on the medium in which the radiometer operates
6. Linearity of response
7. Integration time response
8. Temperature response
9. Polarization sensitivity
10. Sensitivity decay
11. Dark-signal
12. Temporal response
13. Pressure effects

Any field instrument providing suitable data for satellite validation should have a traceable history of calibrations and characterizations. In particular, spectral radiometric responsivity should be determined before and after each major field deployment. Conversely, certain characteristics—such as the angular response—need be determined only once (unless the instrument is modified). Further, among the different characterizations, some should be performed for each individual instrument, such as the determination of the immersion factor of irradiance sensors. Others, such as linearity response, may be confidently applied for each class of radiometers (*i.e.*, those made of identical components for which specific optical characteristics were proven to exhibit equivalent features within a given uncertainty). Table 3.1 summarizes instrument-specific calibrations and characterizations to be performed regularly (regular), occasionally (occasional) and tentatively once (initial), and those not strictly instrument-specific, which can rely on characterizations performed for radiometers of the same class (class-based).

2. RADIOMETRIC RESPONSIVITY

The determination of the absolute radiometric response (*i.e.*, responsivity) of irradiance and radiance sensors requires the availability of a properly furnished and staffed calibration facility. Such a facility must be equipped with suitable stable sources, *e.g.*, lamp standards of spectral irradiance calibrated by NMIs. The facility must also have a variety of specialized radiometric and electronic equipment, including reflectance plaques, spectral filters, integrating spheres, and highly regulated power supplies for the

operation of lamps. Precision electronic measurement capabilities are also needed, both for setting and monitoring lamp current and voltage.

Instrument manufacturers and a few research laboratories are equipped and staffed to perform these calibrations for the ocean color research community. These facilities should perform frequent intercomparisons to ensure the maintenance of the radiometric traceability to NMI standards. An ambitious goal is to perform calibrations from 350 nm to 900 nm with 1% target uncertainty (k = 1) for irradiance and slightly higher for radiance.

Table 3.1. Basic requirements on the type and occurrence of calibrations and main characterizations of field radiometers supporting ocean color validation activities.

	Regular	**Occasional**	**Initial**	**Class-based**
Radiometric responsivity	X			
Spectral response		X		
Out-of-band & stray light		X		
Immersion factor (irradiance)			X	
Immersion factor (radiance)				X
Angular response			X	
Linearity				X
Integration time				X
Temperature response				X
Polarization sensitivity				X
Dark-signal	X			
Temporal response				X
Pressure effects				X

The main standards used for irradiance responsivity are FEL lamps[1] exhibiting assigned scales of spectral irradiance that have been transferred directly, or indirectly via secondary standards, from the scales of radiometric standards maintained by NMIs. The spectral irradiance scales of the FEL lamps are in turn transferred to spectral radiance scales using plaques of known bidirectional reflectance, or integrating spheres, or both.

The SeaWiFS (Sea-Viewing Wide Field-of-View Sensor) Project Office initiated a series of SeaWiFS Intercalibration Round-Robin Experiments (SIRREXs) to assure internal consistency between the laboratories calibrating radiometers for SeaWiFS validation (Mueller 1993 and Mueller *et al.* 1994). The outcome from SIRREX-3 (Mueller *et al.* 1996) and SIRREX-4 (Johnson *et al.* 1996), showed that with properly maintained FEL lamp secondary and working standards, thorough training of laboratory

[1] FEL is an American National Standards Institute (ANSI) lamp type code. The 1000 W FEL lamps used for spectral irradiance calibration are modified by welding on a special base, which has much larger terminals than are provided with the stock commercial bulbs (Walker *et al.* 1987). Following this modification, the spectral irradiance output of each lamp is scanned with a high-resolution double monochromator, to assure that its spectrum is smooth and free from unwanted emission lines. Finally, the candidate calibration source lamp is "seasoned" by burning it initially for approximately 24-hours using a highly regulated current source; its spectral irradiance output and lamp terminal voltage are monitored carefully. Lamps that do not achieve stable performance during the seasoning process are discarded. Several commercial vendors offer both seasoned FEL lamps as well as seasoned lamps with a certified scale of spectral irradiance transferred from another FEL secondary standard lamp acquired directly from the appropriate NMI.

personnel, and careful attention to measurement setups, it is possible to maintain an uncertainty level below 2% for spectral irradiance and 3% for spectral radiance calibrations. Successive, round-robin comparisons of calibration coefficients determined for a reference set of field instruments were implemented to benchmark the internal consistency of calibrations performed at various labs. In particular, SIRREX-6 showed a level of relative uncertainty of approximately 2% across the involved laboratories (Riley and Bailey, 1998). Following this work, a new series of round-robin comparisons called SIMBIOS Radiometric Intercomparison (SIMRIC) based on a transfer radiometer (*i.e.*, the SeaWiFS Transfer Radiometer (SXR); Johnson *et al.* (1998)) directly calibrated by the National Institute of Standards and Technology (NIST), were used to verify the radiance scales of the calibration sources at the various laboratories (Meister *et al.* 2002). Results showed that laboratory and SXR scales agreed within approximately 2% for most spectral bands considered (Meister *et al.* 2002).

The above results clearly indicate that some common calibration traceability must exist. In particular, multiple facilities (*e.g.*, instrument manufacturers, and some research labs or government institutions) should make their standards and protocols directly traceable to NMI scales (Johnson *et al.* 1996). As an example, Fig. 1 shows the schematic of such an organizational structure established within the framework of the SIMBIOS Project.

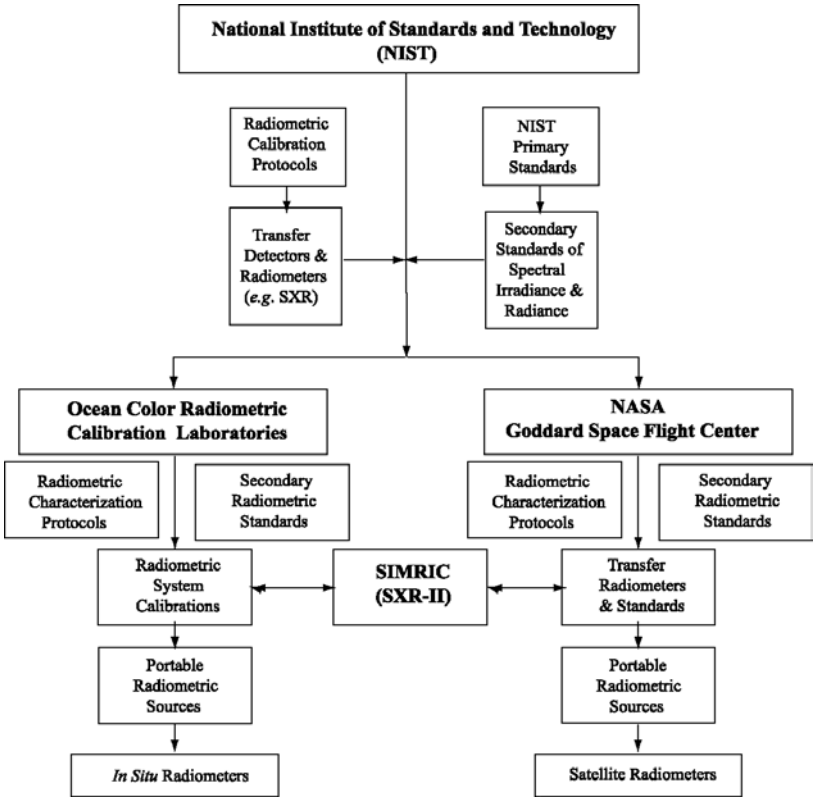

Figure 3.1: The organizational structure for radiometer characterization and calibration established by the ocean color research community within the framework of the SIMBIOS Project.

Spectral Irradiance Calibration

Radiometric calibrations of irradiance sensors can be performed after ascertaining conformity of the sensor angular response to the required cosine function, sensor linearity, spectral sensitivity, and also satisfactory out-of-band blocking or low stray light perturbations.

As already mentioned, radiometric calibrations mostly rely on FEL lamp standards of spectral irradiance. These lamps can be provided by NMIs (*e.g.*, NIST, NPL, PTB) as secondary standards with NMI-traceable spectral irradiance scales. Alternatively, they are available as working standards (*i.e.*, with

calibrations traceable to a secondary standard) from various commercial laboratories and manufacturers. The expanded combined uncertainty (corresponding to a coverage factor $k = 2$ indicating a 95% confidence level) of a NIST-issued secondary standard FEL is approximately 1.7% in the ultraviolet and varies from 0.8% to 0.5% in the visible and near-infrared (Yoon and Gibson 2011).

NIST has delivered guidelines for the setup, alignment, and use of FEL lamp standards (Walker *et al.* 1987). Vendors who manufacture and calibrate these lamps have issued additional user guidelines. The irradiance calibration procedure (Walker *et al.* 1987; Johnson *et al.* 1996) is summarized as follows:

a) The irradiance sensor and a suitable fixture for the FEL lamp are mounted on an optical bench (see Fig. 3.2). The lamp space must be appropriately baffled and draped so that occulting the direct path between lamp and sensor results in a response of less than 0.1% of the unocculted signal. Best practice suggests the lamp and sensor are operated in separate spaces (*e.g.*, rooms) with a variable-sized aperture to confine the lamp flux near the edges of the irradiance collector. The size of the aperture, however, should be large enough to prevent diffractive fringes affecting the irradiance collection area. Curtains and partitions offer an alternative solution to baffle the light source. Regardless of how the baffling is accomplished, the most critical aspect is to eliminate on-axis reflections, *e.g.*, as might result from a flat surface directly behind the lamp and perpendicular to the optical axis (Walker *et al.* 1987). The alignment reference target for FEL lamps, *i.e.*, an alignment jig made of a window with crosshairs etched to mark the location of the lamp filament, is mounted in the lamp holder (see Walker *et al.* (1987) for mechanical specifications).

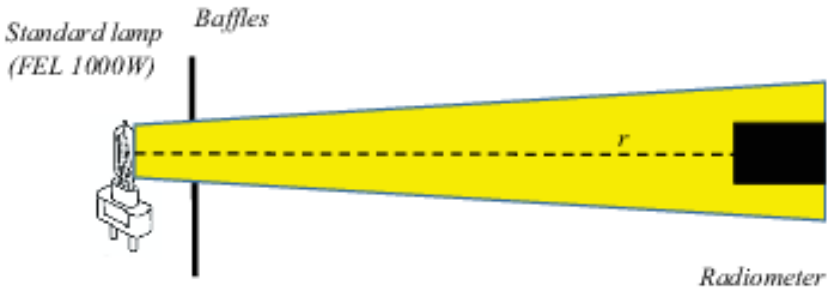

Figure 3.2: A diagram illustrating the principle for absolute irradiance calibrations.

b) An alignment laser beam is directed normal to the target window. The alignment is achieved when the retro-reflection from the window is directed back on the laser aperture.

c) The sensor is mounted on the optical bench with the irradiance collector centered on the alignment laser beam, which marks the optical axis. The collector is aligned normal to the beam using a mirror or a microscope slide held flat against the collector to reflect the beam back through the lamp target crosshairs to the laser aperture.

d) The distance r along the optical path between the collector surface and the terminal posts of the lamp alignment jig is accurately measured (ideally with an electronic ruler). The standard reference distance for all NMI traceable FEL lamp scales of spectral irradiance is $r = 50.0$ cm, measured to the front of the FEL terminal posts.

e) The FEL lamp spectral irradiance standard is inserted into the lamp-holder with its identification tag facing away from the sensor. The lamp terminals are connected to a current-regulated, direct current power supply, with careful attention to ensure proper polarity (as marked on the lamp). The power supply is turned on and ramped-up to the proper current for the particular lamp (as specified within the lamp calibration certificate). A shunt and a voltmeter with an appropriate number of digits should be used to monitor the lamp current to the nearest 0.001 A. Following a 15 min to 30 min warmup, irradiance calibration measurements can be taken. It is emphasized that any deviation from the nominal value of the lamp current would become the source of spectrally dependent biases. The voltage present across the lamp terminals should be measured at frequent intervals during each

calibration run and compared to the voltage measured when the lamp was calibrated (as detailed in the calibration certificate). A significant change in the lamp operating voltage at the specified current indicates that the irradiance output of the lamp has probably changed and that the lamp is no longer usable as a standard of spectral irradiance. It is anticipated that on completion of the calibration session, the lamp current should be ramped down to avoid thermally shocking the filament.

f) An occulting device (*e.g.*, a rod) is placed to obstruct the direct optical path between lamp and collector, then the sensor response to ambient light $DN_{\text{amb}}(\lambda)$ is recorded in digital counts. This operation can be performed after 5 min to 10 min lamp warmup (*i.e.*, when the lamp stabilizes at nearly its final value). If the ambient signal is appreciably higher than the dark-signal measured with the collector completely covered $DN_{\text{dark}}(\lambda)$, then the baffling of the calibration setup is inadequate and should be improved.

g) The occulting device is removed from the optical path and the irradiance sensor response $DN_{\text{r}}(\lambda)$ is recorded. The sensor irradiance responsivity calibration coefficients $F_{\text{E}}(\lambda)$ generally in units of $\mu\text{W cm}^{-2}\text{nm}^{-1}\text{counts}^{-1}$, are determined for each band identified by the wavelengths λ applying the basic equation

$$F_{\text{E}}(\lambda) = \frac{E_{\text{r}}(\lambda)}{DN_{\text{r}}(\lambda) - DN_{\text{amb}}(\lambda)}. \tag{3.1}$$

h) If the lamp is at the standard distance $r = 50.0$ cm, $E_r(\lambda) = E_{50}(\lambda)$, where $E_{50}(\lambda)$ is the certified NMI traceable scale of spectral irradiance rigorously determined at 50 cm. The spectral irradiance responsivity coefficients can then be applied to *in situ* radiometric measurements $DN(\lambda)$ to compute the related irradiance $E(\lambda)$ as

$$E(\lambda) = F_{\text{E}}(\lambda)\left[DN(\lambda) - DN_{\text{dark}}(\lambda)\right] \tag{3.2}$$

where $DN_{\text{dark}}(\lambda)$ is the radiometer dark-signal as determined in the field with the aperture covered.

i) If the irradiance sensor saturates when it is illuminated by the lamp at the standard distance of 50 cm, it is necessary to reduce the irradiance level by increasing the distance *r*.

j) To a first approximation, the irradiance scale $E_{\text{r}}(\lambda)$ is then determined as

$$E_{\text{r}}(\lambda) = E_{50}(\lambda)\frac{(50 + \Delta f)^2}{(r + \Delta f)^2} \tag{3.3}$$

where Δf is the distance offset between the actual reference plane of the lamp filament and the front plane of the terminal posts. The magnitude of this offset is typically $\Delta f \approx 3$ mm (Biggar 1998) with an ±1 mm uncertainty (Yoon *et al.* 2012), but it may vary appreciably among FEL lamps. The value of Δf can be determined for a particular lamp by measuring the irradiance sensor response with the lamp positioned at 50 cm and additionally at a series of N distances r_n (with $n = 1, \ldots, N$) between 50 cm and, for instance, 300 cm. Assuming that the response of the sensor is linear

$$\frac{DN_n(\lambda) - DN_{\text{amb}}(\lambda)}{DN_{50}(\lambda) - DN_{\text{amb}}(\lambda)} = \frac{(50 + \Delta f)^2}{(r_n + \Delta f)^2}. \tag{3.4}$$

The solution to Eq. 3.4 at each distance r_n and center wavelength λ of each spectral band is

$$\Delta f_{n,\lambda} = \frac{X_{n,\lambda} \cdot r_n - 50}{1 - X_{n,\lambda}} \tag{3.5}$$

where $X_{n,\lambda} \equiv \left\{\left[DN_n(\lambda) - DN_{\text{amb}}(\lambda)\right] / \left[DN_{50}(\lambda) - DN_{\text{amb}}(\lambda)\right]\right\}^{\frac{1}{2}}$.

The filament offset may then be computed as the average of the offsets determined at N distances times the number of bands.

When a diffuser collector is used in addition to the lamp filament offset Δf, the denominator of Eq. 3.4 should also account for the distance offset Δd within the diffuser material representing its reference collection plane (which may vary with wavelength). Further, Eq. 3.4 is only valid for an ideal point sensor and source. Deviation from such an ideal condition would then suggest applying correction models accounting for the equivalent size of lamp and collector aperture (Manninen *et al.* 2008). Thus, accounting for the previous elements

$$E_r(\lambda) = E_{50}(\lambda) \frac{(50 + \Delta f)^2 + r_s^2 + r_d^2}{(r + \Delta f + \Delta d)^2 + r_s^2 + r_d^2} \tag{3.6}$$

where r_s and r_d are the equivalent radii of the source and collector aperture.

Spectral Radiance Calibration

Radiance responsivity calibration requires a uniform and near-Lambertian source of known radiance that fills the sensor FOV. The two procedures that are most frequently used to calibrate ocean color radiance sensors are given below.

1. *Reflectance Plaque Radiance Calibration:* An FEL lamp standard of spectral irradiance is used at a distance r to illuminate a plaque of near-Lambertian reflectance with a known bidirectional reflectance distribution function (BRDF) $f_r(\lambda, \theta_o, \theta)$ calibrated for normal incidence illumination, *i.e.*, $\theta_o = 0$, and a viewing angle $\theta = 45°$. The setup is then identical to that described for *Spectral Irradiance Calibration*, with the reflectance plaque in place of the irradiance collector (see Fig. 3.3).

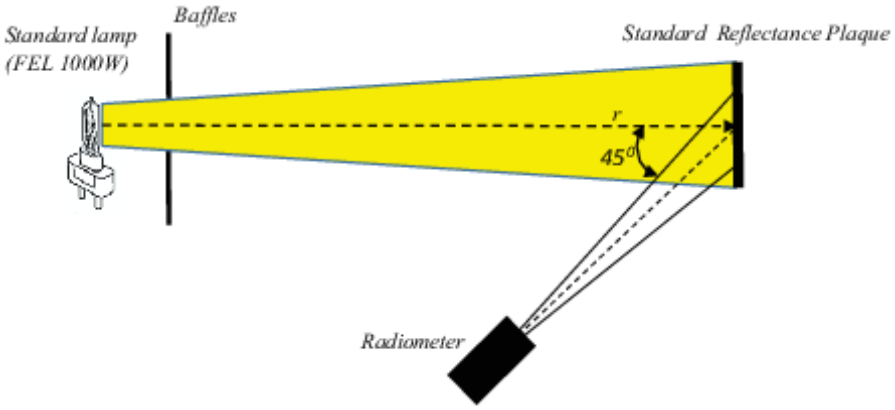

Figure 3.3: A diagram showing the principle for absolute radiance calibrations.

All of the above comments pertaining to effective baffling, and determination of the lamp filament offset, apply to this calibration procedure as well. The procedure (see also Johnson *et al.* 1996) is summarized as follows:

a) The alignment of the lamp optical axis normal to the center of the reflectance plaque is best done using an alignment laser, an FEL alignment jig and a mirror placed against the plaque surface at its center and adjusting the apparatus to achieve retroreflection of the laser beam from both the FEL target and plaque alignment mirror. To avoid damaging the plaque during alignment, a precision frame should hold a flat mirror in the same plane as the plaque.

b) The FEL standard lamp is positioned on an axis normal to the center of the plaque at a distance r. To assure a better uniform illumination across the surface of the plaque, typically r must be greater

than 1.5 m. This minimizes the impact of inhomogeneity of the light projected on the plaque (Hooker *et al.* 2002).

c) The filament offset Δf may be determined by the method described for *Spectral Irradiance Calibration.* If this is done using measurements at varying distances with Eq. 3.5, the FOV of the radiance sensor must be small enough to subtend an area of diameter of a very few centimeters (tentatively 5 cm or less) located at the center of the plaque. If a larger area of the surface is viewed, changes in the spatial distribution of illumination by the FEL may be confounded with the systematic variation associated with the filament offset. Still ignoring the non-ideal point source, it is recommended that a default $\Delta f \approx 3$ mm (Biggar 1998), or an improved one locally determined including both FEL and plaque specific contributions, is applied for radiance calibrations (Meister *et al.* 2002).

d) The radiance sensor is positioned to view the plaque at an angle $\theta = 45°$ measured from the plaque normal. Other angles at which the BRDF of the plaque is known are, in principle, acceptable. It must be established, however, that the plaque fills the sensor FOV and that the presence of the sensor case does not perturb the irradiance on the plaque. The angular alignment of the instrument aperture can be done by rotating the plaque about a vertical axis in the plane of the front surface (measured with an indexing column) by 22.5° and adjusting the instrument to achieve retroreflection (see, Meister *et al.* 2002).

e) The lamp flux is carefully occulted to record the sensor ambient response $DN_{\text{amb}}(\lambda)$. As opposed to the case of *Spectral Irradiance Calibration*, requiring the strict occultation of the flux along the single optical path between lamp and collector, radiance calibration requires that any flux contribution reaching the plaque directly from the lamp is occulted. Finally, the occulter is removed and the response $DN_r(\lambda)$ to radiance reflected from the plaque is recorded.

f) The radiance reflected by the plaque and viewed by the sensor in this geometry is determined as

$$L(\lambda) = \frac{1}{\pi} f_r(\lambda, 0, 45°) E_{\text{r}}(\lambda) \tag{3.7}$$

where the spectral irradiance $E_{\text{r}}(\lambda)$ is calculated using Eq. 3.3.

2. *Integrating Sphere Radiance Calibration:* An alternative approach to calibrating radiance sensors is to view an integrating sphere that is uniformly illuminated by stable and appropriately baffled lamps, with an exit port large enough to completely fill the sensor FOV. Also, the sphere and exit port must be large enough to place the radiance sensor at a distance preventing any significant secondary illumination from the sphere internal walls due to reflections off the sensor entrance optics. In fact, if the sensor is too close, the reflected light increases and distorts the uniformity of the radiance distribution within the sphere. The spectral radiance scale of the integrating sphere can either be determined by an NMI calibration or transferred from the spectral irradiance scale of a FEL lamp standard[2] using the following procedure (Johnson *et al.* 1996).
   a) An irradiance scale transfer radiometer, configured with an integrating sphere having a circular entrance aperture of radius r_2 as its cosine collector, is calibrated using an FEL standard of spectral irradiance by the method outlined for the *Spectral Irradiance Calibration*.
   b) The irradiance scale transfer radiometer is positioned with the entrance aperture parallel to and centered coaxially at a distance d from the circular aperture with radius r_1 of the integrating sphere.

[2] In some laboratories, the radiance scale of a sphere is assumed constant for relatively long periods of time between infrequent scale transfers from an FEL source. Often, these laboratories rely on monitoring the sphere output with detectors at one or more wavelengths. A single wavelength monitor can give a misleading impression of sphere stability, however, as patterns of degradation in sources and optical coatings are often highly wavelength-dependent (J. Butler and G. Meister, Pers. Comm.).

c) The spectral irradiance $E\left(d, r_1, r_2, \lambda\right)$ of the integrating sphere exit port is measured using the irradiance scale transfer radiometer, taking care to subtract the ambient signal collected with the source exit port closed.

d) The spectral radiance scale in the exit aperture of the integrating sphere (Johnson *et al.* 1996) is calculated as

$$L\left(\lambda\right) = \frac{E\left(d, r_1, r_2, \lambda\right) \cdot \left(d^2 + r_1^2 + r_2^2\right)}{\pi \cdot r_1^2} \left(1 + \delta + \delta^2 + \ldots\right) \tag{3.8}$$

where $\delta = r_1^2 r_2^2 \left(d^2 + r_1^2 + r_2^2\right)^{-2}$.

e) Finally, the radiance sensor to be calibrated is positioned in front of the sphere to view the center of the aperture. Its response $DN_{\mathrm{r}}\left(\lambda\right)$ is then recorded.

In either approach, the radiance responsivity calibration coefficients $F_{\mathrm{L}}\left(\lambda\right)$ of the field radiometer, generally in units of μW cm^{-2}nm^{-1}sr^{-1}counts^{-1}, are determined as

$$F_{\mathrm{L}}\left(\lambda\right) = \frac{L\left(\lambda\right)}{DN_{\mathrm{r}}\left(\lambda\right) - DN_{amb}\left(\lambda\right)} \tag{3.9}$$

where $DN_{amb}\left(\lambda\right)$ is the laboratory ambient signal.

The radiance from *in situ* measurements $DN\left(\lambda\right)$ is then computed as

$$L\left(\lambda\right) = F_{\mathrm{L}}\left(\lambda\right)\left[DN\left(\lambda\right) - DN_{dark}\left(\lambda\right)\right] \tag{3.10}$$

where $DN_{dark}\left(\lambda\right)$ is the radiometer dark-signal determined in the field with the aperture covered.

3. SPECTRAL CHARACTERIZATION

Spectral characterization aims to determine the spectral response functions of each band, and additionally determine the out-of-band response of filter-radiometers, or stray light in hyperspectral radiometers. These characterizations imply that a monochromatic source fills the sensor aperture. In the case of radiance sensors, a diffuser placed in front of the optical window can be used to fill the instrument FOV uniformly.

Spectral response function

Center wavelengths and bandpasses of each band are required characterizations for any radiometer. These are determined by measuring the spectral response function, *i.e.*, the passband, for each channel with a scanning monochromatic source exhibiting no stray light and a bandwidth tentatively less than 0.2 nm, which is suitable for most commercial radiometers. For convenience, response functions are commonly normalized to the maximum value. The (nominal) center wavelength is then determined as the wavelength halfway between those at which the normalized response is 0.5 (better quantified through the self-consistent approach detailed in Parr and Johnson (2011)). Similarly, the bandwidth is defined as the passband determined by the full width at half-maximum (FWHM) intensity points.

Detailed knowledge of spectral response functions is needed for accurate radiometric products requiring the convolution of quantities such as the extraterrestrial solar irradiance in the spectral bands.

It is recommended that the internal instrument temperature be monitored during these characterizations, and that they are repeated at two temperatures at least 15 °C apart, *e.g.*, 10 °C and 25 °C. If the temperature-dependent shift detected is greater than 1 nm for either the center wavelength or bandwidth, additional temperature calibration points (*i.e.*, close to 0 °C and to 40 °C) are recommended.

Out-of-band response

Monochromator-based spectral characterizations are not able to adequately measure leakage of broadly distributed out-of-band radiation with high spectral resolution. However, out-of-band radiation can have a significant impact during both calibration and field operation of the radiometers. Because the calibration sources typically have much more flux in the red than the blue, the concern during calibration is the out-of-band long-wavelength light being scattered or transmitted into the shorter wavelength channels. In the field, particularly for the radiometers viewing the surface, or operated in the water, the problem is more related to the flux in the shorter wavelengths, which may lead shorter wavelength light to be scattered or transmitted into the longer wavelength channels. Thus, the out-of-band blocking of the radiometers must be tested occasionally.

In the case of blocking blue light for bands with center wavelengths beyond 540 nm, the lines at 488 nm or at 514.5 nm from a multi-line Ar-ion laser with a prism can be used to measure the out-of-band response. One recommended test that can be performed during absolute calibrations at center wavelengths lower than 640 nm is the sequenced measurement of three Schott BG-18 filters, each 1 mm thick, using an FEL lamp source. The procedure measures the signal using each filter separately, then in combination, and finally compares the transmitted flux. If a significantly lower flux transmitted by the three filters (when they are used in combination) is measured relative to the flux from individual filters, then a spectral leakage is present. At center wavelengths greater than 640 nm, other filters that attenuate the wavelength of interest with a transmission value of less than or equal to 0.1 and which pass shorter wavelength light with significantly greater transmission, should replace the BG-18.

In the case of blocking red light, a convenient way to measure the leakage is to place a long wavelength-pass, sharp-cut, absorbing glass filter that does not exhibit fluorescence between a broadband (*e.g.*, incandescent) source and the sensor. A non-zero response indicates unwanted out-of-band red response and the need for an improved red blocking.

Consideration must also be given to unblocked fluorescence by filters or any other optical component, as an additional possible source of light. In this case, laboratory tests could be performed using filters passing ultraviolet but blocking the visible and near-infrared light components (*e.g.*, UG1).

Stray light perturbations

Equivalent to the out-of-band response for multispectral radiometers, stray light is a significant issue for hyperspectral radiometers calibrated using sources exhibiting a spectral distribution different than those of natural light. Stray light characterization implies determining the spectral stray light response distribution function across the full spectral range of spectrometers. In recent years these characterizations have been performed with high accuracy by NIST using the Spectral Irradiance and Radiance responsivity Calibrations with Uniform Sources (SIRCUS) system based on integrating spheres illuminated by an ensemble of tunable and fixed frequency lasers covering the visible and near-infrared range (Brown *et al.* 2000). This system was specifically applied to characterize stray light at the 10^{-6} level of the Marine Optical Buoy (MOBY) spectrographs of relevance for SVC (Feinholz *et al.* 2009). Alternative and more affordable stray light characterizations can be performed with double monochromators (Talone *et al.* 2016). While the first solution must be applied for each radiometer supporting applications requiring highly accurate measurements (*e.g.*, System Vicarious Calibration (SVC)), the alternative solution is likely applicable for radiometers supporting validation activities.

All the methodologies for the characterization of stray light require that the entrance aperture of sensors is filled with a pure light source having a spectral width much smaller than the sensor bandwidth to accurately determine the line spread functions (LSF) for each band. The inversion of LSF matrices provides the basis for stray light corrections (Feinholz *et al.* 2009, Talone *et al.* 2016).

Stray light characterization is a demanding task. Thus, when applicable, class-based characterizations can be considered for commercial instruments used in validation activities. Some commercial instrument suppliers are capable of delivering spectrometers with stray light correction matrices built into their processing software.

4. IMMERSION FACTORS

Immersion factors account for responsivity variations resulting from changes in the refractive index of the medium in contact with the fore optics (*i.e.*, the cosine collector and the optical window for irradiance and radiance sensors, respectively).

Immersion factor for irradiance sensors

When a diffuser is immersed in water, its light transmissivity is less than in air. Considering that the instrument irradiance responsivity is determined in air, a correction (*i.e.*, the immersion factor) for the change in transmissivity must be applied to irradiance responsivity coefficients for underwater measurements.

The change in transmissivity of a collector when immersed is the net effect of two separate processes, both depending on the relative difference in refractive indices between the diffuser material (*e.g.*, fused silica) and the surrounding medium (*i.e.*, air or water). The first is due to a change in the reflection of light at the external medium-collector interface; the second is due to a change in the reflection of light at the inner (*i.e.*, inside the diffuser) collector-medium interface.

The refractive index of the collector material is always greater than that of either water or air; and because the refractive index of water is greater than that of air, the Fresnel transmission of the water-diffuser interface is greater than that of the air-diffuser interface. Therefore, the initial transmission of light into the irradiance collector is greater in water than in air. However, the transmission of light out of the diffuser into the surrounding medium is greater in water than in air. Therefore, a larger fraction of the light scattered within the diffuser passes back into the water column than would be lost into air. Because the increased flux leaving the diffuser exceeds the gain in the incoming flux, the net effect of these competing processes is a decrease in the transmissivity of the immersed collector (Westlake 1965).

Previous investigations have shown that the immersion factors for irradiance collectors must be characterized experimentally. In fact, some manufacturers only characterize prototypes with a particular collector design and material specification, then successively provide nominal immersion factors for all production radiometers using that collector design. In this respect, Mueller (1995) and Zibordi *et al.* (2004) applied the characterization procedure described below with repeatability better than 1% and observed root-mean-square differences between immersion factors of radiometers from the same series exceeding several percent, with values as large as 10% in some spectral bands.

To measure this effect, a suggested procedure (Aas 1968, Petzold and Austin 1988) is as follows (see the schematic of the measurement setup in Fig. 3.4):

1. The instrument is placed in a tank of water with the irradiance collector leveled and facing upward.
2. A tungsten-halogen lamp with a small filament (to mimic a point source), powered by a stable power supply, is applied as a light source. The measurement system (lamp, radiometer, and water vessel) must be carefully aligned, and the distance of the lamp above the surface of the irradiance collector carefully measured. After lamp warm-up, an initial reading is taken in air before raising the water level in the tank above the dry collector. Lamp voltage and current should be monitored throughout the duration of the characterization to ensure a stable output. As a further assurance of lamp stability, the output flux should be continuously monitored with a separate in-air irradiance sensor (Zibordi *et al.* 2002). The water temperature should also be recorded to accurately determine the water refractive index.
3. The water is raised initially to a carefully measured depth z above the collector surface, and the radiometer outputs are recorded for all bands. Achieving repeatability better than 1% implies careful attention to the cleanliness of the water and removal of any air bubbles from fore optics (Zibordi *et al.* 2002). It is thus recommended to use pure water and a relatively small water tank with an efficient internal baffling (Zibordi *et al.* 2003, Hooker and Zibordi 2005).
4. The water level is then increased stepwise, *e.g.*, in 5 cm increments, and the instrument response measured and recorded for each depth z. A maximum water depth of a few tens of cm (*e.g.*, 40 cm) is normally adequate to obtain data covering a sufficient response range.

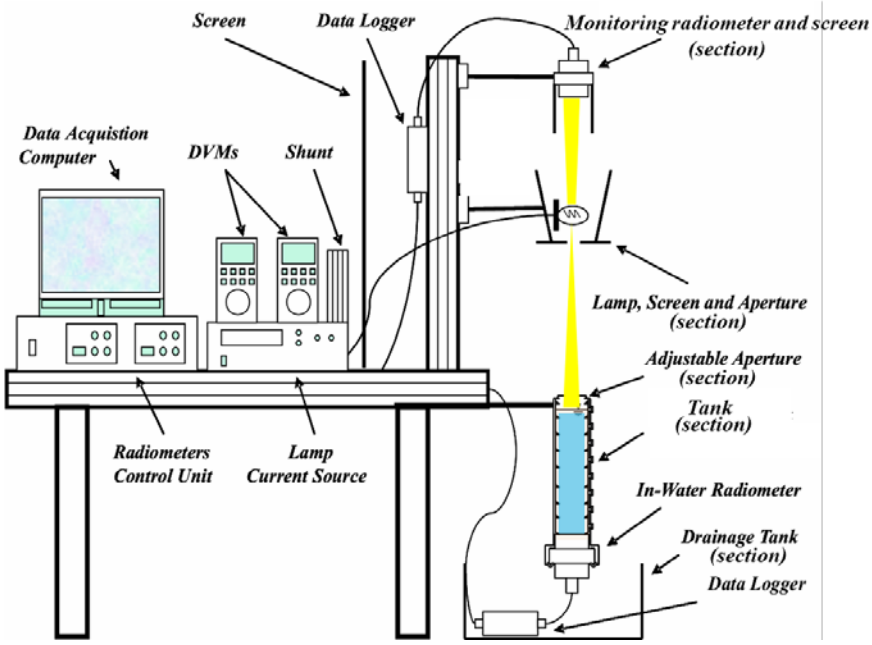

Figure 3.4: Schematic of the measurement setup for determining the immersion factor for irradiance sensors (adapted from Zibordi et al. 2003). The small tank size, which allows for the use of affordable quantities of pure water, requires an efficient internal baffling to minimize stray light.

5. The water level is then lowered, and data recorded over a similar series of incremental depths.
6. A final reading is taken with the water level below the collector after drying it.

A minimum water depth of tentatively 5 cm is recommended to avoid artifacts caused by multiple reflections between the collector and water sub-surface. These reflections would increase the transmitted flux, and therefore, decrease the apparent immersion effects. The magnitude of this artifact increases with a decrease in the minimum depth and an increase in the diameter of the collector.

The amount of flux arriving at the collector varies with the water depth and is a function of several factors:

i. The attenuation at the air-water interface, which varies with wavelength;

ii. The attenuation over the water pathlength, which is a function of depth and wavelength;

iii. The change in the solid angle of the light leaving the source and arriving at the collector, caused by the light rays changing direction at the air-water interface, which also varies with wavelength and water depth.

Using the Fresnel reflectance equations and taking the index of refraction of air as 1, the normal transmittance through the water surface is

$$T_S(\lambda) = \frac{4n_w(\lambda)}{\left[1+n_w(\lambda)\right]^2} \tag{3.11}$$

where $n_w(\lambda)$ is the index of refraction of the water at wavelength λ.

The change with water depth *z* of the refracted solid angle subtended by the collector, as viewed from the lamp filament, is given by

$$G(z,\lambda) = \left\{1-\frac{z}{d}\left[1-\frac{1}{n_w(\lambda)}\right]\right\}^2 \tag{3.12}$$

where *d* is the distance of the lamp source from the collector surface.

The immersion correction factor $F_{\mathrm{i,E}}(\lambda)$ for irradiance is then calculated as

$$F_{\mathrm{i,E}}(\lambda) = \frac{DN_{\mathrm{a}}(0^{+},\lambda)}{DN_{\mathrm{w}}(0^{-},\lambda)} T_{\mathrm{S}}(\lambda) \tag{3.13}$$

where $DN_{\mathrm{a}}(0^{+},\lambda)$ and $DN_{\mathrm{w}}(0^{-},\lambda)$ are in-air and sub-surface irradiances in digital counts. The latter value is determined from the least squares fit as a function of the water depth z_i above the collector of $\ln[DN_{\mathrm{w}}(z_i,\lambda)/G(z_i,\lambda)]$. The factor $G(z_i,\lambda)$ corrects for the geometric effects induced by the change in solid angle of the light leaving the source and arriving at the collector after crossing the air-water interface. $DN_{\mathrm{a}}(0^{+},\lambda)$ and $DN_{\mathrm{w}}(z_i,\lambda)$ are values corrected for the dark-signal.

As already discussed, a high reproducibility of $F_{\mathrm{i,E}}(\lambda)$ determinations imply the use of pure water (*e.g.*, Milli-Q by Millipore Corporation). The actual application of derived $F_{\mathrm{i,E}}(\lambda)$ values to field measurements, then requires corrections accounting for differences in the refractive indices between pure and natural waters as a function of salinity and likely temperature. Because of the difficulty of generating and working with pure seawater, the correction to account for salinity and temperature effects can only rely on experimental estimates of the correction factor to be applied to the pure water calibration. This approach, however, is not expected to appreciably increase the uncertainty assigned to the experimental determination of $F_{\mathrm{i,E}}(\lambda)$.

Immersion factor for radiance sensors

Equivalent to irradiance sensors, the absolute calibration for spectral radiance sensors is performed in air. Thus, when the instrument is submerged in water, a change in responsivity occurs, and a correction must be applied. This change in responsivity is caused by i) a change in transmission through the water-window interface with respect to the transmission of the air-window interface, and ii) change in the solid angle FOV relative to that in air.

Since $n_{\mathrm{w}}(\lambda)$ is a function of wavelength, the correction factor $F_{\mathrm{i,L}}(\lambda)$ is also a function of wavelength. Given that the refractive index of air can be taken as unity at all wavelengths, if $n_{\mathrm{g}}(\lambda)$ is the index of refraction for the material constituting the optical window of the radiance sensor, the correction for the change in transmission through the window, $T_{\mathrm{g}}(\lambda)$, is given by (see Austin 1976)

$$T_{\mathrm{g}}(\lambda) = \frac{\left[n_{\mathrm{w}}(\lambda)+n_{\mathrm{g}}(\lambda)\right]^{2}}{n_{\mathrm{w}}(\lambda)\left[1+n_{\mathrm{g}}(\lambda)\right]^{2}} \tag{3.14}$$

and the correction for the change in FOV is

$$F_{\mathrm{v}}(\lambda) = \left[n_{\mathrm{w}}(\lambda)\right]^{2}. \tag{3.15}$$

For an optical window made of fused silica, the spectral refractive index $n_{\mathrm{g}}(\lambda)$ can be conveniently computed using an empirical fit to the Hartmann formula, as (Ohde and Siegel 2003)

$$n_{\mathrm{g}}(\lambda) = 1.4424 + \frac{7.1661}{\lambda - 144.717} \tag{3.16}$$

where λ is in units of nm. For different materials commonly used for optical windows (*e.g.*, BK-7) the refractive indices are provided by the manufacturers.

The refractive index of seawater $n_{\mathrm{w}}(\lambda)$ can be similarly computed using an empirical fit of the data from Austin and Halikas (1976) for pure water at 22 °C as

$$n_{\mathrm{w}}(\lambda) = 1.325147 + \frac{6.6096}{\lambda - 137.1924}. \tag{3.17}$$

An empirical equation by Quan and Fry (1995) provides an alternative solution to compute $n_{\mathrm{w}}(\lambda)$ as a function of both salinity and temperature.

By combining the corrections $T_{\mathrm{g}}(\lambda)$ and $F_{\mathrm{v}}(\lambda)$, the immersion factor $F_{\mathrm{i,L}}(\lambda)$ for a radiance sensor is given by

$$F_{\mathrm{i,L}}(\lambda) = \frac{n_{\mathrm{w}}(\lambda)\left[n_{\mathrm{w}}(\lambda) + n_{\mathrm{g}}(\lambda)\right]^2}{\left[1 + n_{\mathrm{g}}(\lambda)\right]^2}. \tag{3.18}$$

This equation ideally applies to Gershun tube radiometers with an optical window as fore optics. Because of this, efforts were made to experimentally characterize $F_{\mathrm{i,L}}(\lambda)$ for radiometers exhibiting different optical designs (Zibordi 2006, Zibordi and Darecki 2006, Feinholz *et al.* 2017), where the interaction of light with the various components of the optical system may affect the responsivity.

Two experimental methods were proposed and applied to determine $F_{\mathrm{i,L}}(\lambda)$ (see Zibordi 2006 and Feinholz *et al.* 2017). Following the method proposed by Zibordi (2006), the experimental characterization of $F_{\mathrm{i,L}}(\lambda)$ for radiance sensors is made using in-air and in-water radiance measurements successively, performed at a constant sensor–source distance with the sensor looking vertically down at a stable, homogeneous, and near-Lambertian source immersed in pure water. The measurement procedure is equivalent to that detailed for the *Immersion factor for irradiance sensors*, except that immersed measurements are taken with a single distance *r* between the optical window and source while multiple in-air measurements are taken decreasing the water level z_i and, thus, with diverse water depths $r - z_i$ between the water surface and the optical window (see the schematic of the measurement setup in Fig. 3.5). The diffuse light source can be obtained with an LCD flat-field source (Feinholz *et al.* 2017) operated underneath a water tank with the bottom made of a transparent material (*e.g.*, optical glass), or alternatively a number of quality diffusers illuminated by a halogen-tungsten lamp operated at an opportune distance to increase homogeneity of the resulting diffuse source (Zibordi 2006). This latter solution provides a more uniform spectral distribution of light in the visible and near-infrared spectral region.

Following Zibordi (2006) $F_{\mathrm{i,L}}(\lambda)$ is determined from

$$F_{\mathrm{i,L}}(\lambda) = \frac{DN_a(0^+,\lambda)}{DN_w(0^-,\lambda)} \frac{\Omega_a}{\Omega_w(\lambda)} \frac{1}{T_s(\lambda)} \tag{3.19}$$

where $DN_a(0^+,\lambda)$ and $DN_w(0^-,\lambda)$ are the digital values related to the above- and in-water radiances, respectively. $DN_a(0^+,\lambda)$ is computed as the intercept of the least-squares fit to the distance z_i of the optical window from the water surface, regressed with the log-transformed in-air measurement $DN_a(r-z_i,\lambda)$. It is recalled that $DN_w(0^-,\lambda)$ and $DN_a(r-z_i,\lambda)$ are values corrected for the dark-signal.

The terms Ω_a and $\Omega_w(\lambda)$ are the in-air and in-water solid angle FOVs, respectively: their exact values are not needed because their ratio is known, *i.e.*, $\Omega_a/\Omega_w(\lambda) = n_w^2(\lambda)$. $T_s(\lambda)$ is the normal transmittance through the water surface given by Eq. 3.11. However, if the sensor FOV is larger that a few degrees, $T_s(\lambda)$ should be replaced by the mean of the water surface transmittances determined over the solid angle $\Omega_w(\lambda)$.

The experimental characterization of $F_{\mathrm{i,L}}(\lambda)$ for sample radiometers of the same series did not show appreciable sensor-to-sensor dispersion (Zibordi 2006). However, theoretical and experimental determinations exhibited appreciable differences for some radiometer series (Zibordi and Darecki 2006). These findings suggest that i) values of $F_{\mathrm{i,L}}(\lambda)$ can be applied confidently to radiance sensors of a given

class, still, ii) the experimental characterization of $F_{i,L}(\lambda)$ for sample radiance sensors of each class is desirable to detect differences between theoretical and experimental determinations.

Finally, relative changes of $F_{i,L}(\lambda)$ as a function of the refractive index of natural waters can be easily quantified through Eq. 3.18 as a function of $n_w(\lambda)$ for different temperatures and salinities (Zibordi 2006).

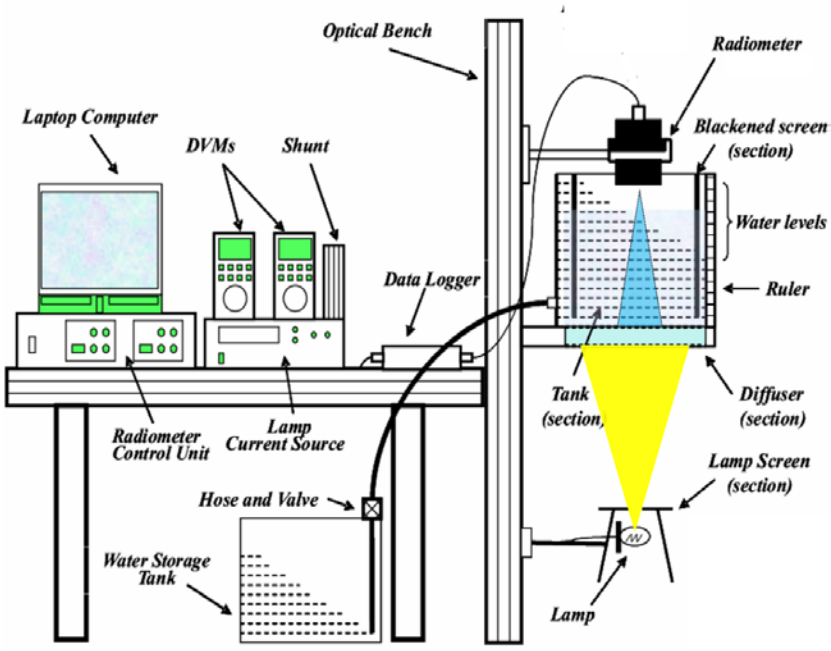

Figure 3.5: Schematic of the measurement setup for determining the immersion factor for radiance sensors (adapted from Zibordi (2006)).

5. ANGULAR RESPONSE

Radiance field-of-view

The radiance FOV does not normally enter into the absolute calibration when a uniform calibration source fully fills the fore optics. However, the radiance FOV of the instrument must be determined during characterization.

Excluding sensors with a very small FOV (*i.e.*, typically smaller than 1°), the determination of the FOV is performed with the instrument operated on a rotational stage with the entrance aperture of the radiometer aligned with the rotation axis. A stable light source with a small filament is placed in front of the instrument several meters away. The distance depends on the FOV of the radiometer and the apparent size of the filament; the latter must be a small fraction (tentatively 1/20) of the radiometer FOV. The on-axis, *i.e.*, 0° , mechanical alignment can be performed using the surface of the optical window as the reference, by simply adjusting the position of the radiometer to get the reflection of the lamp filament to return on-axis. Data should be ideally collected at increments approximately 1/20 of the estimated radiometer FOV over two planes with a positioning uncertainty better than 1/10 of the increment spacing. In the case of in-water characterizations, the in-air measurement angles θ_a need to be converted to the corresponding in-water angles $\theta_w(\lambda)$ using the relation (through the small-angle approximation):

$$\theta_w(\lambda) = \frac{\theta_a}{n_w(\lambda)} \tag{3.20}$$

After normalization of the angular response function to the maximum value, the full-angle FOV is determined as the FWHM of intensity points.

Cosine response

Irradiance sensors are equipped with collectors that should exhibit a cosine response as a function of the incidence angle θ. However, actual collectors always show angular response deviating from this ideal. This deviation becomes a source of error in measurements. Because of this, the directional response of cosine collectors must be characterized.

Due to the different refractive index of the medium in which the radiometers may be operated, the spectral directional response of E_s sensors needs to be determined in air, while the in-water E_d and E_u sensors need to be measured immersed. Considering the large variability affecting the cosine response of instruments within a manufacturing series (Mueller 1995; Zibordi and Bulgarelli 2007; Mekaoui and Zibordi 2013), the angular response of each radiometer should be characterized individually.

A measuring set-up for the characterization of an in-water sensor implies the use of a tank (see schematic in Fig. 3.6). Following Petzold and Austin (1988), the instrument is operated either in-air or in a tank filled with water that is supported by a fixture designed to rotate around an axis through the surface and center of the collector. A tungsten-halogen lamp with a small filament is enclosed in a housing with a small exit aperture and placed 1 m (or more) from a large optical window in the tank or from the collector. The collector is placed approximately 25 cm (or more) behind this window. A circular baffle should be placed immediately in front of the window to reduce stray light. When performing characterizations of immersed radiometers, the use of pure water minimizes scattering effects.

The $\theta = 0$ alignment should locate the center of the collector on the axis of illumination with the collector surface oriented normal to the axis. One method of achieving this alignment is to pass a laser beam through the location of the filament (with aid of a lamp jig) to the center of the collector. The collector is rotated until a mirror held flat against it, reflects the laser beam back on itself. The rotational indexing scale should be zeroed in this position. With $\theta = 90°$ the beam should just graze the collector, while it should remain in the center of the collector at any other smaller angle. The position of the apparatus should be adjusted until these alignment criteria are satisfied. Note that success in this alignment procedure also depends on orienting the illumination axis normal to the tank window. Additionally, the alignment distance must be corrected by accounting for the actual collection plane of the irradiance collector (see the section on *Spectral irradiance calibration*).

Importantly, the alignment procedure and correction for the actual irradiance collection plane should be performed for each collector for radiometers equipped with multiple collectors.

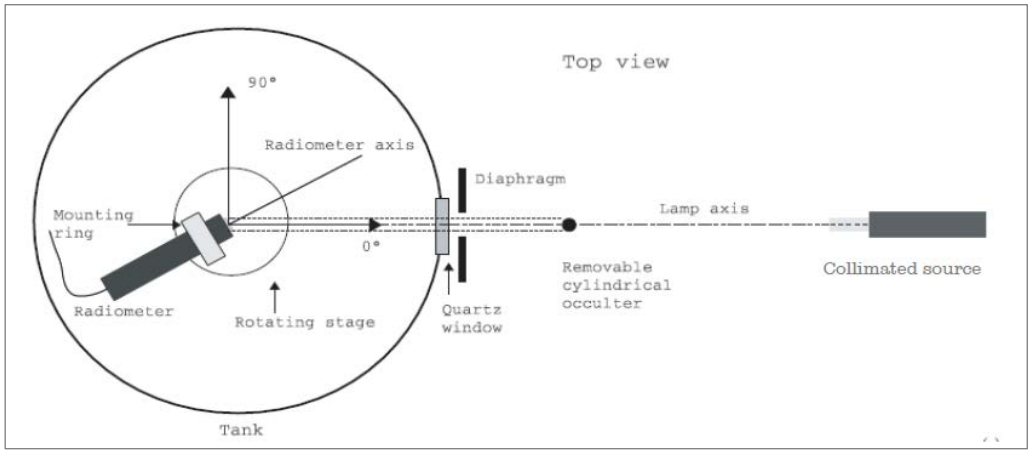

Figure 3.6: Schematic of a measurement setup for the characterization of the angular response of irradiance sensors (adapted from Mekaoui and Zibordi (2013)). Note that in this setup, the lamp is replaced by a collimated source.

Assuming an ideal cosine response, with a lamp-to-collector distance of 1.25 m, the fall-off at the outer edge of a 6 cm diameter collector is 0.9994, or -0.06%, when the diffuser is at θ = 0. The net effect

over the entire area of the diffuser is 0.9997 or -0.03%. When $\theta = 90°$, with the diffuser edge-on to the lamp, the distance to the lamp varies for different points on the surface. The net error over the entire surface for this condition is 0.99997 or -0.003%. All other angles fall between these limiting cases.

The instrument response $DN(0,\phi,\lambda)$ is initially recorded for $\theta = 0$ in the plane determined by the azimuth angle ϕ. The instrument is rotated ideally with 1° increments up to $\theta = 90°$, and the instrument responses $DN(\theta,\phi,\lambda)$ recorded at each angle θ. The specific $DN(0,\phi,\lambda)$ value is acquired at the beginning, middle, and end of each run, then examined as a measure of lamp and instrument stability over the time involved. If the angular indexing mechanism allows rotation in either direction, the procedure should then be repeated for the azimuth ϕ+180° to complete the characterization of the directional response in one full plane perpendicular to the collector surface. If the apparatus allows rotation in one direction only, then the instrument should be rotated about the optical axis (normal to the collector), and the procedure repeated to complete the plane. At least two sets of such runs should be made for different planes through the surface of the diffuser. The directional normalized response of the instrument for each azimuth is expressed as

$$DN_N(\theta,\phi,\lambda) = \frac{DN(\theta,\phi,\lambda) - DN_{amb}(\theta,\phi,\lambda)}{DN(0,\phi,\lambda) - DN_{amb}(0,\phi,\lambda)}. \tag{3.21}$$

For an ideal cosine collector, $DN_N(\theta,\phi,\lambda)$ should equal $\cos\theta$, regardless of ϕ and λ.

Note that the ambient signal $DN_{amb}(\theta,\phi,\lambda)$ should be measured by occulting the direct path between source and collector for each viewing geometry defined by (θ,ϕ).

For convenience, by fitting $DN_N(\theta,\phi,\lambda)$ as a function of θ to a third-order polynomial function (or even higher-order, depending on the features shown by the experimental data), the fitted $DN_{Nf}(\theta,\phi,\lambda)$ can be applied to compute the cosine error for any angle θ

$$f_c(\theta,\phi,\lambda) = \frac{DN_{Nf}(\theta,\phi,\lambda)}{\cos\theta} - 1 \tag{3.22}$$

or, when considering the average response $\overline{DN}_{Nf}(\theta,\lambda)$ of $DN_{Nf}(\theta,\phi,\lambda)$ values over different azimuth angles,

$$f_c(\theta,\lambda) = \frac{\overline{DN}_{Nf}(\theta,\lambda)}{\cos\theta} - 1. \tag{3.23}$$

Applying $\overline{DN}_{Nf}(\theta,\lambda)$, the error $\varepsilon_c(\lambda)$ in measuring the irradiance for a uniform radiance distribution is computed from

$$\varepsilon_c(\lambda) = \frac{\int_\theta^{\pi/2} \overline{DN}_{Nf}(\theta,\lambda)\sin\theta d\theta}{\int_\theta^{\pi/2} \cos\theta\sin\theta d\theta} - 1. \tag{3.24}$$

Similarly, for a radiance distribution of the form $1+4\sin\theta$, which may be used to approximate the in-water upward irradiance, the error is given by

$$\varepsilon_c(\lambda) = \frac{\int_\theta^{\pi/2} \overline{DN}_{Nf}(\theta,\lambda)(1+4\sin\theta)\sin\theta d\theta}{\int_\theta^{\pi/2} \cos\theta\,(1+4\sin\theta)\sin\theta d\theta} - 1. \tag{3.25}$$

The asymmetry of the cosine response can be estimated as the ratio of sums of values at opposite azimuth angles in the same plane, *i.e.*, ϕ and ϕ+180°, according to

$$\delta_c(\phi,\lambda) = \frac{\int_0^{\pi/2} DN_{Nf}(\theta,\phi,\lambda)\sin\theta d\theta}{\int_0^{\pi/2} DN_{Nf}(\theta,\phi+\pi,\lambda)\sin\theta d\theta} - 1. \quad (3.26)$$

Any offset of the average asymmetry with the mechanical axis could be due to any one of the following causes: poor alignment, tilt of the diffuser, a non-centered detector array or nonuniformity of the diffuser. Variations in asymmetry from channel to channel of the same radiometer may be due to the placement of the individual detectors behind the diffuser.

The German Institute of Standardization defined the following performance index (see DIN5032, German Institute of Standardization, 1978) for irradiance collectors determined by the integral of azimuth-independent absolute values of the cosine error for θ from 0 to 85°

$$\left\langle \left| f_c(\lambda) \right| \right\rangle = \int_0^{0.47\pi} \left| f_c(\theta,\lambda) \right| \sin(2\theta) d\theta. \quad (3.27)$$

The value of the index $\left\langle \left| f_c(\lambda) \right| \right\rangle$ is null for ideal cosine collectors and increases with a decrease of the collector performance. Values in the range of 0.01 to 0.05 (*i.e.*, 1% and 5%) were computed for collectors in commercial radiometers (Mekaoui and Zibordi 2013).

By neglecting the sky light and thus only considering the direct sun component, an approximate impact of cosine errors $\varepsilon_c(\theta_0,\lambda)$ in $E_s(\lambda)$ is given by $\varepsilon_c(\theta_0,\lambda) \approx f_c(\theta_0,\lambda)$. However, validation activities imply the delivery of highly accurate values of $E_s(\lambda)$. It is then important to apply corrections to measurements performed with non-ideal cosine collectors, once these are carefully characterized. Following the scheme applied by Zibordi and Bulgarelli (2007) and originally proposed for the ultraviolet spectral region by Seckmeyer and Bernhardt (1993), errors affecting actual measurements can be computed from

$$\varepsilon_c'(\theta_0,\lambda) = \left\langle f_c(\lambda) \right\rangle \frac{I_r(\theta_0,\lambda)}{I_r(\theta_0,\lambda)+1} + f_c(\theta_0,\lambda) \frac{1}{I_r(\theta_0,\lambda)+1} \quad (3.28)$$

where $I_r(\theta_0,\lambda)$ is the diffuse-to-direct irradiance ratio and

$$\left\langle f_c(\lambda) \right\rangle = \int_0^{\pi/2} f_c(\theta,\lambda)\sin(2\theta)d\theta\,. \quad (3.29)$$

Cosine errors affecting field data $\left[DN(\lambda) - DN_{dark}(\lambda) \right]$ are finally corrected by applying the factor

$$\aleph_c(\theta_0,\lambda) = 1 - \varepsilon_c'(\theta_0,\lambda). \quad (3.30)$$

An analysis by Zibordi and Bulgarelli (2007) showed an agreement generally better than 2% between values of $\varepsilon_C'(\theta_0,\lambda)$ computed with the above equation and equivalent values determined with radiative transfer simulations accounting for atmospheric optical properties and the actual characterization of the angular response of the collector. Nevertheless, differences are well below 0.5% for sun zenith angles $\theta_0 < 65°$ and collectors exhibiting performance indices better than 2.5%.

6. LINEARITY OF RESPONSE

The standard method to characterize the linearity of radiometers is conveniently implemented using a point source and applying the inverse-square law. This solution generates different irradiances by changing the distance between source and detector. Practically, it is recommended that characterizations rely on series of measurements ideally performed over the full dynamic range of each spectral band with fluxes incremented or decremented by 5 dB (0.5 log).

It is mentioned that a variety of fluxes can be obtained with 1000 W tungsten-halogen lamps and additionally from 1000 W to 2000 W high-pressure xenon arc-lamps. These arc lamps can produce irradiance levels approximating the full sunlight.

The straightforward characterization for sensor linearity is, however, complicated by several factors. First, the inverse square law exactly applies to a point aperture and a point source. Thus, its inaccuracy

increases with the size of the sensor aperture and the lamp filament, and additionally with a decrease of the distance between the two. This requires applying correction models accounting for the equivalent source and sensor aperture radii (Manninen *et al.* 2008). Further difficulties are created by the need to determine the actual reference planes for lamps and diffusers (see *Irradiance responsivity calibration*).

Defining $DN_r(\lambda)$ and $DN_0(\lambda)$ as the digital values corrected for ambient signal corresponding to measurements performed at sensor-source distances r and r_0, respectively, with $DN_0(\lambda)$ reference value conveniently determined to approximately match half of the counts range, the non-linearity error is given by

$$\varepsilon_l\left(DN_r, DN_0, \lambda\right) = \frac{DN_r(\lambda)}{DN_0(\lambda)} \frac{(r+\Delta_f+\Delta_d)^2}{(r_0+\Delta_f)^2} - 1 \tag{3.31}$$

where Δ_f and Δ_d indicate the filament and collector reference plane offsets, respectively (see the section on *Irradiance Responsivity Calibration*). It is mentioned that Eq. 3.31 neglects the effects of non-negligible size of sensor aperture and source; and in the case of radiometers with variable sampling rate, it assumes that $DN_r(\lambda)$ and $DN_0(\lambda)$ values are taken with the same integration time.

By imposing a linear dependence of non-linearity with digital counts, the non-linearity factor $l(\lambda)$ can be derived from the linear regression of $\varepsilon_l\left[DN_r(\lambda)\right]$ as a function $\left[DN_r(\lambda) - DN_0(\lambda)\right]$ (see Talone and Zibordi 2018) so that

$$\varepsilon_l\left(DN_r, DN_0, \lambda\right) = l(\lambda) \cdot \left[DN_r(\lambda) - DN_0(\lambda)\right]. \tag{3.32}$$

Once characterized, any departure from linearity must be incorporated into the calibration function and properly applied to field measurements. Practically, corrections of raw values $\left[DN(\lambda) - DN_{dark}(\lambda)\right]$ are obtained through the application of the factor

$$\aleph_l(DN, DN_0, \lambda) = 1 - l(\lambda) \cdot \left\{\left[DN(\lambda) - DN_{dark}(\lambda)\right] - DN_0(\lambda)\right\}. \tag{3.33}$$

It should be mentioned that there are other methods that rely on combinations of light sources and allow the individual light sources to be uncalibrated (White *et al.* 2008: Hamadani *et al.* 2016). These methods may be hard to physically implement but they may avoid the problem with non-ideal point sources and deviation from the ideal inverse square law.

7. INTEGRATION TIME RESPONSE

For instruments such as hyperspectral radiometers based on detector arrays, which allow operation with different integration times, the variation in response with integration time must be characterized. This is best done as a separate step after the sensor linearity is determined. Specifically, the integration time characterization is performed in a straightforward manner by looking at a constant source and measuring this source at different integration times. It is particularly important to characterize this at the short end of the integration times that will be used in either field or calibration, as this is the region where non-linear effects take place due to either mechanical shutter-speed limitations, timing offsets, or any other factor related to charge-handling from the elements of the detector array.

8. TEMPERATURE RESPONSE

The various components of a radiometer may be temperature dependent. For instance, silicon detectors commonly applied for ocean color applications, exhibit a significant temperature dependence in the near-infrared spectral region. Because of this, in the absence of any temperature stabilization, the radiometer output may show changes in dark-signal and responsivity. This dependency requires that radiometers undergo a comprehensive temperature characterization at least for a few units of each class or series of instruments. Characterizations for underwater instruments should be performed over at least the 0 °C to 35 °C temperature range, which are easily achievable in controlled conditions. In the case of E_s sensors,

the temperature range should at least embrace 0 °C to 45 °C . Sensors exhibiting temperature coefficients greater than 0.01% per °C over these temperature ranges, should be comprehensively characterized to establish the means and precision with which post-acquisition processing can be applied to correct for temperature dependence. Although exact knowledge of changes in the dark-signal with temperature is fundamental for working at the lowest radiances or irradiances, it should be emphasized that temperature variations in responsivity may induce significant errors.

Possible responsivity changes with temperature must be individually determined across the spectrum. Ideally, any correction should use the temperature of the affected element, which is typically in the interior of the instrument. This is best accomplished by routinely monitoring temperature sensors at critical locations within the radiometer. For the highest precision, dynamic temperature testing involving temporal transients relevant for profiling instruments, as well as possible temperature gradients within instruments, may be appropriate. In any case, at least one thermistor should be operated within the instrument near the detector.

Temperature characterizations imply operating the radiometer in a temperature-controlled chamber while looking at a stable source. Following Zibordi *et al.* (2017), alignment of the different system components (*i.e.*, source, optical window of the chamber, radiometer) should be performed with a laser. Stray light should be minimized using a diaphragm at the entrance window of the measuring chamber. Both the chamber and the internal instrument temperature should be measured to identify conditions of thermal equilibrium inside the instrument allowing measurements in stable conditions. This process should allow performing measurements when all the radiometer components are thermally stabilized. In the challenging condition created by the lack of any temperature measurement inside the instrument, extended time should be provided to the radiometer to stabilize. It is essential to avoid direct illumination of the radiometer by the source between successive temperature tests (if operated at close distance) to avoid heating the fore optics components. Measurements should be performed with increments of at least 5 °C over the expected operating range of the instrument.

The temperature response of radiometers can be defined through the relative difference $\varepsilon_T(T,\lambda)$ between values of $DN_T(T,\lambda)=\left[DN(T,\lambda)-DN_{amb}(T,\lambda)\right]$ determined at temperature T and values of $DN_0(T_0,\lambda)=\left[DN(T_0,\lambda)-DN_{amb}(T_0,\lambda)\right]$ obtained at the reference temperature T_0 (typically set close to 20 °C, which corresponds to the temperature at which radiometers are commonly calibrated for responsivity)

$$\varepsilon_T(T,T_0,\lambda)=100\cdot\left[\frac{DN_T(T,\lambda)}{DN_0(T_0,\lambda)}-1\right] \tag{3.34}$$

where, assuming a linear dependence with temperature of the radiometer responsivity, the fitted values of $DN(T,\lambda)/DN(T_0,\lambda)$ are applied to determine the temperature coefficinet $c(\lambda)$ in units of $(°C)^{-1}$ as a function of $\Delta T=T-T_0$ for each band, so that

$$c_T(\lambda)=\left[\frac{DN(T,\lambda)}{DN(T_0,\lambda)}-1\right]\cdot\Delta T^{-1}. \tag{3.35}$$

The dependence to temperature response in field data $\left[DN(\lambda)-DN_{dark}(\lambda)\right]$ is finally removed by applying the factor

$$\aleph_c(T,T_0,\lambda)=1-c_T(\lambda)\cdot\Delta T. \tag{3.36}$$

9. POLARIZATION SENSITIVITY

Light from the sea has a degree of polarization varying with water constituents and the atmospheric aerosols with impact more pronounced in above-water than in in-water radiometry. Because of this, the polarization sensitivity of radiometers due to individual optical components (*e.g.*, optical windows, lenses, dispersive elements) may become a source of uncertainty in measurements. Thus, at a minimum, the polarization sensitivity of optical radiometers must be determined. Considering that the circular

polarization of radiance in the atmosphere and natural waters is generally negligible, the characterization for polarization sensitivity reduces to linear polarization analysis. This can be achieved by incrementally rotating a linear polarizer positioned between a non-polarized source and the entrance optics of the radiometer. The resulting polarization sensitivity, in percent, can then be expressed as

$$P(\lambda) = 100 \cdot \frac{DN_M(\lambda) - DN_m(\lambda)}{DN_M(\lambda) + DN_m(\lambda)} \tag{3.37}$$

where $DN_m(\lambda)$ and $DN_M(\lambda)$ indicate the minimum and maximum values recorded while rotating the polarizer and corrected for the ambient signal.

In the case of sensitivity to linear polarization tentatively higher than 1%, corrections should be applied for comprehensively characterized radiometers (Meister *et al.* 2005, Talone and Zibordi 2016). In general, best practice would suggest reducing polarization sensitivity through depolarizers placed inside the radiometer optics.

10. SENSITIVITY CHANGE

The responsivity of radiometers may change over time as optical components age (*e.g.*, filters, fore optics). Tracking these changes is essential and imposes pre- and post-field absolute radiometric calibrations and, ideally, regular responsivity checks through portable and stable reference sources during field activities. Responsivity changes of a very few percent (*e.g.*, 2% or greater when supported by regular checks) generally can be corrected assuming linear variations with time. However, if the change is within the expanded uncertainty of the radiometric calibration (Johnson *et al.* 2014), no adjustment is warranted. Conversely, caution is suggested while correcting responsivity changes reaching several percent. In fact, these changes could result from abrupt variations in the characteristics of optical components, such as those subsequent to a deterioration of interference filters due to humidity effects or thermal stress of gratings.

11. DARK-SIGNAL

Radiometers generally exhibit a non-null output signal in the absence of flux at the entrance optics. This signal, which largely varies with temperature and sampling time (*i.e.*, integration time in the case of most hyperspectral radiometers), results from the photodetector dark current and additional contributions such as the electronic offset. Anticipating that the removal of the dark-signal from field data requires dedicated measurements performed during regular above- or in-water operations (see Chapters on *In-water-Radiometry Measurements and Data Analysis* and also *Above-water Radiometry Measurements and Data Analysis*), it is relevant to have frequent characterizations of the dark-signal for each radiometer. In fact, depending on the instrument design and procedures put in place to precisely determine the dark-signal during field activities, frequent characterizations could be relevant for any processing requiring comprehensive knowledge of the radiometer performance with temperature and sampling time, and for the quality assurance of measurements.

The dark-signal characterization must be performed with the entrance optics closed and measuring the output signal as a function of temperature and sampling time.

12. TEMPORAL RESPONSE

The temporal response of a spectrometer may be examined by introducing a step function of near full-scale flux to the system using an electrically operated shutter and measuring the system transient response at 0.1 s, or shorter intervals (depending on sampling rate). The response should be stable within one digital count, or 0.1%, whichever is greater, of the steady-state value in one second or less.

13. PRESSURE EFFECTS

Pressure can cause radiometric measurement errors by deforming irradiance collectors. Pressure coefficients associated with polytetrafluoroethylene (PTFE) based irradiance diffusers are known to exist, but they are not uniform, and there may be hysteresis effects. It is recommended that each type of irradiance

detector be examined for variations in responsivity with pressure. If a significant effect is observed, then pressure-dependent responsivity coefficients should be determined separately for each instrument and collector. The pressure characterization should also test for and quantify hysteresis and temporal transients in responsivity under a time-varying pressure load.

The characterization of pressure effects on optical radiometers is not common practice, and the requisite procedures are not defined.

14. SUMMARY OF TARGET UNCERTAINTIES

This final section aims at summarizing the target measurement uncertainties. Specifically accounting that each individual uncertainty affecting basic radiometric quantities from in- and above-water radiometry should be kept below the ideal thereshold of 1% (see Chapter 1 on *Elements of Marine Optical Radiometry Data and Analysis*). Table 3.2 lists the best-effort uncertainties achievable in the visible spectral region with current technology and expertise.

Table 3.2. Target uncertainties at $k = 1$ for most relevant radiometric quantities.

	L_u	L_i	L_T	E_d	E_u	E_s
Responsivity [%]	2	2	2	1.5	1.5	1.5
Out of band response [%]	1	1	1	1	1	1
Stray light [%]	1[1]	1[1]	1[1]	1[1]	1[1]	1[1]
Immersion factor [%]	0.2			0.5	0.5	
Cosine response [%]				1[2]	2[2]	0.5[1,2]
Linearity [%]	0.1[1]	0.1[1]	0.1[1]	0.1[1]	0.1[1]	0.1[1]
Polarization sensitivity [%]	1	1	1	0.2	0.2	0.2
Sensitivity change [%]	0.2[1]	0.2[1]	0.2[1]	0.2[1]	0.2[1]	0.2[1]

[1] Corrected in the relevant range of variation
[2] With sun zenith angle between 0 and 65°

Table 3.3 summarizes some requirements for spectral bands and radiometer attitude during field operations.

Table 3.3. Target maximum deviations from the nominal values of center wavelengths and width of spectral bands as well as the tolerance on radiometer pointing (*i.e.*, attitude) achievable through best practices.

	L_u	L_i	L_T	E_d	E_u	E_s
Center wavelength [nm]	1	1	1	1	1	1
Band width [nm]	1	1	1	1	1	1
Attitude [°]	5	5	2	2	2	1

15. FUTURE DIRECTIONS

In addition to continuously improving protocols for a comprehensive characterization of radiometers and the implementation of correction schemes reducing uncertainties in field data, it would be relevant to construct libraries of characterization parameters determined across different laboratories for commercial radiometers widely used by the scientific community. Additionally, there is the need for new blue-rich calibration sources better matching the spectral shape of natural light.

REFERENCES

Aas E., 1969: On submarine irradiance measurements. Institute of Physical Oceanography, University of Copenhagen, Copenhagen, Denmark, 23 pp. plus tables and figures.

Austin R.W., 1976: Air-Water Radiance Calibration Factor. Scripps Institution of Oceanography, La Jolla, CA, Technical Memorandum *ML - 76 - 004T*, 8 pp.

Austin R.W. and Halikas G., 1976: The index of refraction of seawater. *SIO Ref. 76-1*, Vis. Lab., Scripps Inst. of Oceanography, La Jolla, California, 64 pp.

Biggar S.F., 1998: Calibration of a visible and near-infrared portable transfer radiometer. *Metrologia*, 35, 701-706.

Brown S.W., Eppeldauer G.P. and Lykke K.R., 2000: NIST facility for spectral irradiance and radiance response calibrations with a uniform source. *Metrologia*, 37, 579-589.

Feinholz M.E., Flora S.J., Yarbrough M.A., Lykke K.R., Brown S.W., Johnson B.C. and Clark D.K., 2009: Stray light correction of the Marine Optical System. *Journal of Atmospheric and Oceanic Technology*, 26(1), 57-73.

Feinholz M.E., Johnson B.C., Voss K.J., Yarbrough M.A. and Flora S., 2017: Immersion Coefficient for the Marine Optical Buoy (MOBY) Radiance Collectors. *Journal of Research of the National Institute of Standards and Technology*, 122, 1-9.

German Institute of Standardization, 1978: *DIN 5032 Teil 1, Deutsche Normen Series*.

Hamadani B.H., Shore A., Roller J., Yoon H.W. and Campanelli M., 2016: Non-linearity measurements of solar cells with an LED-based combinatorial flux addition method. *Metrologia*, 53, 76-85.

Hooker S.B., McLean S., Sherman J., Small M., Lazin G., Zibordi G. and Brown J.W., 2002: The Seventh SeaWiFS Intercalibration Round-Robin Experiment (SIRREX-7), March 1999. *NASA Tech. Memo. 2002-206892, Vol. 17*. Hooker S.B. and Firestone E.R., Eds., NASA Goddard Space Flight Center, Greenbelt, Maryland, 69 pp.

Hooker S.B. and Zibordi G., 2005: Advanced methods for characterizing the immersion factor of irradiance sensors. *Journal of Atmospheric and Oceanic Technology*, 22(6), 757-770.

Johnson B.C., Bruce S.S., Early E.A., Houston J.M., O'Brian T.R., Thompson A., Hooker S.B. and Mueller J.L., 1996: The Fourth SeaWiFS Intercalibration Round-Robin Experiment (SIRREX-4), May 1995. *NASA Tech. Memo. 104566, Vol. 37*, Hooker S.B., Firestone E.R. and Acker J.G., Eds., NASA Goddard Space Flight Center, Greenbelt, Maryland, 65 pp.

Johnson B.C., Fowler J.B., and Cromer C.L., 1998: The SeaWiFS Transfer Radiometer (SXR). *NASA Tech. Memo. 1998-206892, Vol. 1*, Hooker S.B. and Firestone E.R., Eds., NASA Goddard Space Flight Center, Greenbelt, Maryland, 58 pp.

Johnson B.C., Yoon H., Rice J.P. and Parr A.C., 2014: Principles of Optical Radiometry and Measurement Uncertainty. In *Experimental Methods in the Physical Sciences* (*Vol.* 47, pp. 13-67). Academic Press.

Manninen P., Kärhä P. and Ikonen E., 2008: Determining the irradiance signal from an asymmetric source with directional detectors: application to calibrations of radiometers with diffusers. *Applied Optics*, 47(26), 4714-4722.

Meister G., Abel P., Barnes R., Cooper J., Davis C., Godin M., Goebel D., Fargion G., Frouin R., Korwan D., Maffione R., McClain C.R., McLean S., Menzies D., Poteau A., Robertson J. and Sherman J., 2002: The First SIMBIOS Radiometric Intercomparison (SIMRIC-1), April-September 2001, *NASA Tech. Memo. 2002-206892*, NASA Goddard Space Flight Center, Greenbelt, Maryland, 60 pp.

Meister G., Kwiatkowska E.J., Franz B.A., Patt F.S., Feldman G.C. and McClain C.R., 2005: Moderate-Resolution Imaging Spectroradiometer ocean color polarization correction. *Applied Optics*, 44(26), 5524-5535.

Mekaoui S. and Zibordi G., 2013: Cosine error for a class of hyperspectral irradiance sensors. *Metrologia*, 50 (3), 187-199.

Mueller J.L., 1993: The First SeaWiFS Intercalibration Round-robin Experiment SIRREX-1, July 1992. *NASA Tech. Memo. 104566, Vol. 14*, Hooker S.B. and Firestone E.R., Eds., NASA Goddard Space Flight Center, Greenbelt, Maryland, 60 pp.

Mueller J.L., 1995: Comparison of irradiance immersion coefficients for several marine environmental radiometers (MERs), In: Mueller, J.L. and others, Case Studies for SeaWiFS Calibration and Validation, Part 3. *NASA TM 104566, Vol. 27*, Hooker S.B. and Firestone E.R. and Acker J.G., Eds. NASA Goddard Space Flight Center, Greenbelt, Maryland, 67 pp.

Mueller J.L., Johnson B.C., Cromer C.L., Cooper J.W. *et al.* 1994: The Second SeaWiFS Intercalibration Round-robin Experiment SIRREX-2, June 1993. *NASA Tech. Memo. 104566, Vol. 16*, Hooker S.B. and Firestone E.R., Eds., NASA Goddard Space Flight Center, Greenbelt, Maryland, 121 pp.

Mueller J.L., Johnson B.C., Cromer C.L., Hooker S.B., McLean J.T. and Biggar S.F., 1996: The Third SeaWiFS Intercalibration Round-Robin Experiment (SIRREX-3), 19-30 September 1994. *NASA Tech. Memo. 104566, Vol. 34*, Hooker S.B., Firestone E.R. and Acker J.G., Eds., NASA Goddard Space Flight Center, Greenbelt, Maryland, 78 pp.

Ohde T. and Siegel H., 2003: Derivation of immersion factors for the hyperspectral TriOS radiance sensor. *Journal of Optics A: Pure and Applied Optics*, 5(3), L12-L14.

Parr A.C. and Johnson B.C., 2011: The use of filtered radiometers for radiance measurement. *Journal of Research of the National Institute of Standards and Technology*, 116(5), 751-760.

Petzold T.J. and Austin R.W., 1988: Characterization of MER-1032. *Tech.Memo.*EV-001-88t, Vis.Lab., Scripps Institution of Oceanography, La Jolla, California, 56 pp.

Quan X. and Fry E.S., 1995: Empirical equation for the index of refraction of seawater. *Applied Optics*, 34, 3477-3480.

Riley T. and Bailey S., 1998: The Sixth SeaWiFS Intercalibration Round-Robin Experiment (SIRREX-6) August—December 1997. *NASA/TM-1998-206878*. NASA, Goddard Space Flight Center, Greenbelt, Maryland, 26 pp.

Seckmeyer G. and Bernhard G., 1993: Cosine error correction of spectral UV-irradiances. In *Atmospheric Radiation* (*Vol.* 2049, pp. 140-152). International Society for Optics and Photonics.

Talone M., Zibordi G., Ansko I., Banks A.C. and Kuusk J., 2016: Stray light effects in above-water remote-sensing reflectance from hyperspectral radiometers. *Applied Optics*, 55(15), 3966-3977.

Talone M. and Zibordi G., 2016: Polarimetric characteristics of a class of hyperspectral radiometers. *Applied Optics*, 55(35), 10092-10104.

Talone M. and Zibordi G., 2018: Nonlinear response of a class of hyper-spectral radiometers. *Metrologia*, 55, 747-758.

Walker J.H., Saunders R.D., Jackson J.K., and McSparron D.A., 1987: Spectral Irradiance Calibrations. NBS Special Publication 250--20, U.S. Dept. of Commerce, National Bureau of Standards, Washington, DC, 37 pp. plus appendices.

Westlake D. F., 1965: Some problems in the measurement of radiation under water. A review. *Photochemistry and Photobiology*, 4, 849–868.

White D.R., Clarkson M.T., Saunders P., and Yoon H.W., 2008: A general technique for calibrating indicating instruments. *Metrologia*, 45, 199-210.

Yoon H.W. and Gibson C.E., 2011: NIST Measurement Services: Spectral Irradiance Calibrations. NIST Special Publication 250-89, 132 pp.

Yoon H.W., Graham G.D., Saunders R.D., Zong Y. and Shirley E.L., 2012: The distance dependences and spatial uniformities of spectral irradiance standard lamps. In *Earth Observing Systems XVII* (*Vol.* 8510, p. 85100D). International Society for Optics and Photonics.

Zibordi G., 2006: Immersion factor of in-water radiance sensors: assessment for a class of radiometers. *Journal of Atmospheric and Oceanic Technology*, 23(2), 302-313.

Zibordi G. and Bulgarelli B., 2007: Effects of cosine error in irradiance measurements from field ocean color radiometers. *Applied Optics*, 46 (22), 5529-38.

Zibordi G. and Darecki M., 2006: Immersion factors for the RAMSES series of hyper-spectral underwater radiometers. *Journal of Optics A: Pure and Applied Optics*, 8(3), 252-258.

Zibordi G., D'Alimonte D., van der Linde D., Berthon J.-F., Hooker S.B. and Brown J.W., 2003: New Laboratory Methods for Characterizing the Immersion Factor of Irradiance Sensors. *NASA Tech. Memo. 2003-206892, Vol. 26*, Hooker S.B. and Firestone E.R., Eds., NASA Goddard Space Flight Center, Greenbelt, Maryland, 34 pp.

Zibordi G., D'Alimonte D., van der Linde D., Berthon J.-F., Hooker S.B., Mueller J.L., Lazin G. and MacLean S., 2002: The Eighth SeaWiFS Intercalibration Round-Robin Experiment (SIRREX-8), September – December 2001. *NASA Tech. Memo. 2002-206892, Vol. 21*, Hooker S.B. and Firestone E.R., Eds., NASA Goddard Space Flight Center, Greenbelt, Maryland, 43 pp.

Zibordi G., Hooker S.B., Mueller J.L. and Lazin G., 2004. Characterization of the immersion factor for a series of in-water optical radiometers. *Journal of Atmospheric and Oceanic Technology*, 21(3), 501-514.

Zibordi G., Talone M. and Jankowski L., 2017: Response to Temperature of a Class of In Situ Hyperspectral Radiometers. *Journal of Atmospheric and Oceanic Technology*, 34(8), 1795-1805.

Chapter 4: In-Water Radiometry Measurements and Data Analysis

Kenneth J. Voss[1] and Giuseppe Zibordi[2]

[1] *University of Miami, Coral Gables, Florida, USA*
[2] *European Commission, Joint Research Centre, Ispra, Italy*

1. INTRODUCTION

In-water radiometric profiling is a reliable methodology to measure the spectral upwelling radiance $L_u(z,\lambda)$, downward irradiance $E_d(z,\lambda)$ and additionally (desirable to support the quality assurance of profile data products and bio-optical investigations at large, but not a requirement for strict validation activities) the upwelling irradiance $E_u(z,\lambda)$, at various depths *z*. These measurements are commonly performed with profiling systems such as free-falls or floats in conjunction with the collection of above-water downward spectral irradiance data $E_s(\lambda)$. Primary data products from profile measurements, in the context of satellite validation, are the values extrapolated to the sub-surface depth $z = 0^-$: $L_u(0^-,\lambda)$, $E_d(0^-,\lambda)$ and $E_u(0^-,\lambda)$. Reliable extrapolations require measurements collected in the first optical depth and the capability of producing a number of measurements per unit depth to allow the minimization of the perturbing effects due to wave focusing and defocusing.

Radiometric data supporting satellite ocean color validation activities must be acquired during clear sky conditions (at least with clear sun and low cloud coverage) in regions affected by negligible bottom perturbations and located far enough from land to assume negligible adjacency effects in satellite data. The application of this last requirement is challenged by the dependence of adjacency effects on the distance from land and its spectral albedo, and additionally on water reflectance and sensor signal-to-noise ratio (Bulgarelli and Zibordi 2018). For practical use, it is recommended that *in situ* data are collected at a distance from the coast at least exceeding five nautical miles, still recognizing that such a distance my not ensure negligible adjacency effects.

The following sections mostly focus on free-fall optical profiling. When appropriate, alternative in-water methods relying on profiling floats and buoy systems, which share common deployment and data processing elements with free-fall optical profiling, are discussed.

2. MEASUREMENTS

In-water radiometric profiles primarily rely on deployment systems such as free-falls operated up to some tens of meters from deployment platforms (Waters *et al.* 1990, Hooker and Maritorena 2000). These measurement systems, which allow sampling from near the surface up to several tens of meters depth by minimizing the impact of deployment platforms (Gordon 1985, Voss *et al.* 1986), have replaced the previous winched systems requiring extended analysis to quantify superstructure perturbations affecting radiometry data (Doyle and Zibordi 2002).

Besides avoidance of superstructure perturbations, a number of additional deployment requirements must be met to minimize uncertainties in measurements. These imply: i) using radiometers and deployment devices (*e.g.*, free-falls) minimizing the so-called self-shading resulting from the perturbation of the light field by the measurement system itself (Gordon and Ding 1992); ii) producing a statistically significant number of measurements from near the sea surface up to a few meters depth ideally with vertically homogeneous optical properties of the water; iii) determining the pitch and roll of each measuring component (*e.g.*, free fall and above-water reference unit); and, iv) regularly recording system offsets (*i.e.*,

dark-signals for optical sensors and pressure tare for depth sensors) to allow for the removal of potential unwanted errors in recorded data.

Avoidance of perturbations by deployment structures

The complete avoidance of perturbations by deployment structures is a mandatory requirement for all radiometric measurements, and as previously stated, free falls offer the capability of deploying the measurement system far away from the deployment structure. To a first approximation, the minimum safe deployment distance will vary with the optical properties of the water. By considering deployments performed from the stern of a ship with the sun well away from the bow and recognizing that the various quantities measured (*i.e.*, $E_d(z,\lambda)$, $E_u(z,\lambda)$, and $L_u(z,\lambda)$) are affected differently by the deployment structure as a function of distance, a practical approach would suggest profiling at a distance that ensures negligible effects to any quantity in any spectral band. Following Mueller *et al.* (2003), the sampling distance d from large deployment structures should be $d > 3/K_m$, with K_m indicating the minimum spectral value for the sub-surface values of $K_d(\lambda)$, or $K_u(\lambda)$, or $K_L(\lambda)$ (*i.e.*, near-surface diffuse attenuation coefficients determined from profile values as detailed in the section on *Extrapolation of sub-surface values*). Such a conservative approach, however, may greatly overestimate distance in oligotrophic waters.

In the case of $E_s(\lambda)$ measurements, superstructure perturbations can only be avoided by deploying the radiometer above any obstacle that may be seen by the FOV of the radiometer. Such a fundamental requirement is often challenged by the difficulty of reaching the highest locations of deployments structures (*e.g.*, ships) well away from sources of pollution and the operational need to ensure daily maintenance to radiometers. A practical solution is often offered by the use of telescoping poles operated at the most convenient location.

Specific systems, such as profiling floats, may not have E_s sensors (Gerbi *et al.* 2016). In this case $E_s(\lambda)$ can be determined from $E_d(0^-,\lambda)$ (*e.g.*, $E_s(\lambda) \approx 0.96 \cdot E_d(0^-,\lambda)$). It must be recognized, however, that this determination of $E_s(\lambda)$ is affected by focusing and defocusing (Zibordi *et al.* 2004). Because of this, and in view of minimizing uncertainties, it is emphasized that $E_s(\lambda)$ should be derived from in-water determinations of $E_d(0^-,\lambda)$ only if $E_s(\lambda)$ cannot be directly measured. Another alternative, applicable in the absence of both $E_s(\lambda)$ and $E_d(0^-,\lambda)$ values, is provided by the theoretical determination of $E_s(\lambda)$. Such a solution implemented through the computation of the diffuse atmospheric transmittance (Tanré *et al.* 1979), has shown satisfactory results during clear sky conditions (Zibordi 2012), but with greater uncertainty and requiring knowledge of the aerosol optical depth.

Self-shading minimization

Self-shading implicitly effects $E_u(z,\lambda)$ and $L_u(z,\lambda)$ data (Gordon and Ding 1992). This perturbation varies with the size of the radiometers, the water optical properties, and the illumination conditions. Additionally, any auxiliary component of the profiling system, in addition to radiometers, may perturb measurements. Thus, aside from using radiometers and system components with small dimensions, it is recommended that: i) L_u radiometers are always operated on the side of the profiling system directly illuminated by the sun and at a distance from the main components of the device to warrant a clear FOV; and, ii) E_u and E_d radiometers must be located in the lowermost and uppermost locations of the profiling system, respectively, so that no single component of the device falls in their FOV.

Bio-fouling avoidance

Bio-fouling generally affects any optical component operated in water for extended periods. Thus, bio-fouling is not an issue for manually operated systems but is an issue for autonomous floats or buoy systems. Typically, due to the growth of bacteria and algae, the problem can be mitigated by shutters covering the radiometer fore optics when data are not collected, or alternatively installing rings or plates

of copper near the fore optics. In the case of floats, the problem is minimized by positioning the system in deep, cold water when not in operation.

Depth resolution

Waves introduce focusing and defocusing perturbations in profile data (Zaneveld *et al.* 2001). These effects vary with the size of the detector (Darecki *et al.* 2011), the optical properties of water, the deployment speed, the illumination and surface wave conditions, and, when applicable, the integration time. A limited number of data in the extrapolation depth may thus become the source of significant uncertainties in computed sub-surface values. Consequently, it is essential that the density of measurements (*i.e.*, the number of data per unit depth) comprehensively represents the light field variability at each measurement depth (Zibordi *et al.* 2004, D'Alimonte *et al.* 2010). A statistically representative number of data per unit depth requires a low deployment speed or a high sampling rate, or better, a combination of the two (noting that light variability is better captured by decreasing the deployment speed rather than increasing the sampling rate). While some profilers can meet requirements on depth resolution (Hooker *et al.* 2013), others may exhibit limits both in deployment speed (that may not be reduced below a specific limit to ensure an acceptable system attitude while profiling) or in sampling rate. In such a case, a practical solution is offered by the combination of successive individual profiles into a single one or the collection of a single composite profile comprising data from successive concatenated casts (Zaneveld *et al.* 2001, Zibordi *et al.* 2004, Voss *et al.* 2010). This technique, so-called multicasting (see Figs. 4.1 and 4.2), was shown effective in lessening wave perturbations in sub-surface radiometric products from both multispectral and hyperspectral systems (D'Alimonte *et al.* 2018). Importantly, multicasting must not be construed as the averaging of data products from the analysis of independent casts nor the binning of data versus depth across various casts.

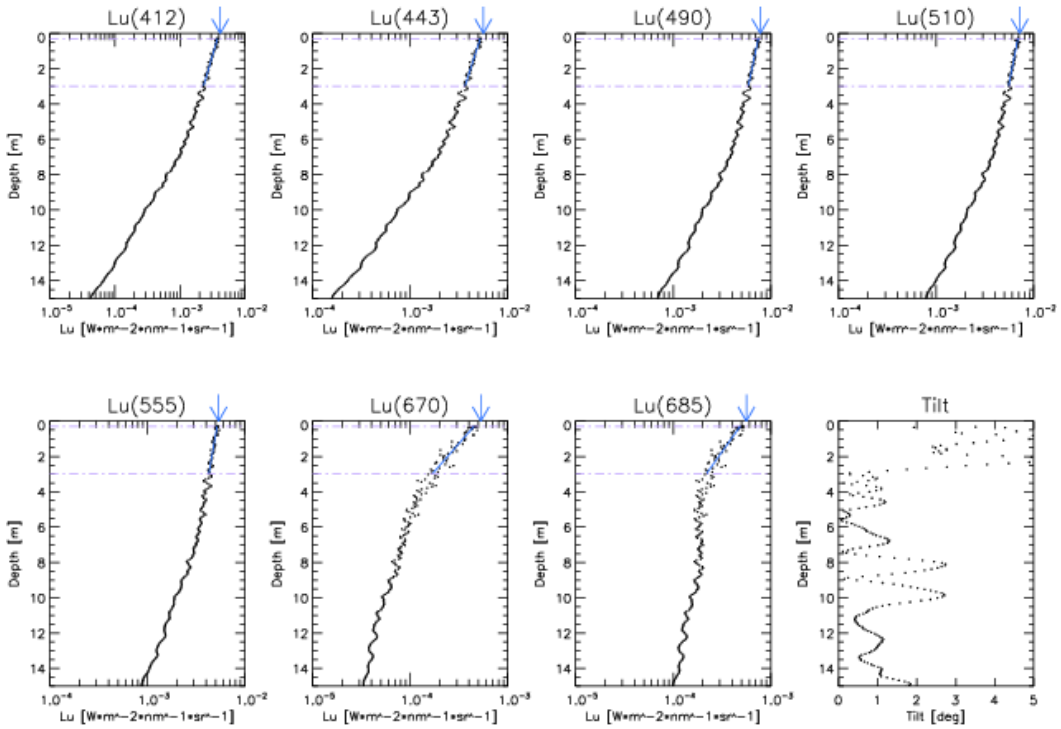

Figure 4.1: An individual multispectral profile of $L_u(z,\lambda)$ *in the 412-685 nm interval. The last panel in the lower row displays the tilt of the* L_u *sensor as a function of depth. The extrapolation chosen between 0.3 m and 3.0 m, includes 40 measurements (i.e., ~15 measurements per meter). The blue arrows indicate the sub-surface extrapolated value.*

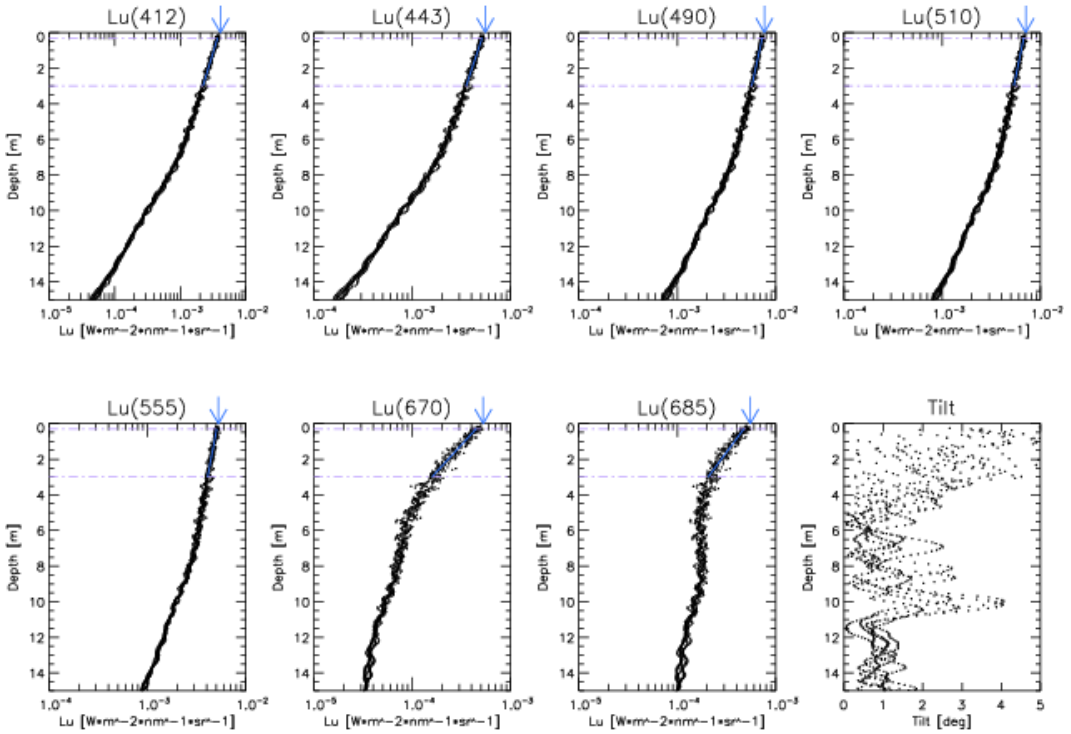

Figure 4.2: A multicast profile comprising 5 consecutive multispectral profiles in the 412-685 nm interval. The last panel on the lower row displays the tilt of the L_u sensor as a function of depth. The extrapolation chosen between 0.3 m and 3.0 m, includes 191 measurements (i.e., ~71 measurements per meter). The blue arrows indicate the sub-surface extrapolated value.

Specific investigations indicated that the density of measurements reducing the uncertainty below a given threshold significantly changes for the various sensors (*i.e.*, L_u, E_d, and E_u) as a function of sea state and optical properties of water. By choosing a 2% uncertainty target for wave perturbations affecting sub-surface values computable from profile data, and combining results from studies on both multispectral and hyperspectral sensors (Zibordi *et al.* 2004, D'Alimonte *et al.* 2018), it is estimated that for the visible portion of the spectrum a minimum of 10, 50 and 20 measurements per meter are required for $L_u(z,\lambda)$, $E_d(z,\lambda)$ and $E_u(z,\lambda)$, respectively. Obviously, a more stringent target uncertainty implies more measurements per unit depth. These measurements per meter, which are a function of the sampling rate, determine the minimum number of independent profiles or concatenated casts necessary to satisfy depth resolution requirements.

It is, however, important to mention that the probability distribution of $E_d(z,\lambda)$ and on a lesser extent of $L_u(z,\lambda)$ and $E_u(z,\lambda)$, is highly asymmetric at shallow depths (Gernez *et al.* 2011). This impacts the sampling of the various radiometric quantities with depth and becomes the source of additional uncertainties affecting extrapolated values.

Depth offset and dark-signal recording

The offsets of depth sensors and the dark-signal of radiometers, *i.e.*, the signals measured with the profiling system out of the water and the optical sensors with the apertures covered, generally exhibit temperature dependence. These depth offsets and dark-signals can easily change with time as a function of the environmental conditions. It is therefore recommended that each sequence of optical measurements is accompanied by their determinations. Also, when there is a large difference between the air and water temperatures, the in-water radiometers should be allowed to equilibrate with water temperature at the beginning of the measurement station. Ideally, thermistors inside radiometers would provide access to

temperature values allowing corrections for non-negligible changes in dark-signals with temperature while profiling.

Besides radiometers, depth sensors also exhibit offset changes with temperature and atmospheric pressure. Since the accuracy of depth is essential for the determination of accurate sub-surface values (see the section on *Operating depths and accuracy* in Chapter 2), the depth offset should always be recorded for each deployment or sequence of deployments.

Measurement sequence

Each measurement sequence should provide contemporaneous measurements of $E_s(\lambda)$, $L_u(z,\lambda)$, $E_d(z,\lambda)$, and ideally $E_u(z,\lambda)$. Best practice suggests that each determination of sub-surface values should rely on profiles (*i.e.*, single or multiple in the case of multicasting) collected during a measurement sequence lasting a very few minutes. Multiple measurement sequences are fundamental to support the quality control of data and additionally to quantify the environmental perturbations affecting $L_u(0^-,\lambda)$, $E_d(0^-,\lambda)$, and $E_u(0^-,\lambda)$. Finally, as already anticipated, each measurement sequence, or multiple sequences, should include specific depth offset and dark-signal measurements.

Essential ancillary data and metadata

Several ancillary data and metadata are required for the processing and quality check of in-water radiometric data. These comprise date and time (UTC); longitude and latitude; bottom depth; cloud cover (likely documented through digital pictures or videos); sea state; wind speed and direction; air and water temperature; barometric pressure; water salinity. Additional quantities needed for the correction of the self-shading perturbations (see next section) are the total spectral absorption coefficient of water $a(\lambda)$ and the spectral diffuse-to-direct irradiance ratio $I_r(\lambda)$. This latter quantity could be determined experimentally from $E_s(\lambda)$ measurements by alternatively measuring the downward irradiance with the direct sun irradiance occulted (*i.e.*, the diffuse component only) and unocculted (*i.e.*, the diffuse plus direct components), both in the absence of tilt perturbations.

The attitude of sensors with respect to the vertical is a critical factor for $E_s(\lambda)$, $E_d(z,\lambda)$, $E_u(z,\lambda)$ measurements and slightly less for $L_u(z,\lambda)$. Thus, in view of allowing the removal of data affected by excessive tilts, it is essential that roll and pitch are measured and recorded concurrently with radiometric values for both in-water and in-air systems. Nevertheless, in the case of systems relying on radiometers delivering data at variable sampling rate (*i.e.*, adjusting the integration time as a function of light intensity), roll and pitch measurements should be oversampled with respect to the radiometric data. This would provide the capability to accurately assess the radiometer attitude for data collected applying a long integration time (*e.g.*, several hundreds of milliseconds) during which the sensor asset may change.

Rotating shadow-bands can be applied to measure the diffuse downward irradiance to determine the ratio $I_r(\lambda)$ (Zibordi *et al.* 2002, Hooker *et al.* 2003). This implies the use of bands with dimension and rotating speed adjusted to allow for occulting the direct sun irradiance at the radiometer collector over several consecutive acquisitions. Most favorable conditions, which would also help to minimize the negative impact of ship motion, are those combining slow speed for the band and high sampling rate for both the radiometric and related roll and pitch data.

It is recommended that both ancillary data and metadata are systematically recorded and properly entered into the data management system in view of supporting their comprehensive exploitation during the successive processing of the in-water radiometric data.

3. DATA ANALYSIS

Data products from profile data are the sub-surface radiometric values $L_u(0^-,\lambda)$, $E_d(0^-,\lambda)$ and $E_u(0^-,\lambda)$, and their respective attenuation coefficients $K_L(\lambda)$, $K_d(\lambda)$ and $K_u(\lambda)$ (see the section on

Extrapolation of sub-surface values), determined in a near-surface extrapolation layer. Accuracy of derived data products, in addition to the accuracy of the depth values and of the calibration and characterization factors applied to radiometry, mostly depend on: i) the minimization of the impact of outliers or in general of any measurement artifact (*e.g.*, elevated tilt); ii) the extrapolation layer selected; iii) the extrapolation method; and, iv) the accuracy of the correction applied for self-shading perturbations.

The values of sub-surface radiometric quantities cannot be directly measured due to wave perturbations. This section introduces the methods required to process profile measurements of $L_u(z,\lambda)$, $E_d(z,\lambda)$ and $E_u(z,\lambda)$ in view of deriving the sub-surface quantities.

Depth offset and dark-signal removal, corrections for the non-ideal performance of sensors, and calibration

The instrument dark-signal in each channel, ideally recorded for each profile or sequence of profiles, must be subtracted from the raw data before any further processing. This also applies to the depth data by accounting for the relative distance offsets between the depth sensor transducer and the aperture of the L_u, E_d and E_u radiometers. All corrections must be applied to minimize the non-ideal performance of the radiometer (*e.g.*, temperature dependence, linearity) in conjunction with the application of immersion factors and the absolute calibration coefficients. The latter should result from pre- and post-field calibrations and eventually the supplementary use of relative field calibrations performed with portable sources to monitor the stability of the sensor responsivity with time.

These early data reduction steps require consistent and comprehensive access to any information needed for the processing and successive re-processing of field measurements. Best practice suggests an efficient data management system ensuring unique association of field data (*i.e.*, profile and, depth offset and dark-signal) to measurement campaigns, stations, casts, essential ancillary data, and, obviously, radiometer tags and their calibration coefficients and correction factors.

Quality assurance of input data

Quality assurance should be applied to field measurements before processing to identify measurement sequences hindered by poor input data. First, in-water profile data and $E_s(\lambda)$ measurements affected by excessive roll or pitch should be removed through the application of tilt thresholds. These thresholds need to be chosen by trading off the number of measurements and the need for accuracy, appreciating that thresholds may vary from case to case as a function of the sea state and of the deployment platform (*e.g.*, the size of the ship). Still, threshold of 2° (and up to 5° for $L_u(z,\lambda)$) should be an upper limit for the in-water data, while it should ideally not exceed 1° or maximum 2° for E_s measurements.

Additional quality checks should remove those measurement sequences affected by significant variability of $E_s(\lambda)$ not explained by tilt perturbations. In particular, understanding the requirement of clear sun and low cloudiness, quality checks applied to $E_s(\lambda)$ values (likely supported by analysis of digital pictures collected during field measurements) should aim at identifying those measurement sequences likely contaminated by clouds (including clouds shadow). These checks should depend on very small thresholds, ideally a few percent change of the measured signal.

Quality checks should apply to differences between the pre- and post-field calibrations of optical sensors. This step may benefit from field checks performed with portable reference sources. Thresholds in calibration differences should obviously account for the deployment duration and the working conditions. When considering well-maintained systems (*e.g.*, regularly cleaned) and operated for a short time (*e.g.*, up to a few weeks), differences between pre- and post-field calibrations should mostly be explained by calibration uncertainties. Slightly larger differences due to the decay over time of the sensitivity of the sensor may imply actions such as interpolation with time of calibration coefficients. A major difference, which may negatively impact the determination of accurate radiometric products, should lead to the

rejection of profile data unless the cause can be isolated to some unique event and a timeline for applying the pre- or post-calibrations determined.

Finally, wave perturbations can significantly impact measurements near the surface. As such, sufficient measurements are required in the very-near-surface to perform regressions, or conversely, in the case of fixed-depth measurements for averaging over a time scale longer than that of surface fluctuations. The number of measurements should then reflect that already indicated in the section on *Depth resolution*. A measurement density not fulfilling requirements in the extrapolation layer should lead to the rejection of the entire profile data.

Normalization by surface irradiance

Restating the fundamental requirement of performing radiometric measurements during ideal illumination conditions (*i.e.*, clear sun and low cloudiness), changes in the illumination condition during measurements simply due to sun zenith changes may affect the accuracy of derived data products. By introducing the time dependence t, these changes are minimized through normalization by $E_s(\lambda,t)$ measured over the duration of a radiometric cast simultaneously with $L_u(z,\lambda,t)$, $E_u(z,\lambda,t)$ and $E_d(z,\lambda,t)$. Recalling that in-water radiometric data and $E_s(\lambda,t)$ measurements are subject to independent filtering for tilt perturbations, the available $E_s(\lambda,t)$ measurements may need to be interpolated to substitute for missing values at times t matching the in-water data.

A fundamental step in data reduction is to account for the effects of changes in the incident light field during data collection. Using $\Im(z,\lambda,t)$ to represent the various radiometric quantities (*i.e.*, $L_u(z,\lambda,t)$, $E_u(z,\lambda,t)$ and $E_d(z,\lambda,t)$), and assuming that the transmission of $E_s(\lambda,t)$ through the surface does not vary with time, changes due to the incident light are accounted for through

$$\Im_0(z,\lambda,t_0) = \frac{\Im(z,\lambda,t)}{E_s(\lambda,t)} E_s(\lambda,t_0) \tag{4.1}$$

where $\Im_0(z,\lambda,t_0)$ is the radiometric quantity normalized to the incident light field at t_0, $E_s(\lambda,t_0)$, with t_0 generally chosen to coincide with the beginning of the acquisition sequence (but, a different reference time can be confidently chosen).

The former normalization process implies the existence of $E_s(\lambda,t)$ collected at the same time t of $\Im(z,\lambda,t)$. This need is challenged by tilts affecting $E_s(\lambda,t)$ measurements (which may lead to the removal of a substantial amount of values) and, additionally, by different sampling rates characterizing radiometers operated with different integration times. Benefitting from the clear sky requirement, the former limitations are solved by linearly interpolating the existing $E_s(\lambda,t)$ as a function of t during measurement intervals not exceeding a very few minutes.

Finally, it is important that the spectral bands of the E_s sensor closely match those of the in-water sensors to avoid introducing spectral artifacts in the normalized data. In fact, any appreciable spectral mismatch of inter-sensor bands would lead to an increase of uncertainties in the normalized and, in general, any derived radiometric quantity.

Extrapolation of sub-surface values

The first step in the determination of sub-surface radiometric values from profile measurements is the determination of the extrapolation interval. Best practice suggests that regressions are performed using measurements in the top optical depth (*i.e.*, between the surface and $1/K_d(\lambda)$). However, inhomogeneity of the extrapolation layer together with focusing and defocusing effects may complicate the determination of the proper depth interval.

The process leading to the determination of the extrapolation interval should benefit from the visualization of profile data at various spectral bands in view of choosing the upper (typically within a few tens of centimeters from the surface) and lower (at least a few meters below the surface) boundaries. Trial linear regressions of log-transformed data as a function of depth, may provide evidence of the actual exponential decay of radiometric values in the extrapolation interval selected. Successive trials and the

analysis of the standard deviation of differences between fitted and actual data at incremental depth intervals may support the selection of the most appropriate extrapolation interval. This processing step should also include filtering outliers that may affect the very near-surface data. A convenient way is to apply a data exclusion threshold based on the standard deviation of the difference between fitted and actual data. For instance, individual data should be removed when the difference between the fitted and actual value exceeds three standard deviations.

The selection of the extrapolation layer can be independently performed for each spectral band. This choice, which allows limiting the impact of inelastic scattering that restricts the depth of the extrapolation layer in the red bands, should only be applied to cases exhibiting high vertical homogeneity of the optically active components across the maximum extrapolation interval. Conversely, in the presence of vertical inhomogeneity, which often occurs in coastal optically complex waters, a single extrapolation layer for all the bands is preferable in view of producing radiometric products for the same water layer and consequently for the same vertical distribution of water constituents.

Omitting the dependence with time and assuming that measurements satisfy the requirement of linear decay of $\ln \Im_0(z, \lambda)$ with depth in the extrapolation interval identified by $z_0 < z < z_1$, the sub-surface values $\Im_0(0^-,\lambda)$ (*i.e.*, $L_u(0^-,\lambda)$, $E_d(0^-,\lambda)$ and $E_u(0^-,\lambda)$) are determined as the exponential of the intercepts from the least-squares linear regressions of $\ln \Im_0(z, \lambda)$ versus z. The negative values of the slopes of the regression fits are the so-called diffuse attenuation coefficients $K_\Im(\lambda)$ (*i.e.*, $K_L(\lambda)$, $K_d(\lambda)$, and $K_u(\lambda)$) for the selected extrapolation interval. Thus, the determination of the sub-surface values is addressed as a linear problem relying on the logarithmic transformation of radiometric data as a function of depth. Specifically, by assuming the exponential decay of $\Im_0(z,\lambda)$ and a constant value of $K_\Im(\lambda)$ in the extrapolation layer

$$\Im_0(z,\lambda) = \Im_0\left(0^-,\lambda\right)\cdot e^{-K_\Im(\lambda)\cdot z} \tag{4.2}$$

in logarithmic scale given by

$$\ln\left[\Im_0(z,\lambda)\right] = \ln\left[\Im_0\left(0^-,\lambda\right)\right] - K_\Im(\lambda)\cdot z \tag{4.3}$$

the determination of $\Im_0\left(0^-,\lambda\right)$ and $K_\Im(\lambda)$ is obtained from the minimization of the sum-of-square errors SSE_L for different depths z_i (with $i = 1, \ldots, N$)

$$SSE_L\left[\Im_0\left(0^-,\lambda\right), K_\Im(\lambda)\right] = \sum_{i=1}^{N}\left\{\ln\left[\Im_0(z_i,\lambda)\right] - \ln\left[\Im_0\left(0^-,\lambda\right) - K_\Im(\lambda)\cdot z_i\right]\right\}^2. \tag{4.4}$$

It is emphasized that the linearity of the log-transformed radiometric profile data with depth is an approximation because of changes in the radiance distribution in the near-surface due to scattering, absorption, wave perturbations, and, additionally, due to inelastic processes such as Raman scattering (Sugihara *et al.* 1984: Stavn and Weidemann 1988: Gordon 1999) and chlorophyll-*a* fluorescence (Gordon 1979) at some wavelengths.

To account for the wave perturbation effect on $E_d(0^-,\lambda)$ and to a lesser extent on $L_u(0^-,\lambda)$ and $E_u(0^-,\lambda)$, an alternative approach for the determination of $\Im_0\left(0^-,\lambda\right)$ and $K_\Im(\lambda)$ is offered by the minimization of the sum-of-square errors SSE_E without using the logarithm of the $\Im_0(z_i,\lambda)$ values (see D'Alimonte *et al.* 2013), *i.e.*,

$$SSE_E\left[\Im_0\left(0^-,\lambda\right), K_\Im(\lambda)\right] = \sum_{i=1}^{N}\left[\Im_0(z_i,\lambda) - \Im_0\left(0^-,\lambda\right)e^{-K_\Im(\lambda)\cdot z_i}\right]^2 \tag{4.5}$$

where minimization techniques such as the Trust-Region algorithm can be applied.

Investigations focussing on the comparison of the two regression approaches (D'Alimonte *et al.* 2013; see also Fig. 4.3) indicated typical differences within 2% for $L_u(0^-,\lambda)$ and values well exceeding 5% for

$E_d(0^-,\lambda)$. These values may, however, become larger without a statistically significant number of measurements per unit depth and the selection of an inappropriate extrapolation layer.

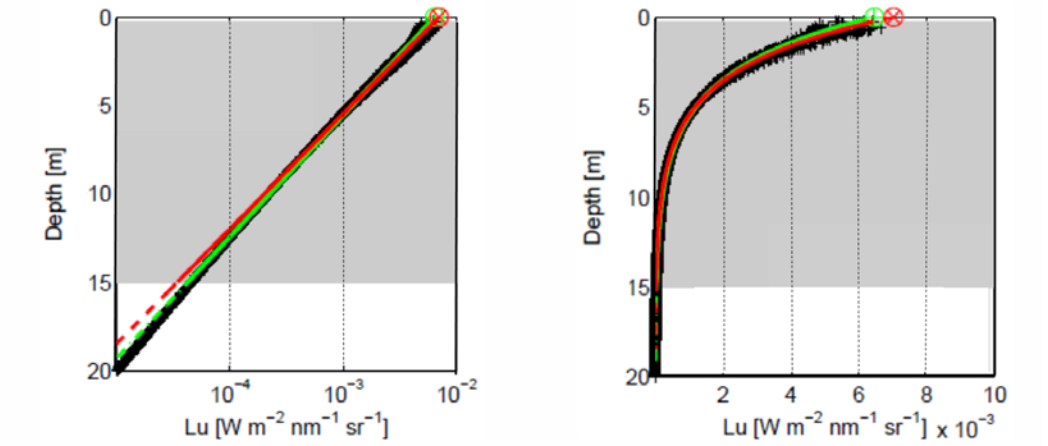

*Figure 4.3. Comparison of extrapolation methods based on logarithmic (green line and symbols) and non-logarithmic (red line and symbols) transformations of data (black symbols) representative of highly scattering waters (redrawn from D'Alimonte et al. 2013), illustrated with both linear (left panel) and logarithmic (right panel) scales. Values resulting from the fit of logarithmically transformed data in the 0.3-15 m extrapolation interval indicate underestimated values of sub-surface L_u (by -8.0%) and of K_L (by 5.5%) with respect to the exponential fit of non-logarithm transformed data (*differences *would decrease through the application of a smaller sub-surface extrapolation layer).*

It is emphasized that extrapolating $E_d(z,\lambda)$, $E_u(z,\lambda)$ and $L_u(z,\lambda)$ to $z=0^-$ becomes very difficult at $\lambda \geq 600$ nm for either method. In fact, with impact increasing from the red to the near-infrared, the rapid decrease in light over an extremely shallow first attenuation length may compete with an increase in flux with depth due to inelastic scattering. Thus, in view of confining uncertainties in sub-surface values within a few percent in these spectral regions, the extrapolations need to be performed using radiometric data collected within the first few tens of centimeters below the surface (Li *et al.* 2016). Still, this could be challenged by waves hindering the capability of assigning accurate depths to radiometric measurements performed within a few centimeters from the surface.

With reference to the depth, it is important to underline the need to assign the exact value *z* to each radiometric measurement by way of accurate depth measurements and rigorous knowledge of the offsets between depth sensor(s) and radiometers. In the case of radiometric and depth data collected at a constant sampling rate, which is typical of multispectral profilers, the association of the exact depth is straightforward: each radiometric value generally has a corresponding simultaneous depth measurement. Conversely, the determination of the exact depth *z* becomes more difficult in the case of radiometric and depth data collected at a variable sampling rate. This is the typical case provided by hyperspectral systems, often exhibiting a diverse sampling frequency for each sensor as a result of using different integration times that may reach several seconds. In such a case, best practice would suggest that the depth *z* assigned to each radiometric value is determined accounting for: i) the exact depths corresponding to the start, and end, of each radiometric measurement performed with given integration time; and ii) a weight based on the diffuse attenuation coefficient (D'Alimonte *et al.* 2018). Specifically, assuming an exponential decay of the radiometric profile data with depth, the value of *z* associated with each radiometric measurement $\Im(z,\lambda,t)$ can be determined as

$$z = \frac{1}{-K^*_{\Im}(\lambda)}\left[\ln\left(e^{-K^*_{\Im}(\lambda)\cdot z^*_s} - e^{-K^*_{\Im}(\lambda)\cdot z^*_e}\right) - \ln\left(-K^*_{\Im}(\lambda)\cdot(z^*_s - z^*_e)\right)\right] \quad (4.6)$$

where $K^*_{\Im}(\lambda)$ is the attenuation coefficient determined from the profile data using an extrapolation interval encompassing the depths z^*_s and z^*_e.

To conclude, in addition to $L_u(0^-, \lambda)$, $E_d(0^-, \lambda)$, ideally $E_u(0^-, \lambda)$, and the related $K_L(\lambda)$, $K_d(\lambda)$, and $K_u(\lambda)$ coefficients, other derived quantities of interest for remote sensing applications are the dimensionless irradiance reflectance at depth 0^-, $R(0^-,\lambda)$ defined as $E_u(0^-,\lambda)/E_d(0^-,\lambda)$, and the Q-factor at nadir, $Q_n(0^-,\lambda)$ in units of sr defined as $E_u(0^-,\lambda)/L_u(0^-,\lambda)$. Finally, fundamental to ocean color applications is the water-leaving radiance $L_w(\lambda)$ in units of $\mu W\ cm^{-2}\ nm^{-1}\ sr^{-1}$ given by

$$L_w(\lambda) = L_u(0^-, \lambda)\frac{1-\rho(\lambda)}{n^2_w(\lambda)} \quad (4.7)$$

where $n_w(\lambda)$ is the spectral refractive index of water and $\rho(\lambda)$ the reflectance factor of the sea surface for near normal incidence. By neglecting the spectral dependence, the term $[1-\rho(\lambda)]/n^2_w(\lambda)$ is often assumed constant and set to 0.543 (Austin 1974). Recent investigations, however, showed that this approximation can introduce spectral uncertainties reaching 1% (Voss and Flora 2017).

Quality control of data products

The quality control of data products can rely on a number of checks. First, $K_{\Im}(\lambda)$ must exhibit positive values, close or exceeding those of pure water. Negative values indicate regression problems likely due to the lack of measurements in the extrapolation layer, high perturbations due to wave focussing and defocussing, or issues with inelastic scattering effects. Additional checks should involve spectral comparisons of $E_s(\lambda)$ and $E_d(0^-,\lambda)$ when both are available. Significant differences exceeding the expected ~4% between the two quantities, may indicate large wave perturbations, or an inappropriate selection of the extrapolation interval, both leading to a poor determination of $E_d(0^-,\lambda)$ data. Large differences between $E_s(\lambda)$ and $E_d(0^-,\lambda)$ may also indicate problems with the attitude of sensors, issues with the sensor calibration or characterization (*e.g.*, cosine and temperature responses), which may lead to differences as a function of the field conditions (*e.g.*, sun zenith angle and, air and water temperature). Finally, when $E_u(0^-,\lambda)$ data are available, unrealistic spectral shape values of $Q_n(0^-,\lambda)$ would again suggest calibration and characterization issues with the related sensors or alternatively extrapolation problems.

Corrections for instrument self-shading

The finite size of underwater radiometers affects the radiance field and induces errors in the measured upwelling radiance and upward irradiance (Gordon and Ding 1992). The problem is further increased by the geometrical complexity of profiling systems composed of radiometers and a number of components of non-negligible size (*i.e.*, hubs, brackets, cables). Therefore, an accurate determination of the shading effects in radiometric measurements performed with profilers implies investigations accounting for the geometric specificity of the various system components (Piskozub *et al.* 2001, Leathers *et al.* 2001, Leathers *et al.* 2004, Shang *et al.* 2017). Still, without minimizing the importance of determining self-shading perturbations from geometrically complex systems, the first level of self-shading correction is possible accounting for the sole radiometers idealized as disks by knowing their diameter, the optical properties of water and the illumination conditions. With reference to this specific correction, Gordon and Ding (1992) evaluated the self-shading error affecting sub-surface upwelling radiance and upward irradiance for an ideal circular sensor of infinitesimal thickness. Through numerical simulations, they estimated errors ranging from a few percent up to several tens of percent. For a given radiometer, the self-shading error is much greater in the near-infrared than in the visible because of the stronger water absorption, and it increases with the concentration of absorbing particles and the absorption coefficient of colored dissolved organic matter.

For practical purposes, the self-shading error $\varepsilon_{\Im}(\lambda)$ for the upwelling radiance or upward irradiance can be defined as

$$\varepsilon_{\Im}(\lambda) = \frac{\Im(0^-,\lambda) - \hat{\Im}(0^-,\lambda)}{\Im(0^-,\lambda)} \tag{4.8}$$

where $\Im(0^-,\lambda)$ indicates the radiometric quantity that would apply in the absence of the instrument, and $\hat{\Im}(0^-,\lambda)$ indicates the experimental quantity determined from field measurements. Gordon and Ding (1992) showed that the error $\varepsilon_{\Im}(\lambda)$ can be expressed as a function of the radius R_d of the radiometer, the absorption coefficient of the medium $a(\lambda)$, the sun zenith θ_0 and the ratio of diffuse-to-direct sun irradiance $I_r(\lambda)$ according to the following parameterization

$$\varepsilon_{\Im}(\lambda) = \frac{\varepsilon_{sun}(\lambda) + \varepsilon_{sky}(\lambda)\cdot I_r(\lambda)}{1 + I_r(\lambda)} \tag{4.9}$$

with

$$\varepsilon_{sun}(\lambda) = 1 - e^{-k_{sun}(\lambda)\cdot a(\lambda)\cdot R_d} \tag{4.10}$$

and

$$\varepsilon_{sky}(\lambda) = 1 - e^{-k_{sky}(\lambda)\cdot a(\lambda)\cdot R_d} \tag{4.11}$$

where $\varepsilon_{sun}(\lambda)$ and $\varepsilon_{sky}(\lambda)$ indicate the errors due to the direct sun irradiance and to diffuse radiance contributions, respectively.

Mueller and Austin (1995) proposed convenient parameterizations for the determination of $\varepsilon_{sun}(\lambda)$ and $\varepsilon_{sky}(\lambda)$ by accounting for the sensor-to-radiometer radius f_R. In particular, for $k_{sun}(\lambda)$ they suggested

$$k_{sun}(\lambda) = (1 - f_R)\cdot k^p_{sun}(\lambda) + f_R \cdot k^e_{sun}(\lambda) \tag{4.12}$$

where $k^p_{sun}(\lambda)$ and $k^e_{sun}(\lambda)$ are terms representing the two extremes of a point sensor or a sensor having the same size as the instrument case, respectively.

Functions for the computation of $k^p_{sun}(\lambda)$, $k^e_{sun}(\lambda)$ and $k_{sky}(\lambda)$, accounting for the additional parameterizations proposed by Zibordi and Ferrari (1995) and formulated using the data published by Gordon and Ding (1992) for $a(\lambda)\cdot R_d < 0.1$ and sun zenith angles $30° < \theta_0 < 70°$, are summarized in Table 4.1.

Actual corrections for self-shading perturbations affecting $\Im(0^-,\lambda)$ are given by

$$\aleph_s(\lambda) = 1 - \varepsilon_{\Im}(\lambda). \tag{4.13}$$

Table 4.1: Functions for the computation of the terms: $k^p_{sun}(\lambda)$, $k^e_{sun}(\lambda)$ and $k_{sky}(\lambda)$. The symbol $\theta_{0w}(\lambda)$ indicates the sun zenith angle in the water (*i.e.*, $\theta_{0w}(\lambda) = \sin^{-1}[\sin\theta_0 / n_w(\lambda)]$).

	L_u	E_u
$k^p_{sun}(\lambda)$	$(2.07 + 00056\cdot\theta_0)/\tan(\theta_{0w})$	$3.41 - 0.0155\cdot\theta_0$
$k^e_{sun}(\lambda)$	$(1.59 + 00063\cdot\theta_0)/\tan(\theta_{0w})$	$2.76 - 0.0121\cdot\theta_0$
$k_{sky}(\lambda)$	$4.61 - 0.87\cdot f_R$	$2.70 - 0.48\cdot f_R$

For computational purposes, the radius of an irradiance sensor approximately corresponds to the radius of the cosine collector. In the case of a radiance sensor, it can be determined as $2h\tan(\theta_F/2)$ where h is the distance between the detector and the optical window of the radiometer, and θ_F is the full-angle FOV.

In the absence of actual determinations of water absorption $a(\lambda)$ for the specific radiometric measurements, its value can be approximated to $a(\lambda) \approx K_d(\lambda)\cos\theta_{0w}$). In addition, in the absence of any experimental determination of the ratio $I_r(\lambda)$, its value can be estimated through theoretical simulations of atmospheric radiative processes.

Uncertainties

The main sources of uncertainty typical of in-water radiometry data products stem from environmental variability and corrections applied to data products (*e.g.*, self-shading). The uncertainties resulting from environmental perturbations such as changes in illumination conditions, the variability of the water optical properties during measurements, and wave perturbations (all affecting sub-surface extrapolations), can be estimated from the standard deviation of sub-surface values $\Im_0\left(0^-,\lambda\right)$ determined from the regression of data from successive radiometric casts.

It is difficult to quantify the uncertainties associated with self-shading for any radiometer system that cannot be idealized as a disk. So, in the case that dedicated computational studies are not available, best practice would suggest a large percentage (*e.g.*, 25%) of the corrections be assigned to the uncertainties.

In the case of the anisotropy corrections, their uncertainties may vary significantly with the correction approach and the water type (Talone et al. 2018). It is suggested that uncertainties make up a large percentage of the corrections in this case too.

Additionally, it is important to consider the determination of radiometric uncertainties affecting derived products such as $R_{rs}(\lambda)$ and $L_{wn}(\lambda)$ resulting from the composition of different data products. For example considering that $L_{wn}(\lambda) = L_w(\lambda)/E_d(\lambda)\cdot E_o(\lambda)$, it is evident that if both the E_d and L_u sensors are calibrated using the same basic source (*e.g.*, a lamp), the systematic component of uncertainties affecting the source cancels out in the ratio. This element should be considered to avoid overestimates of the uncertainties (Zibordi and Voss 2014, Johnson *et al.* 2014).

4. ALTERNATIVE METHODS

In addition to in-water profiling, an alternative in-water radiometric method is provided by the capability of performing measurements at fixed depths. This method is generally implemented through optical buoys specifically designed to host multiple radiometers and to support SVC (Clark *et al.* 1997, Antoine *et al.* 2008) or validation applications at given sites exhibiting unique bio-optical properties. These fixed-depth systems generally provide the possibility of measuring $E_s(\lambda)$, and additionally $L_u(z_i,\lambda)$, $E_d(z_i,\lambda)$, and sometimes $E_u(z_i,\lambda)$, at two or more discrete depths z_i generally set between 1 and 10 m.

A major advantage of fixed-depth systems is the capability of producing a large number of data at each depth (likely benefitting from long integration times), which helps to minimize the impact of wave perturbations through averaging or filtering. The main drawback is the need to implement corrections minimizing the impact of inelastic scattering, which mostly affects the red part of the spectrum or the effects of inhomogeneous vertical distributions of optically significant constituents between the depths of radiometers (Li *et al.* 2016). In fact, as opposed to profiling systems, the availability of measurements at only two or three depths does not allow using regression methods to minimize the impact of a non-exact exponential decay with depth. Still, fixed-depth systems operated in oligotrophic waters can confidently rely on modeling of the in-water radiative processes to determine corrections (Voss *et al.* 2017). An additional element requiring attention is the need to prevent bio-fouling during deployment periods that may last several months.

Another in-water method is that based on floating systems equipped with a single L_u sensor operated at a small depth (*i.e.*, from a few to several tens of centimeters) below the surface and likely several E_d sensors at various depths to allow determination of the near-surface attenuation coefficient (Zibordi *et al.* 2012). These systems, generally designed to be manually operated, provide the advantage of allowing for the collection of a large number of $L_u(z,\lambda)$ values at a depth z close to the sea surface with the additional capability of accounting for the attenuation of the water below the sensor. The appreciable size of system

components hosting the radiometer (*e.g.*, floaters), however, requires dedicated computational efforts to determine self-shading corrections (Leathers *et al.* 2001).

Finally, profiler floats, a subject of recent developments (Gerbi *et al.* 2016), offer the key advantage of operating as profilers and, when at the surface, also acting as floating systems—thus producing both profile and near-surface data.

Last, it is mentioned that processing, quality assurance and control of fixed-depth data from both single- and multiple-depth sensor systems, may benefit from the elements detailed for profiling systems.

5. FUTURE DIRECTIONS

A future objective of in-water profiling radiometry would be the definition of objective extrapolation schemes reducing the impact of subjective decisions, which, despite the adoption of the same protocol, may lead to large uncertainties in data products. From the operational point of view, the development and ongoing maintenance of an open-source community processor for handling and reduction of in-water radiometric measurements—ideally relying on standardized input and output data formats—would be a significant advance for the field.

REFERENCES

Antoine D., Guevel P., Desté J.F., Bécu G., Louis F., Scott A.J. and Bardey P., 2008: The "BOUSSOLE" buoy—A new transparent-to-swell taut mooring dedicated to marine optics: Design, tests, and performance at sea. *Journal of Atmospheric and Oceanic Technology*, 25(6), 968-989.

Austin R.W., 1974: The remote sensing of spectral radiance from below the ocean surface. In: *Optical Aspects of Oceanography*, N.G. Jerlov and E.S. Nielson, Eds., pp 317-344.

Bulgarelli B. and Zibordi G., 2018: On the detectability of adjacency effects in ocean color remote sensing of mid-latitude coastal environments by SeaWiFS, MODIS-A, MERIS, OLCI, OLI and MSI. *Remote Sensing of Environment*, 209, 423-438.

Clark D.K., Gordon H.R., Voss K.J., Ge Y., Broenkow W. and Trees C., 1997: Validation of atmospheric correction over the oceans. *Journal of Geophysical Research: Atmospheres*, 102(D14), 17209-17217.

D'Alimonte D., Shybanov E.B., Zibordi G. and Kajiyama T., 2013: Regression of in-water radiometric profile data. *Optics Express*, 21(23), 27707-27733.

D'Alimonte D., Zibordi G. and Kajiyama T., 2018: Effects of integration time on in-water radiometric profiles. *Optics Express*, 26(5) 5908-5939.

D'Alimonte D., Zibordi G., Kajiyama T. and Cunha J.C., 2010: Monte Carlo code for high spatial resolution ocean color simulations. *Applied Optics*, 49(26) 4936-4950.

Darecki M., Stramski D. and Sokolski M., 2011: Measurements of high-frequency light fluctuations induced by sea surface waves with an Underwater Porcupine Radiometer System. *Journal of Geophysical Research*, 116, C00H9, doi: 10.1029/2011JC007883.

Doyle J.-P. and Zibordi G., 2002: Optical propagation within a three-dimensional shadowed atmosphere–ocean field: application to large deployment structures. *Applied Optics*, 41, 4283–4306.

Gerbi G.P., Boss E., Werdell P.J., Proctor C.W., Haëntjens N., Lewis M.R., Brown K., Sorrentino D., Zaneveld J.R.V., Barnard A.H. and Koegler J., 2016: Validation of ocean color remote sensing reflectance using autonomous floats. *Journal of Atmospheric and Oceanic Technology*, 33(11), 2331-2352.

Gernez P., Stramski D. and Darecki M., 2011: Vertical changes in the probability distribution of downward irradiance within the near-surface ocean under sunny conditions. *Journal of Geophysical Research: Oceans*, 116, C00H07, doi:10.1029/2011JC007156.

Gordon H.R., 1979: Diffuse reflectance of the ocean: the theory of its augmentation by chlorophyll-*a* fluorescence at 685 nm. *Applied Optics*, 18(8), 1161-1166.

Gordon H.R., 1985: Ship perturbations of irradiance measurements at sea, 1: Monte Carlo simulations. *Applied Optics* 24(4) 172-4,182.

Gordon H.R., 1999: Contribution of Raman scattering to water-leaving radiance: A Reexamination. *Applied Optics* 38(15), 3166-3174.

Gordon H.R. and Ding K., 1992: Self shading of in-water optical instruments. *Limnology and Oceanography* 37**,** 491-500.

Hooker S.B. and Maritorena S., 2000: An evaluation of oceanographic radiometers and deployment methodologies. *Journal of Atmospheric and Oceanic Technology*, 17, 811-830.

Hooker S.B., Morrow J.H. and Matsuoka A., 2013: Apparent optical properties of the Canadian Beaufort Sea; Part 2: The 1% and 1 cm perspective in deriving and validating AOP data products. *Biogeosciences*, 10(7), 4511-4527.

Hooker S.B., Zibordi G., Berthon J-F., D'Alimonte D., van der Linde D. and Brown J.W., 2003: Tower-Perturbation Measurements in Above-Water Radiometry. *NASA Tech. Memo. 2003–206892, Vol. 23,* Hooker S.B. and Firestone E.R., Eds., NASA Goddard Space Flight Center, Greenbelt, Maryland, 35 pp.

Johnson B.C., Yoon H., Rice J.P. and Parr A.C., 2014: Principles of Optical Radiometry and Measurement Uncertainty. In *Experimental Methods in the Physical Sciences* (*Vol.* 47, pp. 13-67). Academic Press.

Leathers R.A., Downes T.V. and Mobley C.D., 2001: Self-shading correction for upwelling sea-surface radiance measurements made with buoyed instruments. *Optics Express*, 8(10), 561-570.

Leathers R.A., Downes T.V. and Mobley C.D., 2004: Self-shading correction for oceanographic upwelling radiometers. *Optics Express*, 12(20) 4709-4718.

Li L.H., Stramski D. and Reynolds R.A., 2016: Effects of inelastic radiative processes on the determination of water-leaving spectral radiance from extrapolation of underwater near-surface measurements. *Applied Optics,* 55, 7050-7067.

Mueller J.L. and Austin R.W,. 1995: Ocean Optics Protocols for SeaWiFS Validation, Revision 1. *NASA Tech. Memo. 104566, Vol. 25,* Hooker S.B., Firestone E.R. and Acker J.G., Eds., NASA Goddard Space Flight Center, Greenbelt, Maryland, 67 pp.

Mueller J.L., Morel A., Frouin R., Davis C., Arnone R., Carder K., Lee Z.P., Steward R.G., Hooker S.B., Mobley C.D., McLean S., Holben B.N., Miller M., Pietras C., Knobelspiesse K.D., Fargion G.S., Porter J. and Voss K.J., 2003: Ocean Optics Protocols for Satellite Ocean Color Sensor Validation, Revision 4, Volume III: Radiometric Measurements and Data Analysis Protocols. *NASA/TM-2003-21621/Rev-Vol III*. Mueller J.L., Fargion G.S. and McClain C.R., Eds., NASA Goddard Space Flight Center, Greenbelt, Maryland, 84 pp.

Piskozub J., Weeks A.R., Schwarz J.N. and Robinson I.S., 2000. Self-shading of upwelling irradiance for an instrument with sensors on a sidearm. *Applied Optics* 39(12),1872-1878.

Shang Z., Lee Z.P., Dong Q. and Wei J., 2017: Self-shading associated with a skylight-blocked approach system for the measurement of water-leaving radiance and its correction. *Applied Optics*, 56(25), 7033-7040.

Stavn R.H. and Weidemann A.D., 1988: Optical modeling of clear ocean light fields: Raman scattering effects. *Applied Optics*, 27, 4002-4011.

Sugihara S., Kishino M. and Okami N., 1984: Contribution of Raman scattering to upward irradiance in the sea. *Journal of the Oceanographic Society of Japan*, 40, 397-404.

Talone M., Zibordi G. and Lee Z.P., 2018: Correction for the non-nadir viewing geometry of AERONET-OC above water radiometry data: an estimate of uncertainties. *Optics Express*, 26(10), A541-A561.

Tanré D., Herman M., Deschamps P.Y. and Leffe A., 1979: Atmospheric Modeling for Space Measurements of Ground Reflectances, Including Bidirectional Properties. *Applied Optics*, 18(21), 3587–94.

Voss K.J. and Flora S., 2017: Spectral Dependence of the Seawater–Air Radiance Transmission Coefficient. *Journal of Atmospheric and Oceanic Technology*, 34(6), 1203-1205.

Voss K.J., McLean S., Lewis M., Johnson C., Flora S., Feinholz M., Yarbrough M., Trees C., Twardowski M. and Clark D.K., 2010: An example crossover experiment for testing new vicarious calibration techniques for satellite ocean color radiometry. *Journal of Atmospheric and Oceanic Technology*, 27(10), 1747-1759.

Voss K.J., Gordon H.R., Flora S., Johnson B.C., Yarbrough M., Feinholz M. and Houlihan T., 2017: A method to extrapolate the diffuse upwelling radiance attenuation coefficient to the surface as applied to the Marine Optical Buoy (MOBY), *Journal of Atmospheric and Oceanic Technology*, 34, 1423-1428.

Voss K.J., Nolten J.W. and Edwards G.D., 1986: Ship shadow effects on apparent optical properties. *Ocean Optics VIII*, M. Blizard, Ed., *SPIE*, 637, 186-190.

Waters K.J., Smith R.C. and Lewis M.R., 1990: Avoiding ship induced light field perturbation in the determination of oceanic optical properties. *Oceanogr*aphy, 3, 18-21.

Zaneveld J.R.V., Boss E. and Barnard A., 2001: Influence of surface waves on measured and modeled irradiance profiles. *Applied Optics*, 40, 1442-1449.

Zibordi G., Ruddick K., Ansko I., Moore G., Kratzer S., Icely J. and Reinart A., 2012: In situ determination of the remote sensing reflectance: an inter-comparison. *Ocean Science*, 8(4), 567-586.

Zibordi G. and Voss K.J., 2014: In situ optical radiometry in the visible and near-infrared. In *Experimental Methods in the Physical Sciences* (*Vol.* 47, pp. 247-304). Academic Press.

Zibordi G., 2012: Comment on "Long Island Sound Coastal Observatory: assessment of above-water radiometric measurement uncertainties using collocated multi and hyperspectral systems". *Applied Optics*, 51(17) 3888-3892.

Zibordi G., D'Alimonte D. and Berthon J.-F., 2004: An Evaluation of Depth Resolution Requirements for Optical Profiling in Coastal Waters. *Journal of Atmospheric and Oceanic Technology*, 21(7), 1059-1073.

Zibordi G. and Ferrari G.M., 1995: Instrument self-shading in underwater optical measurements: experimental data. *Applied Opt*ics, 34, 2750-2754.

Zibordi G., Berthon J-F., Doyle J.P., Grossi S., van der Linde D., Targa C. and Alberotanza L., 2002: Coastal Atmosphere and Sea Time Series (CoASTS), Part 1: A Tower-Based Long-Term Measurement Program. *NASA Tech. Memo. 2002–206892, Vol. 19*, Hooker S.B. and Firestone E.R., Eds., NASA Goddard Space Flight Center, Greenbelt, Maryland, 29 pp.

Chapter 5: Above-Water Radiometry Measurements and Data Analysis

Giuseppe Zibordi[1] and Kenneth J. Voss[2]

[1] *European Commission, Joint Research Centre, Ispra, Italy*
[2] *University of Miami, Coral Gables, Florida, USA*

1. INTRODUCTION

Above-water radiometry is a valuable alternative to in-water radiometry for the determination of the water-leaving radiance $L_w(\lambda)$. During the last decades, above-water radiometry has been a matter of extensive investigations leading to a number of alternative measurement methods. The general method presented in the following sections relies on the application of calibrated radiometers allowing for absolute spectral measurements of the total radiance from the sea surface $L_T(\theta,\phi,\lambda)$ (which includes contributions from $L_w(\lambda)$, sky–glitter, and sun–glint) and of the sky $L_i(\theta',\phi,\lambda)$ (*i.e.*, sky radiance), performed with observation geometries defined by the relative azimuth angle between sensor and sun ϕ, and the viewing angle θ specular to θ' (*i.e.*, $\theta' = 180 - \theta$). An additional quantity required for the minimization of changes in illumination conditions during above-water measurements and to compute the remote sensing reflectance $R_{rs}(\lambda)$, is the total downward irradiance $E_s(\lambda)$.

Recognizing the potential for alternative methods—such as those relying on plaques (Carder and Steward 1985, Rhea and Davis 1997, Sydor and Arnone 1997) or polarizers (Fougnie *et al.* 1999)—their application is considerably challenged, however, by non-ideal field implementations (in the case of plaques) and by the application of comprehensive radiative transfer models (in the case of polarizers), which may affect the accurate quantification of the uncertainties of derived data products. Further, with reference to the number of alternative data processing solutions proposed in the literature that center primarily on the optimization of the sky-glint removal and mostly on the minimization of any residual sky radiance affecting $L_w(\lambda)$ (Lee *et al.* 1997, Gould *et al.* 2001, Ruddick *et al.* 2006, Simis and Olsson 2013, Kutser *et al.* 2013, Groetsch *et al.* 2017), the superior performance of these methods is unproven on data collected during clear sky conditions. Because of this, and considering that the objective of this work is focused on above-water radiometry for the validation of satellite ocean color radiometric data products naturally collected during clear sky conditions, the following sections will strictly rely on the basic measurement equation for above-water radiometry performed with calibrated radiometers (Mobley 1999), applicable for both autonomous and manually executed measurements.

Finally, as already indicated for in-water radiometry (see Chapter 4 on *In-Water Radiometry Measurements and Data Analysis*), also above-water radiometry supporting satellite ocean color validation activities must be performed in regions that allow assuming both negligible bottom perturbations and adjacency effects in satellite data (Zibordi *et al.* 2009). In order to minimize the impact of adjacency effects, it is recommended that *in situ* data are collected at a distance from the coast, exceeding at least five nautical miles. However, considering the complex dependence of adjacency effects on the distance from land and its spectral albedo, as well as water reflectance and sensor signal-to-noise ratio, such a minimum distance may not ensure negligible land perturbations in satellite data (Bulgarelli and Zibordi 2018).

2. MEASUREMENTS

Above-water radiometry relying on calibrated radiometers requires measurements of the sky-radiance $L_i(\theta',\phi,\lambda)$ and total radiance from the sea $L_T(\theta,\phi,\lambda)$ performed at given geometries by ensuring minimization of superstructure perturbations such as shading and reflection effects or simply changes in the water surface.

By following Mobley (1999), the measurement equation for the water-leaving radiance $L_w(\theta,\phi,\lambda)$ with measurement geometry determined by (θ, θ', ϕ) and sun zenith angle θ_0, is given by

$$L_w(\theta,\phi,\lambda) = L_T(\theta,\phi,\lambda) - \rho(\theta,\phi,\theta_0,W)L_i(\theta',\phi,\lambda) \quad (5.1)$$

where $\rho(\theta,\phi,\theta_0,W)$ is the sea surface reflectance factor with the wind speed W conveniently expressing the sea state.

Equation 5.1, however, describes an idealized measurement concept. In fact, the sky-radiance contributions to sky-glint may come from a portion of the sky around the direction (θ', ϕ), which varies with the degree of surface roughness. Further, the complexity of the sea surface resulting from the composition of gravity and capillary waves, in combination with parameters such as the instrument field-of-view and integration time, may challenge the capability of determining actual surface reflectance factors. Additional aspects are the skylight polarization and the interaction of this polarization with the sea surface. These elements are introduced and discussed in the following sub-sections with the objective of supporting a robust implementation of above-water radiometry.

Viewing geometry

The minimization of glint perturbations is the main challenge of above-water radiometry. Modeling (Mobley 1999) indicates that a viewing angle θ of 40° and a relative azimuth ϕ of 135° are the most appropriate to minimize sun-glint perturbations. This geometry, however, often conflicts with practical limitations during field deployments. In fact, the use of ϕ = 135° may easily become the source of perturbations in $L_T(\theta,\phi,\lambda)$ measurements because the radiometer necessarily looks at the sea close to the deployment structure or at its shadow. This limitation, which becomes more severe with large sun zenith angles, would suggest that ϕ = 90° is a better solution (see Fig. 5.1), despite the less favorable measurement conditions mostly occurring at mid-high wind speeds (Zibordi *et al.* 2009).

It is thus emphasized that the viewing geometry results from tradeoffs between the measurement conditions minimizing glint effects and those minimizing infrastructure impacts. Regardless of the applied geometry, it is relevant to point out that the non-nadir view characterizing above-water radiometry implies the removal of the viewing angle dependence, which requires the application of correction factors resulting from simulations (see Morel *et al.* 2002). This additional element suggests that the adoption of single measurement geometry (*e.g.*, θ = 40° and ϕ = 90°), as opposed to the application of different geometries adapted to varying measurement conditions, would ensure a higher consistency to data products.

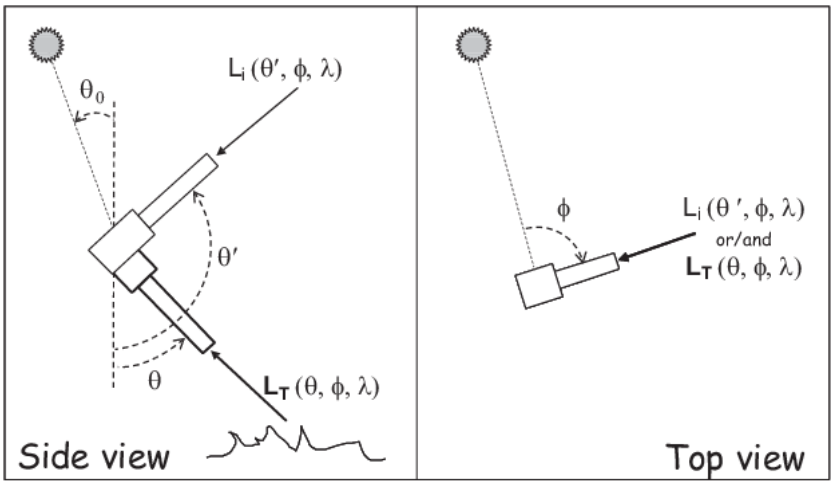

Fig. 5.1: Measurement geometry commonly applied for above-water radiometry (i.e., viewing angle θ of 40° and a relative azimuth ϕ of 90°).

Field-of-view

The full-angle FOV of radiance sensors is not critical in determining $L_w(\lambda)$ from in-water profile data because the (near-nadir) upwelling radiance distribution varies relatively little over nadir angles up to 20°. Conversely, in the case of above-water, the field-of-view is an important factor because of the spatial

variability of the radiance contributions leading to $L_T(\theta,\phi,\lambda)$ and $L_i(\theta',\phi,\lambda)$ measurements. In fact, the spatial and temporal variation of the slope distribution of the wind roughened sea surface (including effects by gravity and capillary waves) may have a large impact on $L_T(\theta,\phi,\lambda)$ data. In particular, a large FOV combined with long integration time (when applicable) may increase the averaging of wave effects. In contrast, a small FOV with short integration time (when applicable) would definitively increase the variability across successive measurements (Carrizo *et al.* 2019). Still, when excluding large full-angle FOV (*e.g.*, greater than 20°), the dependence of $L_i(\theta',\phi,\lambda)$ on FOV is expected to have a secondary impact on the determination of $L_W(\lambda)$.

The literature does not provide clear support regarding the selection of the most appropriate FOV. However, an investigation performed with multispectral radiometers operated with different fore optics allowing for alternative FOVs appears to indicate a preference for small full-angle FOV for $L_T(\theta,\phi,\lambda)$ measurements (tentatively less than 5°) and some flexibility for $L_i(\theta',\phi,\lambda)$ (Hooker *et al.* 2004). Another study, solely based on theoretical simulations (Foster and Gilerson 2016), suggests collecting $L_i(\theta',\phi,\lambda)$ data with a FOV increasing with the sea state. It is mentioned that in the case of $L_T(\theta,\phi,\lambda)$ and $L_i(\theta',\phi,\lambda)$ measurements performed with a 1.2° field-of-view (Zibordi *et al.* 2009), the variability in $L_T(\theta,\phi,\lambda)$ across successive measurements is used to remove those data affected by high variance. This allows for filtering measurements collected during conditions diminishing the accuracy of the surface reflectance factor, which often occur with wind speed tentatively exceeding 5 m s^{-1} and sun zenith lower than 20° (Zibordi 2012).

Finally, a high co-registration of the different spectral bands is the element ensuring that surface effects, and consequently, the sky-glint contributions reaching the sensor FOV arise from the same area of the sea surface. This should discourage the application of filter-wheel radiometers in above-water radiometry because measurements are performed sequentially across the various bands. However, for such instruments, literature shows that strict quality assurance of measurements and quality control of products allows $L_{WN}(\lambda)$ to be obtained with an accuracy comparable to that of above-water systems exhibiting more precise co-registration of spectral bands (Zibordi *et al.* 2012).

Avoidance of perturbations by deployment structures

As with in-water radiometry, $E_s(\lambda)$ measurements are required. Perturbations by superstructures affecting $E_s(\lambda)$ measurements can only be avoided by deploying the radiometer away from sources of pollution and above any obstacle that may be seen in the FOV of the irradiance sensor. Such a fundamental requirement is often challenged by the difficulty in reaching the highest locations of the deployment structures (*e.g.*, ships), and the need to ensure daily maintenance of radiometers. A practical solution is offered often with the use of telescopic poles operated at convenient locations. It is noted that commercial systems may be comprised of L_T, L_i, and E_s radiometers operating in compact configurations. These solutions, however, may prevent optimizing the deployment of the E_s sensor out of superstructure perturbing effects.

When considering $L_i(\theta',\phi,\lambda)$ and $L_T(\theta,\phi,\lambda)$, measurements must also be performed from a location that minimizes both shading and reflections from deployment structures. Generally, a good position for measuring the water-leaving radiance on ships is the bow. This, while steaming with suitable viewing and illumination geometries, ensures measurements with the water surface undisturbed by the ship wake or any associated foam. Major perturbations may result from an unfavorable deployment position with respect to the sun that may lead to viewing an area of the sea surface too close to the superstructure itself. Experimental analysis has shown that, as a rule of thumb, the viewed area should be located at a distance d at least greater than the superstructure height h (Hooker and Morel 2003, Hooker and Zibordi 2005). Still, perturbations by deployment platforms may exhibit spectral dependence with effects more pronounced in the red (Talone and Zibordi 2019). Specifically, in the case of low-reflectance superstructures, perturbations affecting $R_{rs}(\lambda)$ determined with $\phi = 90°$ and $d > h$, are expected to be well below 1% in the visible spectral regios. In contrast, for high-reflectance superstructures (such as white ships), an identical measurement geometry may increase perturbations up to approximately 1% in the blue-green and well exceed 2% in the red.

Overall, the previous findings further reinforce the need to operate above-water radiometers on the uppermost locations of deployment structures in a place allowing a view of the surface well away from superstructures themselves. In the case of fixed structures (*e.g.*, towers or lighthouses), these requirements imply limiting the acquisition of measurements to within specific azimuth limits. In the case of ship measurements, the heading of the ship should be adjusted to warrant fulfillment of the previous distance requirements. In the case of autonomous shipborne measurements, the heading of the ship should be recorded together with the radiometric data to ensure a successive screening of those measurements that do not fulfill the distance requirements.

Dark-signal recording

The dark-signal of sensors generally exhibits a temperature dependence that can easily change with time as a function of operation and environmental conditions. In-air instrumentation often experiences a much bigger temperature range during measurements than in-water instruments. It is thus fundamental that each individual or sequence of measurements is accompanied by offset determinations. Some commercial radiometers are equipped with shutters allowing for the automatic determination of the dark-signal. In this case, too, occasional measurements of the dark-signal obtained by closing the sensor aperture would further support the quality assurance process.

Measurement sequence

Each measurement sequence should provide contemporaneous measurements of $E_s(\lambda)$, $L_i(\theta',\phi,\lambda)$, and $L_T(\theta,\phi,\lambda)$. Still, even though desirable, simultaneous measurements of $L_i(\theta',\phi,\lambda)$ and $L_T(\theta,\phi,\lambda)$ are not strictly necessary during clear sky conditions. Best practice suggests that each above-water determination of $L_w(\theta,\phi,\lambda)$ relies on successive measurements sequences, each one restricted to within a very few minutes, but with each one producing a number of data suitable to investigate the stability of $E_s(\lambda)$ and $L_i(\theta',\phi,\lambda)$ and the variability of $L_T(\theta,\phi,\lambda)$. It is emphasized that the collection of multiple measurement sequences further enables the quality control of data and to additionally quantify the environmental perturbations affecting $L_w(\theta,\phi,\lambda)$.

Essential ancillary data and metadata

A number of ancillary data and metadata are needed for the processing and eventual flagging of above-water radiometry measurements. Data essential for the comprehensive data processing of each measurement sequence include date and time (UTC), longitude and latitude, cloud cover and sea state (likely supported by digital pictures or videos), wind speed and direction, air and water temperature, and barometric pressure. Data quality control also requires that roll, pitch, and heading of sensors are recorded in combination with the radiometric measurements to allow removal of those data affected by excessive tilt effects as well as to identify and remove those data likely affected by the deployment structure. It is specifically recommended that attention to the attitude of sensors with respect to the vertical is a critical factor for the accuracy of $E_s(\lambda)$, and also of $L_i(\theta',\phi,\lambda)$ and $L_T(\theta,\phi,\lambda)$ measurements. Because of this, in the case of systems exhibiting variable sampling rates (*i.e.*, adjusting the integration time as a function of light intensity), roll and pitch measurements should be oversampled with respect to the radiometric data. This would allow proper screening of data affected by significant tilt during integration times that may exceed hundreds of milliseconds.

Finally, in view of supporting the implementation of future processing schemes relying on advanced spectral surface reflectance factors, the aerosol optical properties including at least the optical depth should be measured. It is noted that measurement of the aerosol optical depth is already a requirement for the computation of $E_s(\lambda)$ when this is not actually measured (Zibordi *et al.* 2009).

Equivalent to in-water radiometry, it is fundamental that both ancillary data and metadata are systematically recorded and properly captured in the data management system in view of their comprehensive exploitation during the processing of the above-water radiometric data.

3. DATA ANALYSIS

The data product from above-water radiometry is $L_w(\lambda)$. Its accuracy, in addition to the accuracy of calibration and characterization factors applied to radiometry data, mainly depends on: i) the minimization of measurement artifacts resulting from elevated tilts; ii) the minimization of the impact of wave perturbations in $L_T(\theta,\phi,\lambda)$ data; iii) the accuracy of the surface reflectance factors; and, iv) the accuracy of the correction applied for the minimization of the off-nadir view (*i.e.*, in-water light anisotropy effects). This section provides basic elements in the processing of $L_i(\theta',\phi,\lambda)$, $L_T(\theta,\phi,\lambda)$ and $E_s(\lambda)$ to determine $L_w(\lambda)$.

Dark-signal removal, corrections for the non-ideal performance of sensors, and calibration

The instrument dark-signal in each channel must be subtracted from the raw field data prior to any further processing. Successive steps are the application of any correction minimizing the non-ideal performance of the radiometer in combination with the application of the absolute calibration coefficients accounting for pre- and post-field laboratory calibrations, and eventually supplementary field stability checks performed with portable reference sources.

As already pointed out for in-water methods, these early data reduction steps suggest the need for efficient access to any information required for the processing and successive re-processing of field measurements. This should imply a data management system ensuring a unique association of raw field data to measurement campaigns, stations, casts, essential ancillary data, and, obviously, radiometer tags and their calibration coefficients and correction factors.

Quality assurance of input data

A number of quality assurance steps need to be implemented to identify those data that may be affected by poor measurement conditions (Zibordi *et al.* 2009). Quality checks should first allow removing data affected by excessive tilts (ideally any data affected by tilts higher than 5° for $L_i(\theta',\phi,\lambda)$, 2° for $L_T(\theta,\phi,\lambda)$ and 1° for $E_s(\lambda)$). Still, it is recognized that tilt thresholds should generally result from tradeoffs between the need to preserve a significant number of data and their quality. Thus, chosen thresholds may slightly vary across deployment platforms and sea state.

Additional quality checks should remove those measurement sequences affected by any significant variability of $E_s(\lambda)$, $L_i(\theta',\phi,\lambda)$ and $L_T(\theta,\phi,\lambda)$ not explained by tilt perturbations. Specifically, with the overall requirement of clear sun and low cloudiness, it is fundamental the $L_i(\theta',\phi,\lambda)$ measurements are not affected by clouds shadow or clouds directly seen by the sensor or located in its immediate vicinity (in fact bright clouds occurring in the close vicinity of the portion of sky observed by the L_i sensor could induce significant adjacency effects in measurements). Thus, quality checks applied to $E_s(\lambda)$ and $L_i(\theta',\phi,\lambda)$ should aim at removing those measurement sequences most likely contaminated by clouds. These checks should rely on minimal target thresholds (ideally with 1% or maximum 2% change in the measured signal). Checks on $L_T(\theta,\phi,\lambda)$ data should lead to the removal of those measurement sequences profoundly affected by sun-glint and likely foam perturbations in addition to excessive sky-glint contributions from bright portions of the sky (typical of measurement conditions characterized by a high wind speed: *e.g.*, exceeding 7 ms^{-1}). In such a case, a practical solution is offered by the use of statistical indices, such as the standard deviation, to remove those measurement sequences exhibiting values exceeding thresholds (much stricter for $L_T(\theta,\phi,\lambda)$ than for $L_i(\theta',\phi,\lambda)$). These thresholds are somewhat instrument-specific being a function of FOV and integration time: a large FOV or a high integration time lead to the averaging of glint and any additional surface perturbation.

Finally, quality checks should apply to differences between the pre- and post-field calibrations of optical sensors. This step may largely benefit from field checks performed with portable reference sources. Thresholds in calibration differences should obviously account for the deployment duration and the working conditions. When considering well-maintained systems (*e.g.*, regularly cleaned) and deployed for a short time (*e.g.*, up to a few weeks), differences between pre- and post-field calibrations should be mostly explained by calibration uncertainties. Slightly larger differences, due to actual sensor sensitivity decay with time, may imply actions such as interpolation with time of calibration coefficients. Large, unexplained

differences that may challenge the determination of accurate radiometric products should lead to the rejection of the measurement sequence.

Normalization by Surface Irradiance

Similar to in–water data, the individual measurements of $L_T(\theta,\phi,\lambda)$ and $L_i(\theta',\phi,\lambda)$ should be corrected for illumination changes using the corresponding $E_s(\lambda)$ values. By restating the requirement of clear sun and low cloudiness, and introducing the time dependence t for measurements, changes in the illumination conditions likely only due to changes in the sun position, are minimized through measurements of $E_s(\lambda,t)$ performed simultaneously with the collection of $L_i(\theta',\phi,\lambda,t)$ and $L_T(\theta,\phi,\lambda,t)$.

In agreement with the scheme proposed for in-water radiometry, using $\Im(\theta,\phi,\lambda,t)$ to indicate both $L_i(\theta',\phi,\lambda,t)$ and $L_T(\theta,\phi,\lambda,t)$, changes in illumination are accounted through

$$\Im_0(\theta,\phi,\lambda,t_0) = \frac{\Im(\theta,\phi,\lambda,t)}{E_s(\lambda,t)} E_s(\lambda,t_0) \tag{5.2}$$

where $\Im_0(\theta,\phi,\lambda,t_0)$ is the radiometric quantity normalized to the incident light field at t_0, $E_s(\lambda,t_0)$, with t_0 reference time pertaining to the measurement sequence (*e.g.*, the start of the sequence).

Equivalent to the case of in-water radiometry, the former normalization process implies the existence of $E_s(\lambda,t)$ collected at the same time t of $\Im(\theta,\phi,\lambda,t)$. This need can be challenged by different sampling rates characterizing radiometers operated with diverse integration times. Still, benefitting from the clear sky requirement, the former limitation can be addressed by interpolating the existing $E_s(\lambda,t)$ as a function of t.

Again, a close match between the spectral bands of the E_s sensor and those of the radiance sensors is important to avoid introducing spectral artifacts in the normalized data.

Finally, if $E_s(\lambda)$ measurements are not available, the above-water method described is considered still effective during clear sky conditions when the measurement sequences are restricted to within a very few minutes, albeit at the expense of an increase in uncertainties.

Sea Surface Reflectance Factor

The sea surface reflectance ρ is determined by the total sky-radiance reflected into the FOV of the L_T sensor from the wave-roughened sea surface in the direction (θ,ϕ), divided by sky-radiance into the L_i FOV from the direction (θ',ϕ). The values of ρ as a function of measurement geometry and observation conditions are commonly obtained from simulations, still verifiable through field measurements (Hooker and Zibordi 2005). However, the capability of computing ρ to predict the actual sea-surface-reflectance characterizing measurements depends on the ability to model the surface features and the light contribution reflected into the L_T FOV. This includes the sky radiance from a variety of zenith and azimuth angles (which add to sun-glint or foam contributions) characterized by time scales varying from milliseconds to seconds (as a function of the integration time) and spatial scales varying from a few to several tens of cm^2 (as function of the FOV and sensor height above the sea surface).

The most commonly used surface reflectance factors are those from Mobley (1999). They were determined from simulations performed at λ = 550 nm, accounting for the dependence on the viewing and illumination geometries, and modeling the effects of sea state as a function of wind speed through the Cox-Munk (1954) parameterizations (see Fig. 5.2). The sky radiance distribution was obtained from an irradiance model and experimental sky radiance patterns. While multiple scattering and aerosol effects were implicitly accounted for, the polarization effects were neglected.

A number of investigations indicated non-negligible impact of polarization effects (Harmel *et al.* 2012, Mobley 2015, Hieronymi 2016, D'Alimonte and Kajiyama 2016, Foster and Gilerson 2016, Zhang *et al.* 2017, Gilerson *et al.* 2018) and new reflectance factors at λ = 550 nm were proposed accounting for wave height and slope variance, in addition to polarization effects (Mobley 2015). As opposed to previous values

of ρ, the new ones were determined for a clear purely molecular (*i.e.*, Rayleigh) sky with single scattering approximation. Consequently, this specific ideal case can be considered as representative of extreme polarization conditions because of the absence of depolarization effects from aerosols.

The two sets of surface reflectance factors exhibit marked differences as a function of the viewing and illumination geometries as well as wind speed. When considering measurements performed with low wind speed and away from low sun zenith angles, an experimental assessment of the two sets of reflectance factors indicated slightly better performance for those determined by neglecting the polarization effects (Zibordi 2016). Accounting for this finding and for investigations pointing out the relevance of aerosol contributions and ultimately the non-negligible spectral dependence (Lee *et al.* 2010, Gilerson *et al.* 2018), it is suggested that the operational processing of above-water radiometry data still rely on the ρ values computed neglecting polarization effects (*e.g.*, Mobley 1999). Obviously, spectral values of surface reflectance factors comprehensively accounting for polarization effects as a function of aerosol-type and -load should be applied as soon as available and verified.

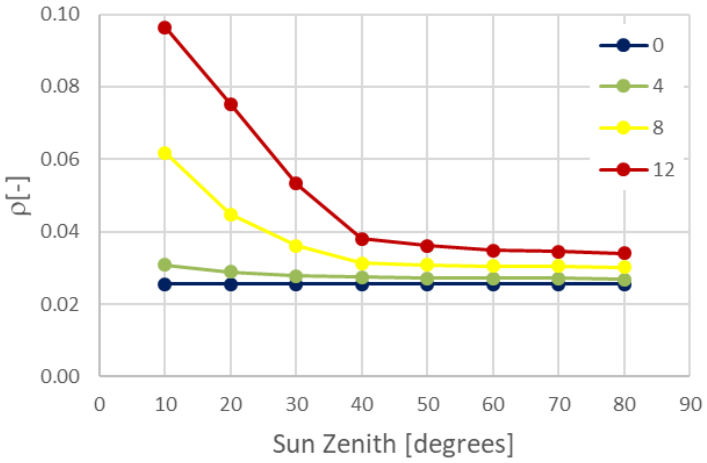

Figure 5.2: Values of ρ from Mobley (1999) as a function of sun zenith (in the range from 10° to 80°) and wind speed (in the range from 0 to 12 m s^{-1}), for viewing geometries determined by $\theta = 40°$ and $\phi = 90°$.

Determination of L_w

$L_T(\theta,\phi,\lambda)$ and $L_i(\theta',\phi,\lambda)$ values applied for the computation of $L_w(\theta,\phi,\lambda)$ through Eq. 5.1 should be obtained from the averaging of *n*-independent measurements satisfying filtering criteria to remove those individual $L_T(\theta,\phi,\lambda)$ values affected by significant glint and foam perturbations.

Some investigations showed the benefit of using the mean of $L_T(\theta,\phi,\lambda)$ relative minima determined from a percentage of the quality-checked ones (Zibordi *et al.* 2002, Hooker *et al.* 2002): *i.e.*, only a fraction of the measurements exhibiting the lowest values are retained for successive processing. This solution, only supported by experimental evidence for relatively low wind-speed (generally lower than 5 ms^{-1}), further minimizes the impact of values affected by significant glint contamination in the quality checked measurement sequences. The number of values to be averaged may range from a few up to tens of percent (typically between 5% and 20%) of the available data, depending on instrument characteristics such as FOV and integration time and the data collection scheme.

It is important to appreciate that the averaging of $L_T(\theta,\phi,\lambda)$ values relying on relative minima collected during the measurement sequence, may lead to an underestimate of the sky-glint correction (Zibordi *et al.* 2009, Zibordi 2012). However, this is expected to only have a significant impact on data collected with high sea state and low sun zenith angles only, which are conditions generally removed by the quality assurance of individual measurement sequences.

The averaging of $L_i(\theta',\phi,\lambda)$ data for each measurement sequence should not undergo any restriction, given the clear sky conditions. However, in the case of simultaneous measurements of $L_T(\theta,\phi,\lambda)$ and $L_i(\theta',\phi,\lambda)$, the averaging of $L_i(\theta',\phi,\lambda)$ data should be performed using the measurements corresponding to those applied for the determination of the $L_T(\theta,\phi,\lambda)$ mean value.

Quality control of data products

The quality control should focus on data products, *i.e.*, $L_w(\lambda)$ or $L_{wn}(\lambda)$, exhibiting negative values (not explained by uncertainties) indicating over-correction of the sky-glint contribution, or exhibiting excessively high values in the near-infrared as a result of under-correction of sky-glint perturbations or a large impact of sun-glint, foam or even of the deployment superstructure. Additional quality check, still qualitative, should evaluate the consistency among successive $L_w(\lambda)$ or $L_{wn}(\lambda)$ spectra ideally expected to exhibit close values unless affected by changes in water properties or illumination conditions.

Corrections for non-nadir view

It is important to recall that $L_w(\theta,\phi,\lambda)$ is determined for a non-nadir view, which implies the need to remove the viewing angle dependence. This is achieved through

$$L_w(\lambda) = L_w(\theta,\varphi,\lambda)\frac{\Re_0}{\Re(\theta,W)}\frac{Q(\theta,\varphi,\theta_0,\lambda,\tau_a,IOP)}{Q_n(\theta_0,\lambda,\tau_a,IOP)} \tag{5.3}$$

where the ratio of $\Re_0$ (*i.e.*, $\Re(\theta,W)$ at $\theta = 0$) to $\Re(\theta,W)$ accounts for changes in surface reflectance and refraction, and the ratio of $Q(\theta,\phi,\theta_0,\lambda,\tau_a,IOP)$ to $Q_n(\theta_0,\lambda,\tau_a,IOP)$, *i.e.*, the Q-factors at viewing angle θ and at nadir (*i.e.*, $\theta = 0$), minimize the effects of the anisotropic radiance distribution of the in–water light field as a function of the water *IOP*s, the observation and illumination geometries defined by θ, ϕ and θ_0, and the atmospheric optical properties by the aerosol optical depths τ_a during clear sky conditions.

In Case-1 waters, the IOPs can be solely expressed as a function of the chlorophyll-*a* concentration, *Chla*. For this specific case, a fully *Chla*-based correction approach can benefit from tabulated values of $\Re(\theta,W)$ and of the Q-factors produced through simulations (Morel *et al.* 2002). It is anticipated that, for actual computations, the ratio $Q(\theta,\phi,\theta_0,\lambda,\tau_a,Chla)/Q_n(\theta_0,\lambda,\tau_a,Chla)$ needs to be replaced by actually available values of $f(\theta_0,\lambda,\tau_a,Chla)/Q(\theta,\phi,\theta_0,\lambda,\tau_a,Chla)$ and $f(\theta_0,\lambda,\tau_a,Chla)/Q_n(\theta_0,\lambda,\tau_a,Chla)$. This exchange of quantities is supported by the fact that $f(\theta_0,\lambda,\tau_a,Chla)$, which relates the irradiance reflectance to IOPs through the ratio of backscattering to absorption coefficients, does not depend on θ. It is finally mentioned that the dependence on τ_a of both $Q(\theta,\phi,\theta_0,\lambda,\tau_a,Chla)$ and $f(\theta_0,\lambda,\tau_a,Chla)$, is small with respect to that of the other quantities. Because of this, the tabulated values of $Q(\theta,\phi,\theta_0,\lambda,\tau_a,Chla)$ and $f(\theta_0,\lambda,\tau_a,Chla)$ are provided for a maritime aerosol with optical depth $\tau_a = 0.2$ at 550 nm.

The alternative IOP-based correction approach for bidirectional effects applicable to both Case-1 and optically complex waters (Lee *et al.* 2011) has the advantage of not requiring any additional input other than the measured $L_w(\theta,\phi,\lambda)$. This approach relies on the following equation to determine the inherent optical properties from $L_w(\theta,\phi,\lambda)$

$$L_w(\theta,\phi,\lambda) = E_s(\lambda)\left\{\left[G_0^w(\theta,\phi,\theta_0) + G_1^w(\theta,\phi,\theta_0)\cdot\frac{b_{bw}(\lambda)}{\kappa(\lambda)}\right]\cdot\frac{b_{bw}(\lambda)}{\kappa(\lambda)} + \left[G_0^p(\theta,\phi,\theta_0) + G_1^p(\theta,\phi,\theta_0)\cdot\frac{b_{bp}(\lambda)}{\kappa(\lambda)}\right]\cdot\frac{b_{bp}(\lambda)}{\kappa(\lambda)}\right\} \tag{5.4}$$

where the coefficients G_0^w, G_1^w, G_0^p, G_1^p are the model parameters, $b_{bw}(\lambda)$ and $b_{bp}(\lambda)$ the pure sea water and particle backscattering coefficients, respectively, with $\kappa(\lambda) = a(\lambda)+b_b(\lambda)$ and $b_b(\lambda) = b_{bw}(\lambda)+b_{bp}(\lambda)$, and $a(\lambda)$ total seawater absorption coefficient.

Once the values of $a(\lambda)$ and $b_b(\lambda)$ are derived, their value is used to calculate $L_w(\lambda)$ by applying the parameters G_0^w, G_1^w, G_0^p, G_1^p for $\theta = 0$ through

$$L_w(\lambda) = E_s(\lambda)\left\{\left[G_0^w(0,0,\theta_0) + G_1^w(0,0,\theta_0)\cdot\frac{b_{bw}(\lambda)}{\kappa(\lambda)}\right]\cdot\frac{b_{bw}(\lambda)}{\kappa(\lambda)} + \left[G_0^p(0,0,\theta_0) + G_1^P(0,0,\theta_0)\cdot\frac{b_{bp}(\lambda)}{\kappa(\lambda)}\right]\cdot\frac{b_{bp}(\lambda)}{\kappa(\lambda)}\right\}\cdot \quad (5.5)$$

An evaluation of the *Chla*- and IOP-based approaches (Gleason *et al.* 2012) indicated a superior performance of the first method in Case-1 waters (see Eq. 5.3) and conversely of the second one in optically complex waters (see Eq. 5.5). An analysis of the uncertainties affecting corrections determined for the latter approach applicable to optically complex waters indicated relative uncertainties for corrections varying between 20% and 35% independent from wavelength and water type (Talone *et al.* 2018).

Uncertainties

Key uncertainties affecting above-water radiometric measurements are those associated with environmental perturbations, the accuracy of the surface reflectance factors, and the corrections for the non-nadir view (extensive analysis are available in Gergely and Zibordi (2013) and Carrizo *et al.* (2019)).

Uncertainties due to environmental perturbations can be quantified from the standard deviation of $L_w(\lambda)$ values determined from consecutive measurement sequences (likely not significantly affected by sun-glint). These uncertainties would embrace wave effects and the impact of changes in illumination conditions and water type.

The determination of uncertainties and biases affecting the surface reflectance factors and corrections for the non-nadir view would imply comparisons with *in situ* reference measurements performed with alternative methods expected to provide highly accurate values of $L_w(\lambda)$ (*e.g.*, in-water radiometry). Because of this, these uncertainties and biases are difficult to quantify. Still, at the very least, the precision of the applied surface reflectance factors and corrections should be investigated through sensitivity analysis addressing the impact of uncertainties affecting the input parameters in the processing chain.

4. ALTERNATIVE METHODS

A number of methods have been proposed and applied for the determination of $L_w(\lambda)$ from above-water radiometry. These include the use of plaques, which provide the major advantage of operating with non-calibrated radiometers (Carder and Steward 1985, Rhea and Davis 1997, Sydor and Arnone 1997). This approach implies viewing the plaque with the radiance sensor, alternatively applied to gather the radiance from the sky and sea, with geometry equivalent to that detailed in the previous sections. However, the correct maintenance of the plaque during field operations and the fundamental need to ensure a perfectly horizontal and unobstructed application of the plaque, challenge this method.

An alternative above-water method relies on the combination of polarized measurements of the radiance from the sea and modeled sky-radiance computed with the aid of measured values of the aerosol optical depth (Fougnie *et al.* 1999). This method has the advantage of highly reducing the sky-glint by measuring only the vertically polarized component of $L_T(\theta,\phi,\lambda)$ and consequently minimizing the dependence of measurements from the reflectance of the sea surface. The accuracy of the method, however, largely depends on the capability of accurately modeling the residual sky-glint radiance and accounting for the non-zero polarization of $L_w(\lambda)$.

A further alternative method is the skylight-blocked approach (Tanaka *et al.* 2006, Lee *et al.* 2010, Lee *et al.* 2013). This *hybrid* method leads to the direct measurement of the water-leaving radiance $L_w(\lambda)$ from a radiance sensor, operated just above the water surface through a floating system equipped with a screen blocking the skylight around the sensor. Compared to classical in-water radiometry, this method does not imply radiance measurements performed at various depths to extrapolate sub-surface radiance values, while still sharing the need for self-shading corrections (Lee *et al.* 2013, Shang *et al.* 2017). The advantage of the skylight-blocked approach with respect to classical above-water radiometry is its independence from the reflectance of the sea surface as there is no contribution by sun- and sky-glint. Still, a definitive assessment of the method requires additional investigations determining most favorable operational conditions (*e.g.*, sea state limits, likely depending on the floating components of the

measurement system), widespread inter-comparisons of derived radiometric data products performed using reference data from consolidated methods, and finally comprehensive investigations of the uncertainties affecting measurements and data products.

5. FUTURE DIRECTIONS

Many inter-comparisons between data products from in-water and above-water methods have been proposed during the last two decades (*e.g.*, Toole *et al.* 2000, Hooker *et al.* 2004, Zibordi 2016). These clearly show significant incremental improvements in both the practice and understanding of above-water radiometry. For instance, recent comparisons of $L_w(\lambda)$ and $L_{WN}(\lambda)$ products performed during clear sky conditions, illustrate the basic equivalence of above- and in-water measurement methods (Zibordi 2012) with differences largely explained by the combined uncertainties assigned to the data products. Still, it is fundamental to continue producing accurate *in situ* measurements through alternative approaches relying on state-of-the-art methods and technology, to explore biases and uncertainties affecting above-water data products further and provide evidence of advances.

When considering specific investigations relevant to above-water radiometry, many issues still require attention. These include: exploring the impact of FOV and sensor height; the application of glint-filtering schemes to $L_T(\theta,\phi,\lambda)$ supported by objective criteria likely function of sun zenith and wind speed; assessing cloud contamination by exploiting $L_i(\theta',\phi,\lambda)$ and $E_s(\lambda)$ spectral features; more extended analysis of the impact of superstructures on $L_T(\theta,\phi,\lambda)$; and finally producing spectral surface reflectance factors ρ with assigned uncertainties fully accounting for polarization effects, slope and wave height, multiple scattering and, aerosol type and load.

Finally, equivalent to the case of in-water radiometry, the development and sustained maintenance of an open-source community processor for the handling and reduction of above-water radiometry data, would ensure access to state-of-the-art processing solutions to any member of the community.

REFERENCES

Bulgarelli B. and Zibordi G., 2018: On the detectability of adjacency effects in ocean color remote sensing of mid-latitude coastal environments by SeaWiFS, MODIS-A, MERIS, OLCI, OLI and MSI. *Remote Sensing of Environment*, 209, 423-438.

Carder K.L. and Steward R.G., 1985: A remote-sensing reflectance model of a red tide dinoflagellate off West Florida. *Limnology and Oceanography*, 30, 286-298.

Carrizo C, Gilerson A., Foster R., Golovin A. and El-Habashi A., 2019: Characterization of radiance from the ocean surface by hyperspectral imaging. *Optics Express*, 27(2), 1750-1768.

Cox C. and Munk W., 1954: Measurement of the roughness of the sea surface from photographs of the sun's glitter. *Journal of the Optical Society of America*, 44, 11838-11850.

D'Alimonte D. and Kajiyama T., 2016: Effects of light polarization and waves slope statistics on the reflectance factor of the sea surface. *Optics Express*, 24(8), 7922-7942.

Foster R. and Gilerson A., 2016: Polarized transfer functions of the ocean surface for above-surface determination of the vector submarine light field. *Applied Optics*, 55(33), 9476-9494.

Fougnie B., Frouin R., Lecomte P. and Deschamps P.-Y., 1999: Reduction of skylight reflection effects in the above-water measurement of diffuse marine reflectance. *Applied Opt*ics, 38, 3844-3856.

Gergely M. and Zibordi G., 2013. Assessment of AERONET-OC L_{wn} uncertainties. *Metrologia*, 51(1), 40-47.

Gilerson A., Carrizo C., Foster R. and Harmel T., 2018: Variability of the reflectance coefficient of skylight from the ocean surface and its implications to ocean color. *Optics Express*, 26(8), 9615-9633.

Gleason A.C., Voss K.J., Gordon H.R., Twardowski M., Sullivan J., Trees C., Weidemann A., Berthon J.-F., Clark D.K. and Lee Z.P., 2012: Detailed validation of the bidirectional effect in various Case I and Case II waters. *Optics Express*, 20(7), 7630-7645.

Gould R.W., Arnone R.A. and Sydor M., 2001: Absorption, Scattering, and Remote-Sensing Reflectance Relationships in Coastal Waters: Testing a New Inversion Algorithm. *Journal of Coastal Research*, 17(2), 328-341.

Groetsch P.M., Gege P., Simis S.G., Eleveld M.A. and Peters S.W., 2017: Validation of a spectral correction procedure for sun and sky reflections in above-water reflectance measurements. *Optics Express*, 25(16), A742-A761.

Harmel T., Gilerson A., Tonizzo A., Chowdhary J., Weidemann A., Arnone R. and Ahmed S., 2012: Polarization impacts on the water-leaving radiance retrieval from above-water radiometric measurements. *Applied Optics*, 51(35), 8324-8340.

Hieronymi M., 2016: Polarized reflectance and transmittance distribution functions of the ocean surface. *Optics Express*, 24(14), A1045-A1068.

Hooker S.B. and Morel A., 2003: Platform and environmental effects on above-water determinations of water-leaving radiances. *Journal of Atmospheric and Oceanic Technology*, 20(1), 187-205.

Hooker S.B., Lazin G., Zibordi G. and McLean S., 2002: An evaluation of above-and in-water methods for determining water-leaving radiances. *Journal of Atmospheric and Oceanic Technology*, 19(4), 486-515.

Hooker S.B. and Zibordi G., 2005: Platform perturbations in above-water radiometry. *Applied Optics*, 44(4), 553-567.

Hooker S.B., Zibordi G., Berthon J.-F. and Brown J.W., 2004: Above-water radiometry in shallow coastal waters. *Applied Optics*, 43(21), 4254-4268.

Kutser T., Vahtmäe E., Paavel B. and Kauer T., 2013: Removing glint effects from field radiometry data measured in optically complex coastal and inland waters. *Remote Sensing of Environment*, 133, 85-89.

Lee Z.P., Carder K.L., Steward R.G., Peacock T.G., Davis C.O. and Mueller J.L., 1997: Remote sensing reflectance and inherent optical properties of oceanic waters derived from above-water measurements. In *Ocean Optics XIII* (*Vol.* 2963, pp. 160-166). International Society for Optics and Photonics.

Lee Z.P., Du K., Voss K.J., Zibordi G., Lubac B., Arnone R. and Weidemann A., 2011: An inherent-optical-property-centered approach to correct the angular effects in water-leaving radiance. *Applied Optics*, 50(19), 3155-3167.

Lee Z.P., Ahn Y.H., Mobley C. and Arnone R., 2010: Removal of surface-reflected light for the measurement of remote-sensing reflectance from an above-surface platform. *Optics Express*, 18(25), 26313-26324.

Lee Z.P., Pahlevan N., Ahn Y.H., Greb S. and O'Donnell D., 2013: Robust approach to directly measuring water-leaving radiance in the field. *Applied Optics*, 52(8), 1693-1701.

Mobley C.D., 1999: Estimation of the remote-sensing reflectance from above-surface measurements. *Applied Optics* 38, 7442-7455.

Mobley C.D., 2015: Polarized reflectance and transmittance properties of windblown sea surfaces. *Applied Optics*, 54(15), 4828-4849.

Morel A., Antoine D. and Gentili B., 2002: Bidirectional reflectance of oceanic waters: accounting for Raman emission and varying particle scattering phase function. *Applied Optics*, 41(30), 6289-6306.

Rhea W.J. and Davis C.O., 1997: A comparison of the SeaWiFS chlorophyll and CZCS pigment algorithms using optical data from the 1992 JGOFS Equatorial Pacific Time Series. *Deep Sea Research II* 44, 1907-1925.

Ruddick K.G., De Cauwer V., Park Y.J. and Moore G., 2006: Seaborne measurements of near infrared water-leaving reflectance: The similarity spectrum for turbid waters. *Limnology and Oceanography* 51(2), 1167-1179.

Shang Z., Lee Z.P., Dong Q. and Wei J., 2017: Self-shading associated with a skylight-blocked approach system for the measurement of water-leaving radiance and its correction. *Applied Optics*, 56(25), 7033-7040.

Simis S.G. and Olsson J., 2013: Unattended processing of shipborne hyperspectral reflectance measurements. *Remote Sensing of Environment*, 135, 202-212.

Sydor M. and Arnone R.A., 1997: Effect of suspended and dissolved organic matter on remote-sensing of coastal and riverine waters. *Applied Opt*ics, 36, 6905-6912.

Talone M., Zibordi G. and Lee Z.P., 2018: Correction for the non-nadir viewing geometry of AERONET-OC above water radiometry data: an estimate of uncertainties. *Optics Express*, 26(10), A541-A561.

Talone M. and Zibordi G. 2019: Spectral assessment of deployment platform perturbations in above-water radiometry. *Optics Express* 27(12), A878-A889.

Tanaka A., Sasaki H. and Ishizaka J., 2006: Alternative measuring method for water-leaving radiance using a radiance sensor with a domed cover. *Optics Express*, 14(8), 3099-3105.

Toole D.A., Siegel D.A., Menzies D.W., Neumann M.J. and Smith R.C., 2000: Remote-sensing reflectance determinations in the coastal ocean environment: impact of instrumental characteristics and environmental variability. *Applied Optics*, 39, 456-468.

Zhang X., He S., Shabani A., Zhai P.W. and Du K., 2017: Spectral sea surface reflectance of skylight. *Optics Express*, 25(4), A1-A13.

Zibordi G., Hooker S.B., Berthon J.-F. and D'Alimonte D., 2002: Autonomous above-water radiance measurements from an offshore platform: a field assessment experiment. *Journal of Atmospheric and Oceanic Technology*, 19(5), 808-819.

Zibordi G., 2012: Comment on "Long Island Sound Coastal Observatory: assessment of above-water radiometric measurement uncertainties using collocated multi and hyperspectral systems". *Applied Optics*, 51(17), 3888-3892.

Zibordi G., 2016: Experimental evaluation of theoretical sea surface reflectance factors relevant to above-water radiometry. *Optics Express*, 24(6), A446-A459.

Zibordi G., Mélin F., Berthon J.-F., Holben B.N., Slutsker I., Giles D., D'Alimonte D., Vandemark D., Feng H., Schuster G. and Fabbri B.E., 2009: AERONET-OC: a network for the validation of ocean color primary products. *Journal of Atmospheric and Oceanic Technology*, 26(8), 1634-1651.

Zibordi G., Ruddick K., Ansko I., Moore G., Kratzer S., Icely J. and Reinart A., 2012: In situ determination of the remote sensing reflectance: an inter-comparison. *Ocean Science*, 8(4), 567-586.